

Description of Solutes/Solids Interactions by Supercritical Fluid Chromatography

Vom Promotionsausschuss der

Technischen Universität Hamburg

zur Erlangung des akademischen Grades

Doktor-Ingenieurin (Dr.-Ing.)

genehmigte Dissertation

von

Miaotian Sun

aus

Qingdao, China

2023

Betreuer/1st Gutachter: Jun.-Prof. Dr. Pavel Gurikov (TUHH)

2nd Gutachterin: PD Dr. habil. Monika Johannsen (TUHH)

3rd Gutacher: Prof. Dr. habil. Philip Jäger (TU Clausthal)

Tag der mündlichen Prüfung:

29. August 2022

Acknowledgement

First and foremost, I am extremely grateful to my supervisor, Jun. -Prof. Dr. Pavel Gurikov for his invaluable advice, continuous support, and patience during my PhD study. Pavel is not only my mentor but also a dearest friend. Without his persistent encouragement, this work would never have been completed. I would also like to thank PD Dr. Monika Johannsen for accepting me for this doctoral program and introducing me to the fascinating world of supercritical fluid chromatography. She has always been supportive and kind to me. My genuine gratitude goes to Prof. Dr. Irina Smirnova. She is my royal model as a female scientist, one who has inspired me to become a researcher. The teaching opportunity she gave me was one of the best experiences in my memory. In addition, I also appreciate Prof. Dr. Philip Jäger for being the reviewer of my thesis, who raised critical questions and gave valuable advice.

My gratitude extends to all the members of V-8, Institute of Thermal Separation Processes. They were never stingy to share their opinions and never hesitated to help. Special thanks go to my precious friends met in V-8, Joana, Fynn, Imke, Tamara, Sheila, Simon, Raman, Steffi, Andreas, Victor, Stephan, Olli, Marc, Alberto, Xixi, René, Thomas, Ilka, Robert and Michal. It was their companionship that made my study and life in Hamburg a wonderful time. There are no words that can express my appreciation to those working experience in V-8, the experience learning the German engaging, rigorous, yet open-minded work culture, the experience exchanging ideas with researchers from all over the world and the experience interacting with such a diverse group of students and co-workers .

Finally, I would like to thank my parents. Without their tremendous understanding and support, it would not have been possible for me to complete my study. Although they were on the other side of the globe, I never felt their care and love had left me for a second.

Summary

Supercritical fluids, especially supercritical carbon dioxide (sc-CO₂), have gained great attention in recent years as green media in various processes to meet the increasing high requirement for safety of food, natural products and pharmaceuticals. No matter which process is employed (impregnation, adsorption or extraction), it involves the interaction between at least one solute and a solid material. Thus, in the aim of process improvements, a fast and robust approach to quantify the interactions in sc-CO₂ is demanded. In this work, supercritical fluid chromatography (SFC) is adopted for this purpose.

First of all, the experimental set-up was examined. Special attention was given to the reliable measurements of hold-up time, working region at single phase and the reproducibility of retention factors. Retention data at various pressures (150-300 bar), temperatures (25-60°C) and modifier concentrations (5-20 vol.% methanol in CO₂) were then collected for various solutes on four silica matrices by SFC. Due to the low polarity of pure sc-CO₂, the elution of most solutes is only possible with binary mixtures of sc-CO₂ and modifier (methanol in this work), where the masking effect of methanol is of great importance on the interactions. The adsorption isotherms of methanol on each applied silica matrix were therefore carefully determined by frontal analysis.

The strength and characteristics of solutes/solids interactions shall be described by proper retention models. Two categories of models were developed. One relates the retention factors to the molecular properties of solutes, which is based on the linear solvation energy relationships (LSER). The other emphasizes on the modifier effect which adopted the parameters obtained from the adsorption isotherms of methanol. The models were validated and applied to generate a comprehensive description of solutes-solids interactions at various operational conditions.

Abstract

Knowing the interactions between a solute and an adsorbent is of great importance for the design of various green processes which utilize supercritical carbon dioxide (sc-CO₂) as a solvent. In this work, by means of supercritical fluid chromatography (SFC) the thermodynamics of such systems have been studied. A wide range of polar and nonpolar solutes was used whereas methanol acted as the modifier. The retention data for various systems on four silica matrices was collected at various pressures, temperatures and modifier concentrations by SFC. Subsequently, two different types of retention models, one focusing on solute properties and the other modifier effects, were developed with the goal to generate a more accurate description of the solute-solid-interactions in sc-CO₂.

Abstrakt

Das Verstehen und Beschreiben der Wechselwirkungen zwischen gelösten Stoffen in einer fluiden Phase und Feststoffen spielt eine gewichtige Rolle bei der Auslegung grüner Prozesse, in denen überkritisches CO₂ (sc-CO₂) als Lösungsmittel genutzt wird. In dieser Arbeit wird mit Hilfe der überkritischen-Fluid-Chromatographie (SFC) die Thermodynamik ebensolcher Systeme untersucht. Dabei wird eine große Bandbreite an polaren und nicht-polaren Stoffen mit Methanol als Begleitstoff versetzt. Die Retentionsergebnisse für mehrere Systeme auf vier unterschiedlichen Silika-Matrizen sind für unterschiedlichen Konzentrationen von beigefügten Stoffen, Drücken und Temperaturen bestimmt worden. Zusätzlich sind zwei unterschiedliche Typen von Retentionsmodellen entwickelt worden mit dem Ziel, eine möglichst hohe Genauigkeit der Wechselwirkungen zwischen den gelösten Stoffen und dem Feststoff in sc-CO₂. Das erste Modell legt den Fokus auf die Eigenschaften des gelösten Stoffes und das zweite auf den Einfluss des Begleitstoffs Methanol.

Publication List

- [1] R. Subrahmanyam, P. Gurikov, P. Dieringer, M. Sun, I. Smirnova, On the Road to Biopolymer Aerogels—Dealing with the Solvent, *Gels*. 1 (2015) 291–313. <https://doi.org/10.3390/gels1020291>.
- [2] S. Reiser, M. Sun, M. Johannsen, M. Türk, Influence of Chemical Nature of Carrier Materials on the Dissolution Behavior of Racemic Ibuprofen, *J. Supercrit. Fluids*. 132 (2018) 91–98. <https://doi.org/10.1016/j.supflu.2017.02.015>.
- [3] M. Sun, S. Ruiz, M. Johannsen, I. Smirnova, P. Gurikov, Retention Characteristics of Silica Materials in Carbon Dioxide/Methanol Mixtures Studied by Inverse Supercritical Fluid Chromatography, *J. Chromatogr. A*. 1588 (2019) 127–136. <https://doi.org/10.1016/j.chroma.2018.12.053>.
- [4] M. Sun, Z. Ülker, Z. Chen, S. Deeptanshu, M. Johannsen, C. Erkey, P. Gurikov, Development and Validation of Retention Models in Supercritical Fluid Chromatography for Impregnation Process Design, *Appl. Sci.* 11 (2021). <https://doi.org/10.3390/app11157106>.

Abbreviations

Abbreviation	Meaning
ABPR	Automated Back Pressure Regulator
Adj. R ²	Adjusted R ²
BET	Brunauer-Emmett-Teller
C18	Octadecylsilane
C8	Octylsilane
DIM	Dual Influential Model
FTIR	Fourier Transform Infrared Spectroscopy
HPLC	High Performance Liquid Chromatography
iSFC	Inverse Supercritical Chromatography
LSE	Linear Solvation Energy Relationship
MRM	Mixed-Retention Model
PAH	Polycyclic Aromatic Hydrocarbons
PDA	Photodiode Array
RP-HPLC	Reversed-Phase High Performance Liquid Chromatography
RSE	Relative Standard Error
RSS	Residual Sum of Squares
RT	Room Temperature
Sc-CO ₂	Supercritical Carbon Dioxide
SFC	Supercritical Fluid Chromatography
TMS	Trimethylchlorosilane

Symbols

A_s	Specific surface area
a, b, A, B, F	Empirical parameters in DIM
$A_{Kaibara}, B_{Kaibara}$	Empirical parameter from Kaibara et al.
A_{Lee}, B_{Lee}	Empirical parameter from Lee et al.
$A_{Nah}, B_{Nah}, C_{Nah}, D_{Nah}$	Empirical parameter from Nahum et al.
$A_{Sch}, B_{Sch}, C_{Sch}$	Empirical parameter from Schoenmakers et al.
c	Modifier concentration
c_s	Concentrations of the solute in the stationary phase
c_m	Concentrations of the solute in the mobile phase
c_w	Water concentration
D	Partition/distribution coefficient
E_{co}	Cohesive energy
H_s^r	Henry's constant of the solute
\bar{h}_m^∞	Infinite-dilution partial molar enthalpy of the solute in the mobile phase
\bar{h}_s^∞	Infinite-dilution partial molar enthalpy of the solute in the stationary phase
k	Retention factor
k_0	Retention factor at zero modifier concentration
k_c	Retention factor for completely covered surface by modifier
k_{CBP}	Retention factors contribution for chemically bonded phase
K_{eq}	Adsorption equilibrium constant
$K_{eq,L}$	Adsorption equilibrium constant (Langmuir)
$K_{eq,lin}$	Adsorption equilibrium constant (Linear)
k_{silano}	Silanophilic retention factor
$k_{silano,0}$	k_{silano} in the absence of water

k_{sil}	Retention factors contribution for the adsorption on the silanol groups
$k_{sil,0}$	k_{sil} in pure CO ₂
k_{solv}	Solvophobic retention factor
K_w	Equilibrium constant of water
$k_{w,Snyder}, S_{Snyder}$	Empirical parameter from Snyder <i>et al.</i> [58]
L_c	Column length
\dot{m}	Mass flow
M	Empirical parameter in MRM
p	Pressure
p_c	Critical pressure
p^0	Vapor pressure of the pure solute
p^r	Reference pressure
q	Amount of solute adsorbed on the stationary phase/loading
q_{max}	Maximum loading
q_{mod}	Loading of modifier
r_c	Column inner radius
T	Temperature
T_c	Critical temperature
t_{BT}	Breakthrough time
t_M	Hold-up time
t_R	Retention time
v	Molar volume
v^0	Molar volume of the pure solute
\dot{V}_{avg}	Average volumetric flow rate
V_c	Column geometrical volume
V_m	Volumes of the mobile phase
$V_{M,p}$	Plant hold-up volume
$V_{M,c}$	Column hold-up volume

\bar{v}_m^∞	Infinite-dilution partial molar volume of the solute in the mobile phase
V_s	Volumes of the stationary phase
\bar{v}_s^∞	Infinite-dilution partial molar volume of the stationary phase
w	Mass fraction
w_s	Mass fraction of the mobile phase fluid in the stationary phase
x_m	Mole fraction of the modifier in the binary mobile phase
x_s	Mole fraction of the modifier in the stationary phase
y^σ	Mole-fraction solubility
$\alpha_{m,P}$	Isobaric expansivity of the pure mobile phase
$\alpha_{s,P}$	Isobaric expansivity of the stationary phase
β	Phase ratio, V_s/V_m
$\beta_{m,T}$	Isothermal compressibility of the pure mobile phase
$\beta_{s,T}$	Isothermal compressibility of the stationary phase
Γ	Molar concentration of unit surface area
δ	Hildebrand solubility parameter
ε_e	External porosity
ε_i	Internal porosity
ε_{tot}	Total porosity
θ	Modifier surface coverage
μ_s^∞	Infinite-dilution chemical potential
ρ	Density
φ_m^∞	Fugacity coefficient of the solute at infinite-dilution in mobile phase
φ_o	Volume fraction of organic modifier

Table of Contents

1 Introduction	1
1.1 Significance of the problem	1
1.2 Objectives.....	3
2 State of the Art.....	4
2.1 Introduction to SFC.....	4
2.2 Modifier effects in SFC	5
2.2.1 Modifier	5
2.2.2 Mobile-phase effects	6
2.2.3 Stationary-phase effects	7
2.3 Inverse chromatography.....	9
2.3.1 Determine properties by SFC.....	9
2.3.2 Retention models in RP-HPLC.....	12
2.3.3 Retention models in SFC	16
2.4 Surface chemistry of silica aerogels	19
3 Material and Methods	22
3.1 Chemicals.....	22
3.1.1 Solvents	22
3.1.2 Solutes	22
3.2 Chromatography.....	22
3.2.1 Packing of columns.....	22
3.2.2 SFC system	26

3.2.3	Hold-up time and retention data	26
3.3	Frontal analysis	29
3.3.1	Theory.....	29
3.3.2	Generation of breakthrough curves.....	30
3.3.3	Determination of crucial parameters	33
	Results and Discussion	37
4	Methodological Aspects	37
4.1	Measurement of t_M	37
4.2	Working region	39
4.3	Stability of columns.....	43
5	Analysis of Modifier Adsorption.....	46
5.1	Isotherm models	46
5.1.1	Experimental	46
5.1.2	Comparison with literature	50
5.2	Temperature and pressure influence.....	52
5.2.1	Temperature	52
5.2.2	Pressure.....	55
5.3	Surface coverage	56
6	Model Development.....	60
6.1	Linear solvation energy relationships	60
6.1.1	Data acquisition and evaluation	62
6.1.2	Model screening.....	62
6.1.3	Evaluation of the models.....	66

6.2	Retention models.....	69
6.2.1	Dual influential model (DIM).....	69
6.2.2	Mixed-retention model (MRM).....	72
6.2.3	Summary of DIM and MRM.....	73
6.2.4	Evaluation of DIM.....	75
6.2.5	Evaluation of MRM.....	80
7	Modifier Effects on Solute-Matrix Interaction	85
8	Other Factors Influencing Interactions	89
9	Transferability of the Free Energies	95
10	Conclusions and Outlook	97
11	References	100
12	Appendix.....	115
12.1	Introduction to REFPROP	115
12.2	A statistical test for outliers.....	116
12.3	Experimental data for LSER.....	117
12.4	Adsorption isotherms fitted into BET	123
12.5	Paired t-test for correction factor	127
12.6	List of Tables.....	129
12.7	List of Figures.....	131

1 Introduction

1.1 Significance of the problem

The interaction between solutes and solids is a fundamental phenomenon in nature, which exist in gas, liquid, and supercritical fluids. Supercritical fluids, especially supercritical carbon dioxide (sc-CO₂), have gained great attention in recent years as green media due to the increasing high requirements for safety of food, natural products, pharmaceuticals, and nutraceuticals. Sc-CO₂ has firmly established itself in the biomedical field wherein demands for safety are at highest level [1–4]. It is applied as the media in various processes, including impregnation, adsorption, and extraction, to produce materials greatly contributing to the life quality. Selected examples include: drug delivery implants, such as contact lenses [5] to treat ophthalmic diseases; polyethylene coated hip and knee endoprosthesis impregnated with α -tocopherol (vitamin E) through sc-CO₂ [6]; urinal stents with active compounds impregnated by means of sc-CO₂ [7]. Each of the above mentioned emerging application involves at least a solute such as a drug and a solid such as an implant. Thus, a deeper understanding of the interactions of solutes dissolved in the sc-CO₂ and solids are crucial for the development of new materials and processes. Fast and efficient methods to quantify these interactions in sc-CO₂ are needed urgently.

Further propagation of sc-CO₂ is, however, limited by the lack of fundamental knowledge when compared with classic processing media [8]. Although this problem has different faces, the most fundamental and thus crucial aspect is the thermodynamic foundations. More specifically, regardless of what process with sc-CO₂ is particularly employed (impregnation, adsorption or extraction), from thermodynamic point of view, the supercritical phase with a solute of interest is in equilibrium with a solid material. Even though numerous systems have been experimentally studied, consistent and comprehensive mathematical description of interactions in sc-CO₂ is missing.

In the literature, there are two major methods for studying equilibria in supercritical solvents: static and dynamic ones. The key idea of the static methods is to prepare a mixture of a given composition followed by exposure to desired conditions ($p - T$)

until an equilibrium is reached. Then, the composition of phases is analyzed without disturbing the equilibrium and translated into a corresponding point in the phase diagram. Such methods are generally of high precision and have widely been applied for studying solubility of organics in sc-CO₂ [9,10], liquid-liquid equilibria [11] and adsorption equilibria between drugs and polymers [12].

The static method and some other methods (e.g., calorimetry) are, however, of a limited value when a fast and accurate screening of various solutes and/or adsorbents is required. To ensure high throughput, dynamic methods are preferred. They rely on the fact that thermodynamic and kinetic properties of any process are fundamentally linked to each other. One common example is the distribution of the solute between an adsorbent and flowing fluid in a chromatographic experiment, where retention time and peak shape can be used to obtain the distribution coefficient and adsorption isotherm. Thus, chromatographic experiments with a solid phase used as stationary phase can deliver the fundamental information about phase equilibria.

In this work, to distinguish from physical characterization and separation applications, chromatographic methods for thermodynamic property determinations are referred to as the “inverse chromatography”. Although the supercritical fluid chromatography (SFC), wherein supercritical carbon dioxide serves as the mobile phase, is a well-established analytical separation technique, inverse version of SFC, is much less explored due to two reasons:

- (a) Both pressure and temperature significantly influence the retention factor k making theoretical interpretation of the retention difficult.
- (b) Low solvation power of pure sc-CO₂ towards even moderately polar solutes requires an addition of organic solvents (modifiers) leading to an even more complex thermodynamic picture.

1.2 Objectives

With the ultimate goal of building a framework for the rational selection of the porous carriers for a given active compound based on molecular interactions acting between them in sc-CO₂ related processes, this initial work aims to develop a robust method to describe the solute-solid-interactions by inverse supercritical chromatography (iSFC).

The objectives to achieve the aim of the work can be summarized as follows:

1. Exploration of the possibility of using porous solid matrices of interest as stationary phase and measure the retention factors of a wide range of solutes on these matrices accurately in SFC.
2. Measurement of the modifier adsorption equilibria at different temperature and pressure and study their effects on interactions in sc-CO₂.
3. Study on different models applied in SFC from literature and research on possibilities of modification or improvement.
4. Development and validation of retention models for the estimation of retention factors for solutes in pure sc-CO₂ using retention data obtained in sc-CO₂/modifier mixtures from experimentally measurable retention factors.
5. Employment of the iSFC technique in a combination with the retention models to characterize solute-solid-interactions and study the temperature, pressure and modifier influence.

2 State of the Art

2.1 Introduction to SFC

Supercritical fluid chromatography (SFC) is a separation technique, which most commonly employs sc-CO₂ as mobile phase. Supercritical fluids are fluids above their critical pressure and temperature [13]. These fluids have densities and solvation powers similar to those of common liquids, but lower viscosities and better diffusion properties [14]. In practice, the research areas of SFC also include fluids in the subcritical state, when only one of the two conditions (pressure and temperature) is fulfilled. After five decades of development [15], SFC has become an important separation tool widely applied to analysis and separation of substances in various fields, like pharmaceuticals, food, natural products and agricultural byproducts [16,17]. In addition, SFC is also becoming a powerful tool to determine thermodynamic properties as so-called “inverse chromatography” [18,19]. This work focuses on the latter application. A detailed introduction can be found in chapter 2.3.

SFC may be performed either in capillary columns or in packed columns. Both approaches have been demonstrated numerous times in the literature [20,21]. Capillary columns are longer and have lower internal diameters than packed columns. Their stationary phases are coated on the inner wall of the column. In packed columns, the stationary phase is directly filled inside [22]. Packed columns are employed in this work. Bare silica or bonded phases on porous silica are by far the most widely used stationary phases for SFC. The applied spherical silica-based particles mostly have diameters between 1 and 10 µm with pore size between 6 and 30 nm and surface areas between 100 and 350 m²/g [22,23].

Sc-CO₂ is adopted as the mobile phase for SFC mainly because of its relatively low critical point ($T_c = 30.98\text{ }^{\circ}\text{C}$, $p_c = 73.77\text{ bar}$ [24]), low cost, the non-toxicity, the availability with high purity and the miscibility to a large variety of organic solvents [17]. However, due to its non-polarity, the solvation power of CO₂ is limited for polar solutes. Thus, an organic solvent or so-called “modifier” is added to CO₂ to extend its solvation power [17]. Modifiers can significantly affect the retention of the solutes which will be further explained in the next chapter 2.2 Modifier effects in SFC.

2.2 Modifier effects in SFC

2.2.1 Modifier

There are several primary parameters in SFC that can be altered to achieve or enhance separation of solutes. These parameters include temperature, pressure, and mobile phase composition (modifier content), apart from the selection of the chromatographic columns [15,25] (Table 2.1). As for the mobile phase composition, many researchers have reported that the addition of organic compounds like methanol, ethanol, or isopropanol, can improve peak shape, alter solute retention and enhance separation [26,27]. These organic solvents are often referred to as modifiers. Modifiers are also widely used in supercritical fluid extraction. They are added to CO₂ as modifiers to increase the solvation power of the resulting extraction fluid as CO₂ has a limited solvation power for polar solutes and fails to solvate or efficiently extract polar molecules [28].

Nowadays, an SFC mobile phase commonly assumes a pure or mixture of CO₂ and modifiers. Typical modifiers are alcohols like methanol, ethanol and isopropanol, or other solvents like acetonitrile, chloroform and ethyl acetate.

Table 2.1: Chromatography classifications and their available control parameters [15].

	GC	LC	SFC
Pressure	No	No	Yes
Temperature	Yes	Yes	Yes
Modifier	No	Yes	Yes

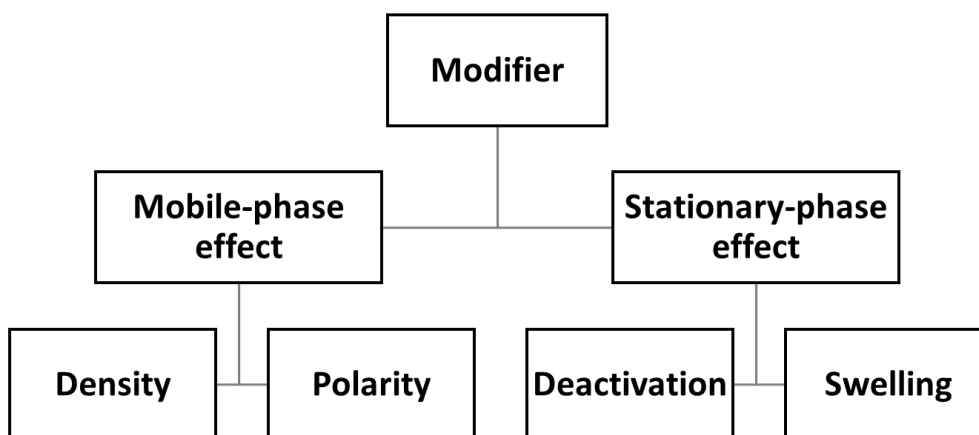


Figure 2.1: Effects of modifiers in SFC [29].

As the solute retention in SFC is governed by both the properties of mobile phase and stationary phase, the introduction of a modifier to the mobile phase can lead to changes in the nature of either or both of these phases [21,29]. Thus, the effects of modifiers are classified into two categories: the mobile-phase effect and the stationary-phase effect, as depicted in Figure 2.1.

2.2.2 Mobile-phase effects

Mobile-phase properties that can be varied by modifiers include density and polarity. The addition of a modifier to CO₂ vary the mobile phase density, compared to pure CO₂ under the same temperature and pressure conditions. For non-polar modifiers (e.g. hexane), the density effect might be the most critical effect, since these modifiers neither lead to drastic change in the mobile phase polarity nor deactivate the adsorptive sites on stationary phase [21]. However, in case of more polar solutes and modifier (like methanol), the density effect is less important. Berger et al. [30] reported that, when using more polar solutes and modifier, the composition changes produced significant retention shifts at constant density, which were larger than those as a result of density changes at constant composition. The shifts in retention were largely due to changes of solute-solvent interactions rather than density changes.

The introduction of modifier into the CO₂ can alter the nature and extent of the physical (or chemical) interactions between the solute and the mixed mobile phase [31]. These changes in the nature of the interactions caused by modifiers can be

detected by a spectroscopic measurement of solvatochromic shifts (color change due to a change in solvent polarity), which was reported by Deye et al. [32]. They selected Nile Red as the solvatochromic dye and dissolved the dye in the mixtures of methanol in CO₂, with the compositions of methanol varying from 1% to 100%. The wavelengths of adsorption maxima were collected by a spectrophotometer and the transition energies for the dye Nile Red were calculated and regarded as a measure of the "solvent strength". As a result, the wavelengths of adsorption maxima of Nile Red rose change with the increasing methanol fraction, which means the corresponding transition energies vary. Though the value of "solvent strength" was actually related to the solute(dye)-solvent interactions instead of the elution strength usually defined in adsorption chromatography, it provided an approximate correlation to solvent polarity. The solubility enhancement of solutes was also observed in binary solvent mixture of modifier and CO₂, which was believed to have close relationship to the complex interactions between modifier in the mobile phase. These intermolecular forces may include dispersion forces, dipole-dipole forces, and specific interactions like hydrogen bonding [33].

2.2.3 Stationary-phase effects

The stationary-phase effects include deactivation of the adsorptive sites on packed material (or on the column wall for capillary columns), as well as additional effects like swelling and changing the polarity of stationary phase.

In some studies, which focused on reversed phase columns in SFC, polar compounds were often found to give asymmetric peaks. The phenomenon was usually attributed to the residual silanol groups remaining on the silica-packing materials, which adsorb polar solutes. These materials were prepared by reaction of the silylating reagent (e.g., chloro- or alkoxysilanes) with the silanol groups on the silica material. However, owing to reactivity differences of the individual silanol groups, also to the steric constraints, it is unlikely to modify all the silanol groups [34]. Silanol groups can be further end-capped, which improves the deactivation but only partially shields the rest silanols on the surface. Polar organic modifiers are then often used to passively deactivate the active sites by competitive adsorption with solutes on the stationary phase.

Many researchers have reported such influence on the silanol groups. Blilie et al. [26] compared the retention of a medium polar compound nitro-PAH (polycyclic aromatic hydrocarbons) on two C18 (octadecylsilane) columns under the same temperature, pressure condition and with the same methanol volume fraction. One column contained appreciable high amounts of silanols while the other had been treated to remove silanol groups. It was shown that the peak shape obtained from the later column was largely symmetric even without modifier and the retention time was lower. However, the peak of a more polar solute benzoic acid still tailed badly without modifier. They suggested the decrease of retention with small amounts of alcohols was due to the deactivation of the adsorbent whereas the retention with high amounts of alcohols depended on the “solvent strength” of the mobile phase. The final effect of adding a modifier was a combination of both the deactivation effect and solubilizing effect. Their results showed that 1% modifier was sufficient to obtain symmetric peaks for the nitro-PAH.

Zou et al. [35] used phenol as a probe for silanol activity in SFC, as its efficiency and peak symmetry indicated the extent of silanol coverage by modifier adsorption. It was shown that the apparent efficiency and peak symmetry of the solute have reached maximum, when modifier fraction is low. The results implied that small amount of modifier can almost fully deactivate the stationary phase.

In addition to the deactivation effect, modifiers may also physically swell the stationary phase and change the polarity of the stationary phase [31]. This effect has mostly reported for polymeric stationary phases [36].

2.3 Inverse chromatography

Besides its important role in analytical field, SFC has become a powerful tool to measure thermodynamic properties providing insights of transport phenomena and fluid-phase equilibria [18,19]. This field of application is called “inverse chromatography”. By applying appropriate models, the types of the solute-solid interactions can be categorized, and their strengths can be analyzed. Moreover, many useful thermodynamic properties, such as solubility, partition coefficient, relative molar volume and molar enthalpy, can be derived from the retention factor of a solute on a stationary phase in pure sc-CO₂ by SFC. However, in practice, modifiers must be applied to elute polar solutes. Therefore, retention models which contain both two contributions, the experimental determined retention factor k and the hypothetical k_0 in pure sc-CO₂, are of interest. With such models, k_0 can be derived from experimental data and thereafter be used to calculate thermodynamic properties.

In the following sub-sections of this chapter, the models to determine thermodynamic properties, the complexity brought by the modifier, the retention models with potential to untangle this complexity and a solvation parameter model, which studies the interaction types and strengths, are introduced.

2.3.1 Determine properties by SFC

The applications of inverse SFC to determine thermodynamic properties in pure CO₂ fall into two categories: (a) to derive properties from solute retention factor directly and (b) to derive properties by changing the retention factor with pressure and temperature [19].

Deriving properties from retention factor

Two major properties can be derived from retention factors directly. They are the solute solubilities in supercritical fluids and the solute partition coefficients between sc-CO₂ and the stationary phase.

The solubility isotherms can be derived from the following equation:

$$y^\sigma = \left\{ \frac{P^0 V_s}{H_s^r V_m v_s} \exp \left[\frac{v^0 (P^r - P^0)}{RT} \right] \right\} \frac{v_m}{k} = [C(T)] \frac{v_m}{k} \quad \text{Eq. 1}$$

where y^σ is the mole-fraction solubility. H_s^r is the Henry's constant of the solute in the stationary phase at reference pressure P^r . P^0 is the vapor pressure of the pure solute at the column temperature. V_s and V_m are the volumes of the stationary and the mobile phase in the column, and v_s and v_m donate the molar volumes of the two phases. The molar volume of the pure solute is represented by v^0 . R is the molar gas constant and T is the column temperature. When $[C(T)]$ is fixed by a single independent value of solubility and the v_m is calculated from an equation of state, the whole solubility isotherm can be determined at a certain pressure. This approach has been applied in numerous studies to extend the solubility data base of supercritical fluids. The selected solutes applied CO₂ as media include polycyclic aromatic hydrocarbons [37–40], n-alkanes [41], and metal-ligand complexes [40].

Another important parameter, the partition or distribution coefficient of solutes D in chromatography can be easily calculated by:

$$D = \frac{c_s}{c_m} = k \frac{V_m}{V_s} \quad \text{Eq. 2}$$

where c_s and c_m are the molar concentrations of the solute in the stationary and the mobile phase. The quotient V_m/V_s is called the phase ratio. The partition coefficients of numerous solutes between sc-CO₂ and various stationary phases including crosslinked polymers [42–45] and bonded phases [46] were determined by this approach.

Deriving properties by changing retention factor with temperature and pressure

By changing pressure at a constant temperature, the change in the solute retention factor can be used to derive the difference between the partial molar volumes of solutes in the mobile and the stationary phase by the following equation:

$$\left(\frac{\partial \ln k}{\partial P} \right)_T = \frac{\bar{v}_m^\infty - \bar{v}_s^\infty}{RT} - \beta_{m,T} - \frac{V_s}{V_m} \beta_{s,T,\sigma} - \frac{1}{RT} \left(\frac{\partial \mu_s^\infty}{\partial w_s} \right)_{T,P,n_s} \left(\frac{\partial w_s}{\partial P} \right)_{T,\sigma} \quad \text{Eq. 3}$$

where \bar{v}_m^∞ and \bar{v}_s^∞ are the infinite-dilution partial molar volumes of the solute in the mobile and stationary phase. The two compressibilities, $\beta_{m,T}$ is the isothermal compressibility of the pure mobile phase and $\beta_{s,T,\sigma}$ is the isothermal compressibility of the stationary phase at saturation with the mobile phase. The parameter μ_s^∞ is the infinite-dilution chemical potential of the solute in the stationary phase and w_s is the mass fraction of the mobile phase fluid in the stationary phase. Subscript n_s refers to insolubility of the stationary phase in mobile phase and σ refers to the saturation of the stationary phase with the dissolved mobile phase. This approach has been applied to determine the partial molar volumes of hundreds of solutes at infinite-dilution in sc-CO₂ including aromatic hydrocarbons [42,46–51], n-alkanes [47], terpenic alcohols [52], coenzyme Q10 [53], vitamin E [54], etc.

By changing temperature at a constant pressure, the change in the solute retention factor can be used to derive the difference between the partial molar enthalpies of solutes in the mobile and the stationary phase by the following equation:

$$\left(\frac{\partial \ln k}{\partial T}\right)_P = \frac{\bar{h}_s^\infty - \bar{h}_m^\infty}{RT^2} - \alpha_{m,P} - \frac{V_s}{V_m} \alpha_{s,P,\sigma} - \frac{1}{RT} \left(\frac{\partial \mu_s^\infty}{\partial w_s}\right)_{T,P,n_s} \left(\frac{\partial w_s}{\partial T}\right)_{P,\sigma} \quad \text{Eq. 4}$$

where \bar{h}_m^∞ and \bar{h}_s^∞ are the infinite-dilution partial molar enthalpies of the solute in the mobile and stationary phase. The two expansivities, $\alpha_{m,P}$ is the isobaric expansivity of the pure mobile phase and $\alpha_{s,P,\sigma}$ is the isobaric expansivity of the stationary phase at saturation with the mobile phase. This approach was employed to obtain partial molar enthalpies for aromatic hydrocarbons [42,46,50,51,55] and hexasubstituted benzenes [56] in sc-CO₂.

Complexity associated with modifier

All the equations of the above introduced approaches contain the retention factor k in pure supercritical fluids (k_0) which means modifiers shall not present. When taking modifier into consideration, the three-component-system (solute, stationary phase and mobile phase) becomes more complicated. In order to apply the thermodynamic models, more assumptions must be suggested which leads to higher possibility of inaccuracies. More parameters will be involved in the calculation which demands

application of certain equation of states which are difficult to access [19,57]. The following equation describes the change in solute retention factor with the mole-fraction of modifier in the mobile phase at a constant temperature and pressure:

$$\begin{aligned} \left(\frac{\partial \ln k}{\partial x_m}\right)_{T,P,n_s} &= \left(\frac{\partial \ln \varphi_m^\infty}{\partial x_m}\right)_{T,P} - \zeta_m - \frac{V_s}{V_m} \zeta_s \left(\frac{\partial x_s}{\partial x_m}\right)_{T,P,n_s,\sigma} \\ &\quad - \frac{1}{RT} \left(\frac{\partial \mu_s^\infty}{\partial x_s}\right)_{T,P,n_s} \left(\frac{\partial x_s}{\partial x_m}\right)_{T,P,n_s,\sigma} \end{aligned} \quad \text{Eq. 5}$$

where φ_m^∞ is the fugacity coefficient of the solute at infinite-dilution in the binary mobile phase. The two mole fractions, x_m is the mole fraction of the modifier in the binary mobile phase and x_s is the mole fraction of the modifier in the stationary phase.

Application of this equation sets a much higher bar for experimental set-up. It requires a stable pumping system which delivers the binary solvent at a very well defined composition at precisely controlled temperature and pressure. [19]. Moreover the correct stationary-phase terms in the equation requires composition data of sorption from the binary mixture into the stationary phase, which is mostly unavailable in literature and difficult to determine [57].

On the other hand, an alternative way is to find reliable retention models which predict the retention factor at zero modifier concentration, k_0 , from the experimental determined k and thereafter apply k_0 in the thermodynamic equations, such as Eq. 1 to Eq. 4 to derive useful properties. The following sections provide inspirations to develop such models.

2.3.2 Retention models in RP-HPLC

Retention models in RP-HPLC is a starting point to develop SFC models thanks to pioneer researchers' hard work. This section will introduce several typical retention models in RP-HPLC before taking a further step to those of SFC.

Snyder et al. [58] have proposed a 2-parameter empirical retention model for RP-HPLC. This model is a linear approximation of the relationship between $\lg k$ and the volume fraction of organic modifier (φ_o), which was given by,

$$\lg k = \lg k_{w,Snyder} - S_{Snyder} \varphi_o \quad \text{Eq. 6}$$

where k is the retention factor. The parameter φ_o is the volume fraction of the organic modifier. The parameter $k_{w,Snyder}$ is an extrapolated value of k using only water as the mobile phase, and with no added organic modifier. The parameter S_{Snyder} is a parameter specific for a given solute and mobile-phase organic modifier. The two parameters are regarded as a measure of hydrophobic character of the solute [58]. In their studies, octylsilane (C8) columns were used, and methanol/water and acetonitrile/water were taken as mobile phases.

It has been observed by Schoenmakers et al. that the $\lg k$ vs. φ_o gives a non-linear relationship, when k was determined in a wide range of modifier concentration [59]. A quadratic approximation has been given by,

$$\lg k = A_{Sch} \varphi_o^2 + B_{Sch} \varphi_o + C_{Sch} \quad \text{Eq. 7}$$

where A_{Sch} , B_{Sch} and C_{Sch} are empirical coefficients.

Kaibara et al. [60] suggested the following form for retention in RP-HPLC,

$$\lg k = A_{Kaibara} \cdot \lg \frac{1}{c} + B_{Kaibara} \quad \text{Eq. 8}$$

where c is the organic modifier concentration in the mobile phase, and $A_{Kaibara}$ and $B_{Kaibara}$ are empirical coefficients which evaluate solute hydrophobicity. In their work, methanol, ethanol and acetonitrile were modifiers, and columns like C18, C8, TMS (trimethylchlorosilane) were used as stationary phases.

Lee et al. [61] proposed the relationship between the retention factor and the organic modifier content in RP-HPLC,

$$k = A_{Lee} + \frac{B_{Lee}}{\varphi_o} \quad \text{Eq. 9}$$

where A_{Lee} and B_{Lee} are experiment coefficients, φ_o is the volume fraction of the organic modifier. The modifiers used were methanol and acetonitrile and the column was packed with C18 particles.

All the models mentioned above considered mainly the solvent effect (solvophobic interaction). Besides the solvent effect, Nahum et al. [62] assumed that the retention of the solute was caused also by the stationary effect (silanophilic interaction), thus a “dual retention mechanism”. In general, there are still abundant silanol groups on the surface of alkyl-silica stationary phase. The solutes molecules can bind to these silanol groups, besides interact with the inert alkyl chains (solvophobic, or hydrophobic). The retention factor is expressed as the sum of the two retention factors, solvophobic, k_{solv} , and silanophilic, k_{silano} ,

$$k = k_{solv} + k_{silano} = A_{Nah} \cdot \exp(B_{Nah}\varphi_w) + \frac{1}{C_{Nah} + D_{Nah}\varphi_w} \quad \text{Eq. 10}$$

or

$$k = A_{Nah} \cdot \exp[B_{Nah}(1 - \varphi_o)] + \frac{1}{C_{Nah} + D_{Nah}(1 - \varphi_o)} \quad \text{Eq. 11}$$

where φ_w is the volume fraction of water and φ_o is the volume fraction of organic modifier. A_{Nah} , B_{Nah} , C_{Nah} , D_{Nah} are characteristic constants of the chromatographic systems. The first term of the equation decreases whereas the second term increases with increasing modifier volume fraction (φ_o). As a result, this model predicts a minimum in the plot of retention factor (k) against modifier composition (φ_o). The general effect of organic modifier is the result of the countervailing solvophobic and silanophilic forces on retention. In their work, two C18 columns were used as stationary phases, methanol/water as mobile phase.

Table 2.2: Summary of retention models in RP-HPLC. (Water is applied as mobile phase in all cases below.)

Reference	Model	Stationary Phase	Modifier
Snyder et al. [58]	$\lg k = \lg k_{w,Snyder} - S_{Snyder}\varphi_o$	C8	Methanol, acetonitrile
Schoenmakers et al. [59]	$\lg k = A_{Sch}\varphi_o^2 + B_{Sch}\varphi_o + C_{Sch}$	C18	Methanol, ethanol, propanol
Kaibara et al. [60]	$\lg k = A_{Kaibara} \cdot \lg \frac{1}{c} + B_{Kaibara}$	C18, TMS	C8, Methanol, ethanol, acetonitrile
Lee et al. [61]	$k = A_{Lee} + \frac{B_{Lee}}{\varphi_o}$	C18	Methanol, acetonitrile
Nahum et al. [62]	$k = k_{solv} + k_{silano}$ $= A_{Nah} \cdot \exp(B_{Nah}\varphi_w)$ $+ \frac{1}{C_{Nah} + D_{Nah}\varphi_w}$	C18	Methanol
Bij et al. [63]	$k = k_{solv} + k_{silano}$ $= k_{solv} + \frac{k_{silano,0}}{1 + K_w c_w}$	C18	Methanol, acetonitrile

Bij et al. [63] from the same group, also supported the dual retention mechanism, in which the solute retention was a result of both solvophobic (hydrophobic) and silanophilic interactions between the solute and stationary phases. The more polar component (i.e., water) acts as a masking agent of the surface silanol groups. The value of the overall retention factor (k) is given by,

$$k = k_{solv} + k_{silano} = k_{solv} + \frac{k_{silano,0}}{1 + K_w c_w} \quad \text{Eq. 12}$$

where $k_{silano,0}$ is the retention factor increment for silanophilic binding in the absence of a masking agent (water). K_w is the equilibrium constant for the binding of the masking agent to the stationary phase, whereas c_w is its concentration in the mobile phase.

Table 2.2 is a summary of the retention models introduced in this section.

2.3.3 Retention models in SFC

As discussed in the previous section, many retention models have been proposed in reversed-phase liquid chromatography (RP-HPLC), however, comparatively few have been developed for SFC. There are models for normal-phase liquid chromatography as well, however, less studies than RP-HPLC. Thus, the RP-HPLC models are usually adopted as a starting point for SFC but due to the differences between their stationary and mobile phases, these models are to be modified carefully.

For instance, the RP-HPLC stationary phases are non-polar, like octadecylsilane bonded silica. Although many have reported the applications of SFC on non-polar columns [64,65], the mostly widely used stationary phases are bare silica and silica-based monomeric sorbents, like 3-aminopropyl-, 3-cyanopropyl-, or a spacer bonded propanediol-siloxane [66], thus mostly the polar normal phase liquid chromatography (NP-HPLC) stationary phases. As for the mobile phase, RP-HPLC generally involves a binary mixture of water and an organic modifier, like methanol, acetonitrile, or tetrahydrofuran. While SFC uses aqueous-free solvents CO₂ together with an organic modifier. The absence of water in the mobile phase can cause drastic differences between RP-HPLC and SFC behaviors [66].

Two prominent classes of retention models reported for SFC are introduced in the following sections: the solvation parameter model and the mixed retention model (MRM). The solvation parameter models focus on the analysis of the interaction types and strengths in a system while by applying a mixed retention model, the theoretical retention factor at zero modifier concentration, k_0 , can be extracted for determination of thermodynamic properties such as partition coefficients, solubilities, molar volumes, and molar enthalpies. The two classes of models have the potential to compensate each other and give a more comprehensive picture of the interactions between the solutes and solids in sc-CO₂.

Linear solvation energy relationship

The solvation parameter model describes the retention of a solute in terms of different solvent-solvent and solute-solvent intermolecular interactions in the mobile and stationary phases. Abraham et al. [67] proposed that the retention factor (k) was related to the total solvation free energy and $\lg k$ was decomposed into contributions for cavity formation and interactions like dispersion, electron lone pair, dipole-type and hydrogen bonding, by using a linear solvation energy relationship (LSER). These types of interactions are schematically shown in Figure 2.2.

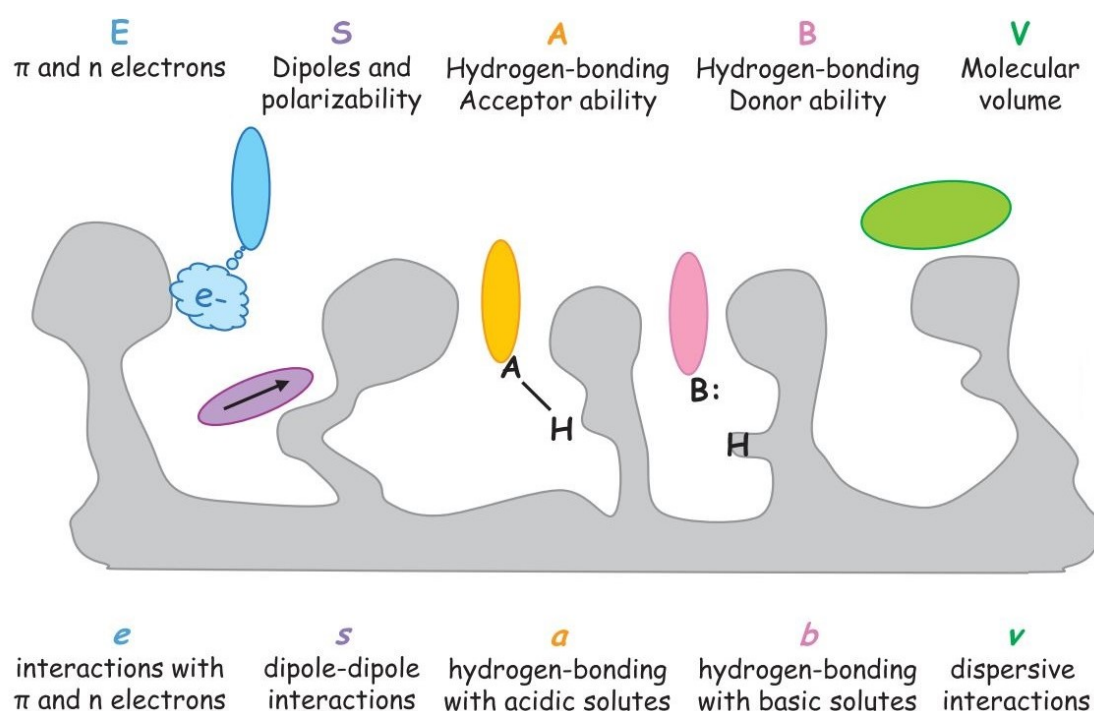


Figure 2.2: Principle of the solvation parameter model: interactions related to each solute descriptor. Figure from West et al. [68].

In a mathematical form the LSER model reads as follows:

$$\lg k = c + eE + sS + aA + bB + vV \quad \text{Eq. 13}$$

where the capital letters $\{E, S, A, B, V\}$ represent the Abraham solute descriptors, related to certain interaction properties. E is the excess molar refraction and models polarizability contributions from n and π electrons; S is the solute dipolarity/polarizability; A and B are the solute overall hydrogen-bond acidity and basicity; V is the McGowan characteristic volume. The lower-case letters $\{e, s, a, b, v\}$

are the system constants, which are related to the complementary effects obtained by multi-linear regressions of the retention data for a certain number of solutes with known descriptors [68]. Addition of a modifier can either promote or suppress a particular type of these molecular interactions.

Pyo et al. [69] applied the LSER regression on the solute on an ODS capillary column. In their study, the coefficients b and s were found to decrease greatly from neat CO₂ mobile phase to 2% methanol fraction. Thereafter, the two coefficients decreased gradually with increasing methanol concentration. They suggested that the predominant effect of modifier on the C18 stationary phase was covering the silanol groups on the surface, when a small amount of modifier (<2%) was added. When more modifier is added, another effect like the increase in the mobile phase density (higher elution strength) becomes more important.

Mixed Retention Model

In the mixed retention model, the deactivation of adsorptive sites on the stationary phase is regarded as the predominant effect of the modifier, compared to the other mobile phase effects (density, polarity).

Janssen et al. [31] derived a retention model for solutes in SFC, using C18 stationary phase or other chemically bonded phases. Two mechanisms were assumed to contribute independently to the overall retention: the first mechanism was the retention of the solute with the chemically bonded phase, while the second was the adsorption of solute on silanol groups on the surface. The effect of silanol groups are suppressed if the modifier is added, thus this part of retention increment has a dependence on the modifier concentration. This contribution of the silanol groups was assumed to be related to the portion of accessible silanols (bare, not occupied by modifier molecules), which could be described by a Langmuir adsorption isotherm of the modifier. The retention model is given by,

Eq. 14

$$k = k_{CBP} + k_{sil} = k_{CBP} + k_{sil,0}(1 - \theta)$$

where k_{CBP} and k_{sil} are the retention factors for the interactions with the chemically bonded phase and for the adsorption on the silanol groups. Parameter $k_{sil,0}$ is the

contribution of the silanol groups to the retention factor with neat CO₂ as mobile phase, i.e., at zero modifier concentration, and θ is the fraction of sites occupied by modifier. In their work, the stationary phase was octadecyl-modified silica, whereas the modifiers were ethanol and tetrahydrofuran. They also found that the retention factors of solutes like phenanthrene and 4-pentoxo-4'-cyano-biphenyl had decreased with hexane as the modifier, which was believed not to exhibit any interaction with the silanol groups on the stationary phase, nor to show specific interaction with the solute molecules in the mobile phase. This result was explained by the density changes in the mobile phase.

2.4 Surface chemistry of silica aerogels

Silica aerogels are low-density highly porous solids which possess an open structure [70,71]. They are prepared by means of the sol-gel process, which involves the hydrolysis and polycondensation of silicon alkoxides. First, the gel is created in a solution, and then the liquid component is removed slowly by supercritical drying to maintain the structural shape. This process is detailed in literature [72,73].

Due to its unique structure, silica aerogels have found place in several applications in the fields of pharmacy/agriculture, electronic, chemistry, and so on. Some of its properties are shown in Table 2.3, whereas some of its applications are summarized in Figure 2.3.

Table 2.3 Most important properties of silica aerogels. Summarized from [70,71,74,75].

Typical properties of silica aerogels	
Density	0.003 - 0.15 kg/m ³
Specific surface area	500 - 1600 m ² /g
Mean pore diameter	20 - 50 nm
Water resistance	Durably hydrophobic up to 250 °C (in air)
Temperature stability	Up to 500 °C

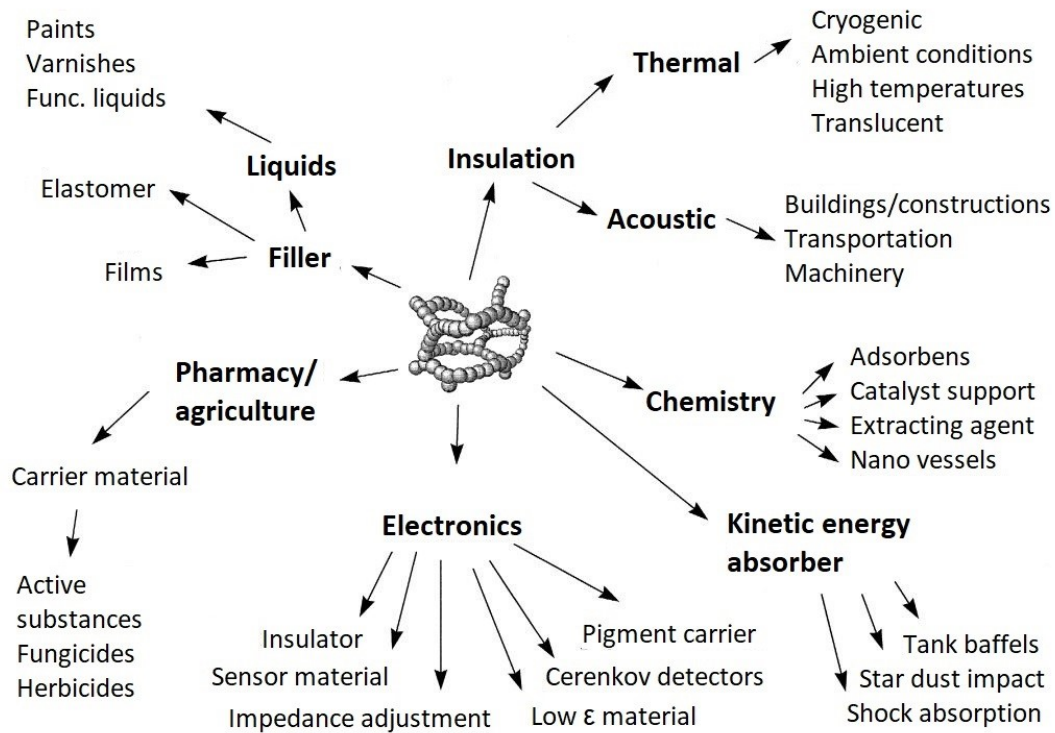


Figure 2.3: Application fields of silica aerogels. Extracted from [74].

The surface of silica aerogels can be either hydrophobic or hydrophilic depending on the different precursors chosen and different production process they went through. The Si-OH groups present in the aerogel structure are the main source of hydrophilicity. The hydroxyl groups act as active sites of adsorption for their specific interaction with molecules which are capable of forming hydrogen bonds or, more generally, undergoing donor-acceptor interaction. In addition, same as other amorphous silica, the surface of the silica aerogel is terminated with three types of silanol groups: (i) isolated silanols, (ii) vicinal silanols and (iii) germinal silanols as illustrated in Figure 2.4. In addition, there are also siloxane groups on the surface of silicas [76,77].

Different degrees of hydrophobicity can be added by surface modifications, which are done by replacing the hydroxyl groups with different functional groups through various processes in wet or dry state or in sc-CO₂ [70,71,75]. Some examples of the functional groups are: alkyl-, aryl- and amino groups [70,78].

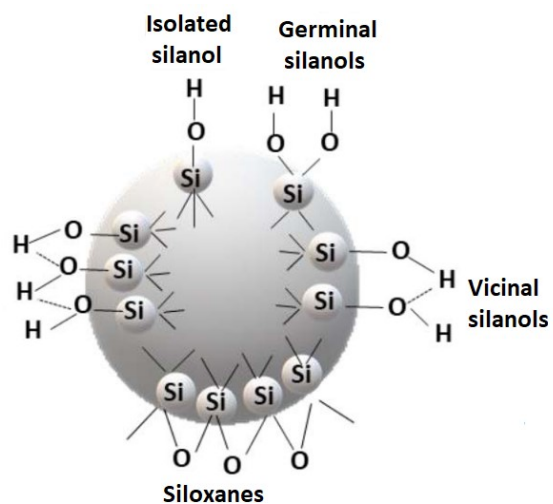


Figure 2.4: Different types of silanol groups and siloxane bridges on the surface of amorphous silica gel [76,77].

3 Material and Methods

3.1 Chemicals

3.1.1 Solvents

As a mobile phase, sc-CO₂ is used together with an organic modifier (mainly methanol) in order to increase the polarity of the mobile phase. CO₂ with purity level of 99.995% is used (Westfalen Austria GmbH). The cylinder capacity is 50 L. As for organic modifiers, high-quality chromatography grade solvents are used. Methanol and isopropanol are obtained from Roth, hexane from Honeywell and Ethanol from Sigma Aldrich.

3.1.2 Solutes

All the studied solutes and their suppliers are listed in Table 3.1.

3.2 Chromatography

Chromatographic experimental set-ups and procedures are described in this chapter.

3.2.1 Packing of columns

In this work, silica aerogel (SIL-Aerogel) and three commercial silica gels, Kromasil® 60-5-SIL (SIL-60), 100-5-SIL (SIL-100) and 300-5-SIL (SIL-300) from AkzoNobel, Bohus, Sweden, were employed as stationary phases. Silica aerogel was prepared from sodium silicate solution neutralized with sulfuric acid followed by extensive washing with water, solvent exchange to ethanol and finally supercritically dried with carbon dioxide. The silica gel and aerogel properties are listed in Table 3.2.

Table 3.1: Summary of solutes.

Solute	Supplier	State at RT*	Working wavelength (nm)
Phenol	Sigma Aldrich	Solid	210/211
Toluene	Roth	Liquid	207/240
Naproxen	Merck	Solid	220
Nicotinamide	Merck	Solid	210
Ketoprofen	Merck	Solid	254
Romarinic acid	Partner institution	Solid	330
Nitrous oxide	Westfalen/Sigma Aldrich	Gas	195
Benzene	Merck	Liquid	204
Caffeine	Merck	Solid	209
Pyridine	Merck	Solid	250
p-Nitrophenol	Honeywell	Solid	202
Vanillin	Roth	Solid	225
Benzoic acid	Roth	Solid	226
Nicotinamide	Sigma Aldrich	Solid	213
Ethyl benzoate	Sigma Aldrich	Solid	226
Anisole	Sigma Aldrich	Solid	216
p-Cresol	Sigma Aldrich	Solid	221
Nitrobenzene	Sigma Aldrich	Solid	202
p-Nitrotoluene	Sigma Aldrich	Solid	202
Butyl benzoate	Sigma Aldrich	Solid	226
Anthracene	Sigma Aldrich	Solid	232
Naphthalene	Fluka	Solid	211

*RT stands for room temperature.

Table 3.2: List of employed stationary phases and their textural properties.

Column	Kromasil® 60-5-SIL	Kromasil® 100-5-SIL	Kromasil® 300-5-SIL	Aerogel
Abbreviation	SIL-60	SIL-100	SIL-300	SIL-Aerogel
*Particle size, μm	6.2	6.1	6.2	17.4
**Mean pore diameter, nm	4	6	23	27
**Specific surface area, m^2/g	540	320	110	858
**Specific pore volume, cm^3/g	1.1	0.9	0.9	5.2
Column hold-volume, mL	0.690	0.676	0.663	0.624
Total porosity, -	0.831	0.814	0.798	0.751

* Measured by electrical sensing zone particle analyzer and scanning electron microscope.

** Measured by N_2 -adsorption.

All columns studied in this work were self-packed in the lab. A slurry method and a dry method were applied for packing.

Slurry method:

A slurry of Kromasil particles (20% in excess of the total volume of the column) in hexane was prepared and filled into an empty HPLC column (50 mm length and 4.6 mm internal diameter). Cellulose and metal filters were located at the outlet of the HPLC column followed by its sealing with an end fitting. The remaining slurry was filled into a feeder that was connected to the column inlet. Fresh hexane was pumped through the system for several minutes at 400 bar back pressure (Figure 3.1, (a)). The column was then disconnected from the feeder and excess particles were gently scraped away from the top of the column. The outlet was covered by cellulose filter and metal fine mesh and sealed with an end fitting.

Dry method:

Packing of silica aerogel was done in dry state as the material is sensitive to liquids. The dry method applied in this work consisted of successive filling of the column with crushed silica aerogel particles assisted by an upturned vibromixer (Chemap AG,

Switzerland), see Figure 3.1, (b). Once the column was filled, it was installed into the SFC equipment to compact the bed in sc-CO₂ flow (1 ml/min, 40 °C, 150 bar, 24 h). If a void volume was found in the column after the compaction, it was filled again with fresh aerogel. The packing process was repeated until the column was filled completely.

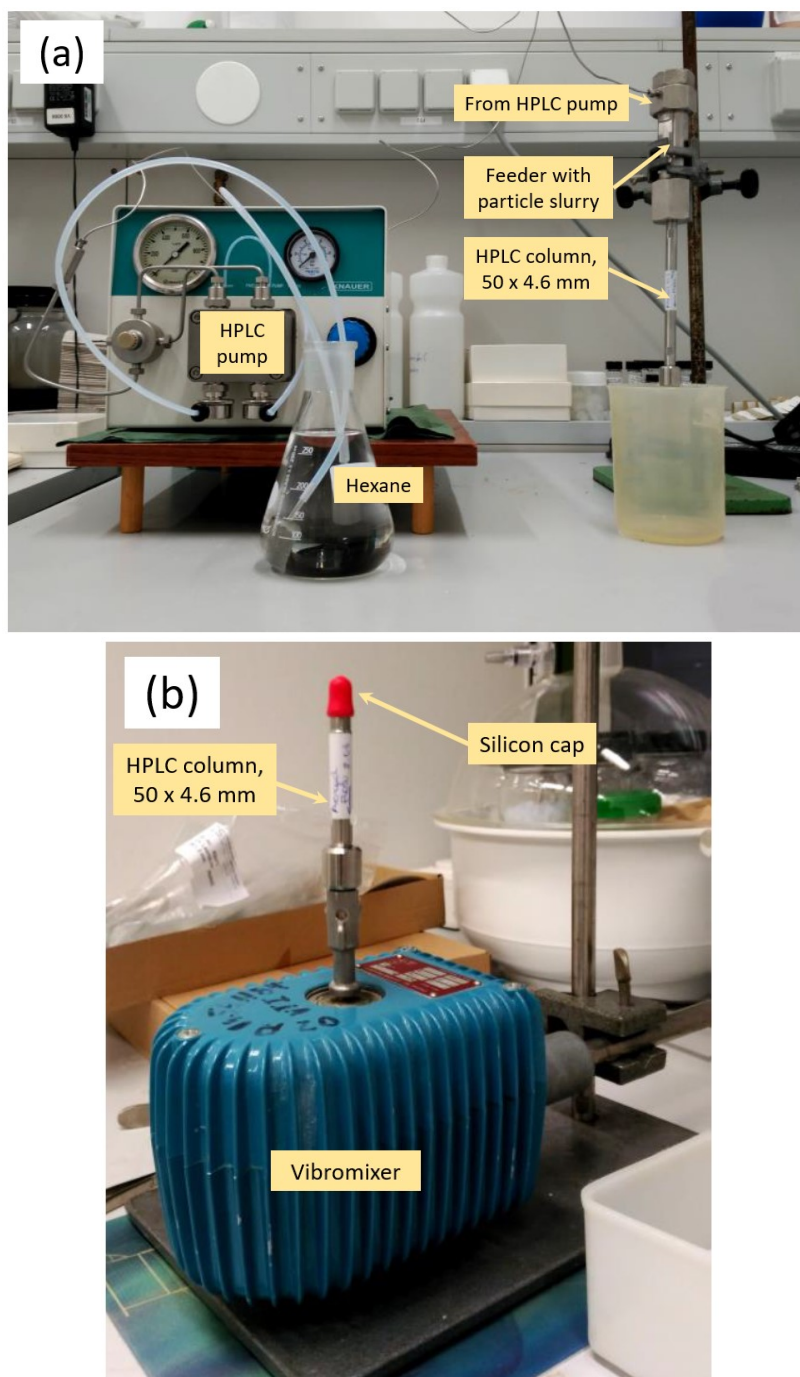


Figure 3.1: Column packing set-ups. Two set-ups were applied: (a) slurry packing method for Kromasil particles and (b) dry packing for silica aerogel.

3.2.2 SFC system

The experiments were carried out on a Waters ACQUITY UPC² supercritical fluid chromatography in this work. It consists of 5 blocks: The photodiode array (PDA) detector, column manager, convergence manager, sample manager and binary solvent manager (Figure 3.2). The wavelength range of the PDA detector is from 190 to 800 nm. Two columns are allowed in the column manager, each equipped with a preheater, which allows to achieve temperatures from room temperature to 90 °C in 0.1 °C increments. An automated back pressure regulator (ABPR) is installed in the convergence manager with a precision of ± 0.5 bar. The sample manager is the so-called auto-sampler as in other chromatography systems. Separated pumping systems in the solvent manager are used for the CO₂ and the modifier. The pumping system of CO₂ is modified and features a two-stage Peltier cooling. The operating flow rate is from 0.01 to 4 mL/min in 0.001 mL increments.

3.2.3 Hold-up time and retention data

Sample preparation

The solutes which are solids at room temperature were dissolved in methanol to a concentration of 0.1 g/L. Liquid solutes were injected directly at 100% concentration. UV spectra of each solute were recorded at 10% modifier concentration and were tested at different modifier concentrations to identify a working wavelength for the PDA detector. The selected working wavelengths are given in Table 3.1.

Hold-up time

Preliminary experiments were performed to identify the most suitable tracer compound for the determination of the hold-up time, t_M . It was found that most of the volatile organic solvents suggested in the literature showed certain retention. Similar findings have been reported earlier [79]. To minimize the systematic error, a method was adopted from the work by Vajda and Guiochon [80], who successfully employed N₂O as a tracer in SFC. This method has been validated in a later work by Åsberg et al., where the void volume determined by N₂O was proved independent on the modifier fraction [81]. A solution of N₂O in methanol was prepared by bubbling N₂O at

ambient conditions for a minute. Obtained solution was well sealed and used within a week. Sharp peaks of nitrous oxide were recorded at 195 nm.

Collection of retention data

Mobile phase was pumped at a flow rate of 2 mL/min with 0 to 30 vol.% methanol. Temperature and pressure were varied from 25 and 60 °C and 150 and 300 bar, respectively. The numerical values of the operational conditions were assumed to be equal to the set values of Waters ACQITY UPC² software Empower [82]. The difference between the actual and set operational conditions was neglected in this study based on the result of another study with the same equipment by Forss et al. [83]. It was shown that the temperature differences between actual and set values were below 1.4 °C, the modifier fraction differences below 1.3 % and pressure differences below 11 bar. The samples were injected into the SFC system and had volumes of 2 µL. Each injection was repeated at least twice. The PDA detector signal was recorded for each compound at its specific working wavelength.

The time at which the maximum signal appears was taken as the retention time t_R . Retention and hold-up times of all solutes were measured at least in triplicate and averaged. The averaged values were used to calculate the retention factor as:

$$k = \frac{t_R - t_M}{t_M} \quad \text{Eq. 15}$$

The methanol concentration was varied from 0 to 30 vol.%. Retention factors were plotted against methanol concentration to generate a retention profile.

Although tailing occurred for some of the compounds, the peak maximum method was adopted to determine the retention times following previous studies [84], where the retention time of each compound is recorded at the apex of the peak. The moment analysis [85,86], which takes the peak distribution into consideration, would potentially improve the accuracy of the analysis, however, is beyond the scope of this work.

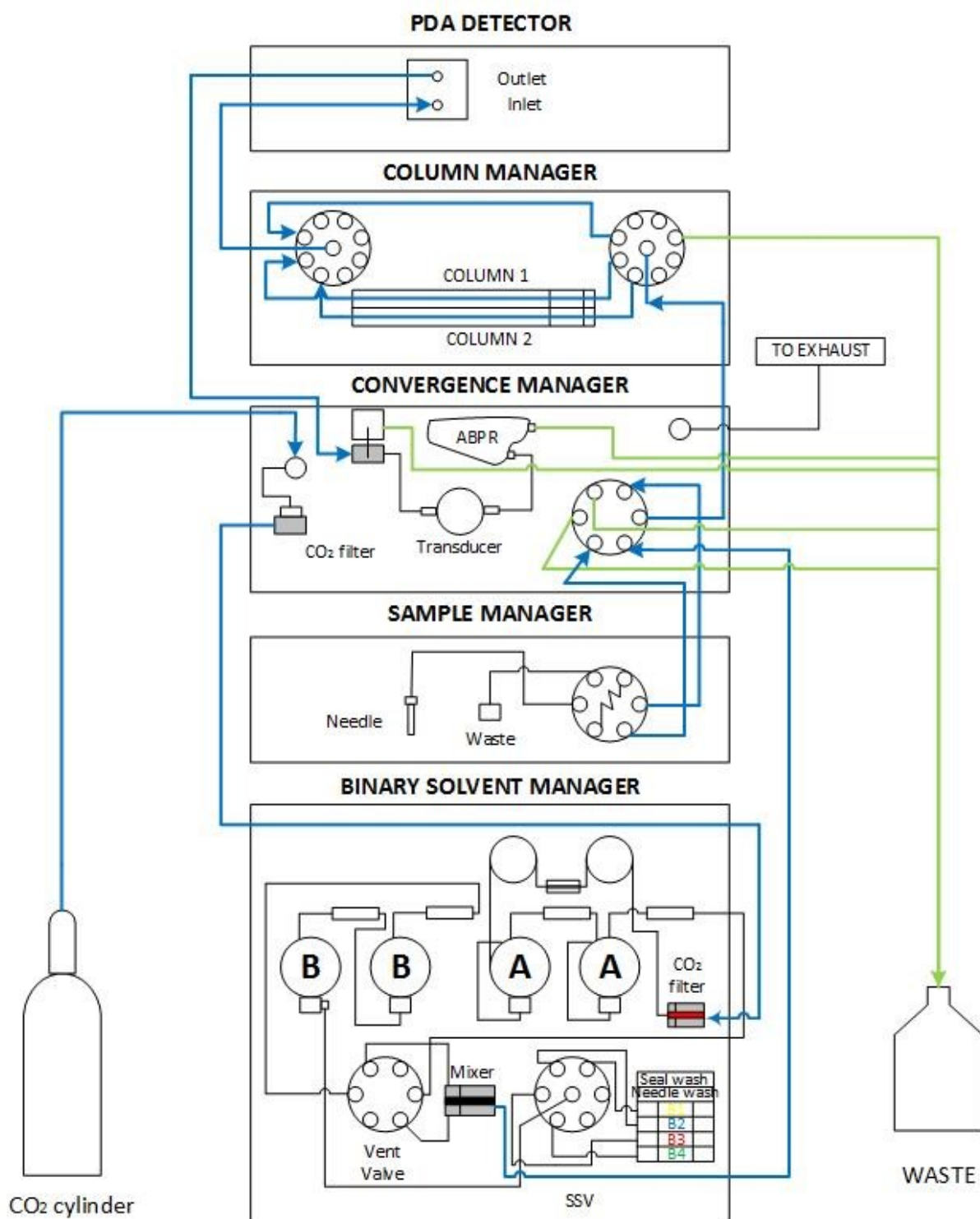


Figure 3.2: Flow diagram of Waters UPC². Blue line: principal connections; green line: to waste. Adapted from the graphical navigator view of Waters' webpage, 2017.

3.3 Frontal analysis

Methanol adsorption isotherms were measured by frontal analysis in this study.

3.3.1 Theory

A typical methodology of frontal analysis is as follows: the column is initially equilibrated with pure CO₂ ($c_1 = 0$) or with CO₂-solute mixture having a concentration of c_n . Then, the solute concentration of the feed (inlet flow) is changed into a new concentration c_{n+1} at the time point t_{inject} . The change of the feed concentration from c_n to c_{n+1} leads to a breakthrough curve, as is shown in Figure 3.3. A new equilibrium state is established when the outlet concentration becomes the feed concentration c_{n+1} . Based on the overall mass balance, the amount of solute adsorbed on the stationary phase (q), which is denoted by the area enclosed between the solid and dotted lines (hatched region A in Figure 3.3), can be calculated by:

$$\begin{aligned}
 V_{M,p} \cdot (c_{n+1} - c_n) + V_c \cdot [\varepsilon_{tot} \cdot (c_{n+1} - c_n) + (1 - \varepsilon_{tot}) \cdot (q_{n+1} - q_n)] \\
 = \dot{V}_{avg} \cdot \int_{t_{injection}}^{t_{plateau}} (c_{n+1} - c) \cdot dt \\
 = \dot{V}_{avg} \cdot (c_{n+1} - c_n) \cdot (t_{BT,n} - t_{injection})
 \end{aligned}
 \tag{Eq. 16}$$

The solute that accumulates in the system can be divided into three categories: (1) those inside the plant (extra-column), (2) those in the mobile phase inside the column and (3) those adsorbed on the stationary phase. $V_{M,p}$ is the plant hold-up volume (without column) and V_c is the column geometrical volume. The total porosity of the column, ε_{tot} , is the sum of the internal porosity (ε_i) and the external porosity (ε_e). (The internal porosity is the volume fraction of column that is available to the stagnant mobile phase, while the external porosity corresponds to the volume available to the flowing mobile phase percolating through the bed of the stationary phase [87]). The corresponding loadings at the initial and the later equilibrium states are represented as q_n and q_{n+1} . The outlet concentration profile reaches a plateau at $t_{plateau}$ and t_{BT} is the breakthrough time. On an ideal breakthrough curve, t_{BT} is at the inflection point $t_{inflection}$ (seen in Figure 3.3). In this work, an integration method was adopted to

estimate t_{BT} from experimental data. \dot{V}_{avg} is the volumetric flow rate of the mobile phase. Methods to determine all the necessary parameters are described in 3.3.3 Determination of crucial parameters.

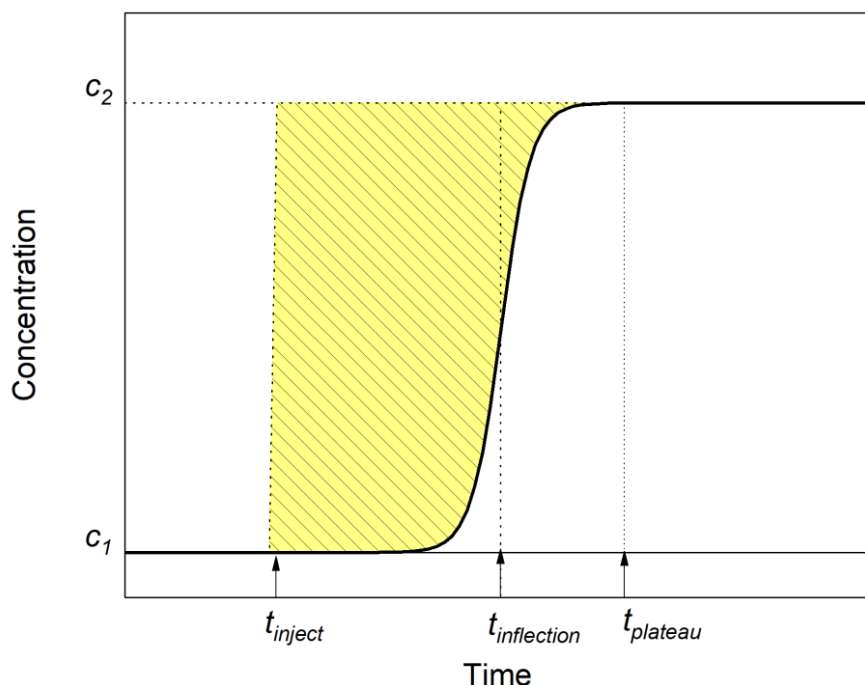


Figure 3.3: Ideal breakthrough curve for adsorption of a pure component in frontal analysis.

3.3.2 Generation of breakthrough curves

The crucial step of frontal analysis is to generate breakthrough curves. The SFC system Waters ACQUITY UPC² was applied for this part of work. Detailed description of the equipment is given in section 3.2.2.

Staircase method

The column was first equilibrated with 100% CO₂ for 15 minutes to remove the methanol residues. The column temperature was kept constant. After a stable baseline was established, the modifier pump was programmed to deliver methanol continuously at a stepwise flow of 11 rates: 0.01, 0.02, 0.04, 0.06, 0.10, 0.16, 0.20, 0.24, 0.30, 0.35, 0.40 mL/min. A 5-minutes time interval was set to achieve a new adsorption equilibrium at each modifier concentration which was observed as a new

plateau formed. Meanwhile the total volumetric flow rate was remained at 2.00 mL/min. A detailed view of the set values is provided in Table 3.3.

Table 3.3: Experimental settings for frontal analysis.

No.	$\varphi_{\text{methanol}}$ [vol%]	t [min]	$\dot{V}_{\text{methanol}}$ [mL/min]	\dot{V}_{CO_2} [mL/min]
0	0	0 - 5.00	0	2.00
1	0.5	5.00 - 10.00	0.01	1.99
2	1	10.00 - 15.00	0.02	1.98
3	2	15.00 - 20.00	0.04	1.96
4	3	20.00 - 25.00	0.06	1.94
5	5	25.00 - 30.00	0.10	1.90
6	8	30.00 - 35.00	0.16	1.84
7	10	35.00 - 40.00	0.20	1.80
8	12	40.00 - 45.00	0.24	1.76
9	15	45.00 - 50.00	0.30	1.70
10	17.5	50.00 - 55.00	0.35	1.65
11	20	55.00 - 60.00	0.40	1.60

The breakthrough curves were recorded by the PDA detector at 200 nm. Measurements were carried out at the column temperature 30 to 60 °C and the back pressure 120 to 240 bar. Temperatures and pressures were pre-set and recorded. Figure 3.4 shows an example of the breakthrough curves of one staircase frontal analysis on the SIL-300 column.

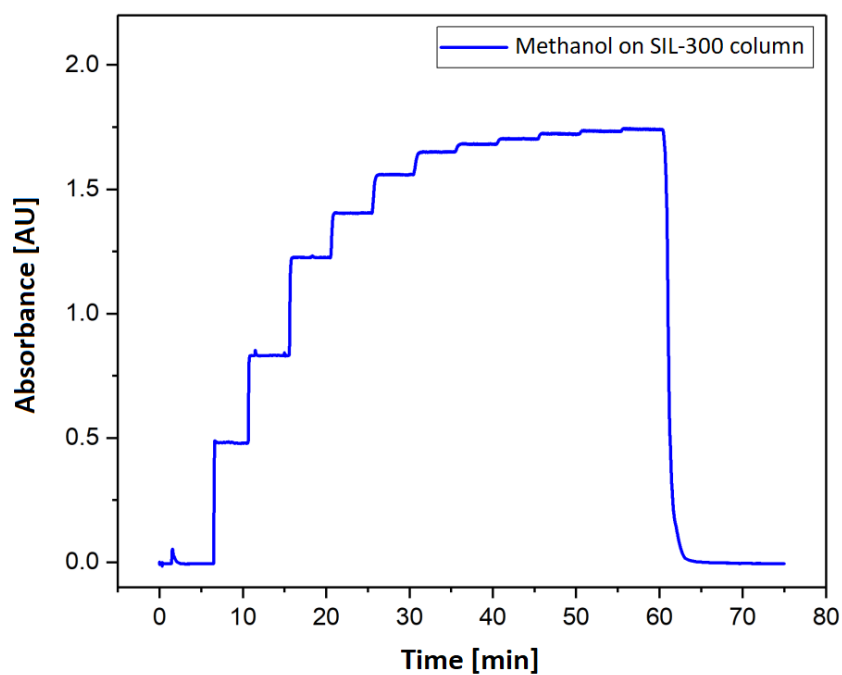


Figure 3.4: An example of breakthrough curves of a staircase frontal analysis of methanol on SIL-300 column. (SFC condition: 200 bar, 40 °C, flow rate 2.0 mL/min, UV 200 nm).

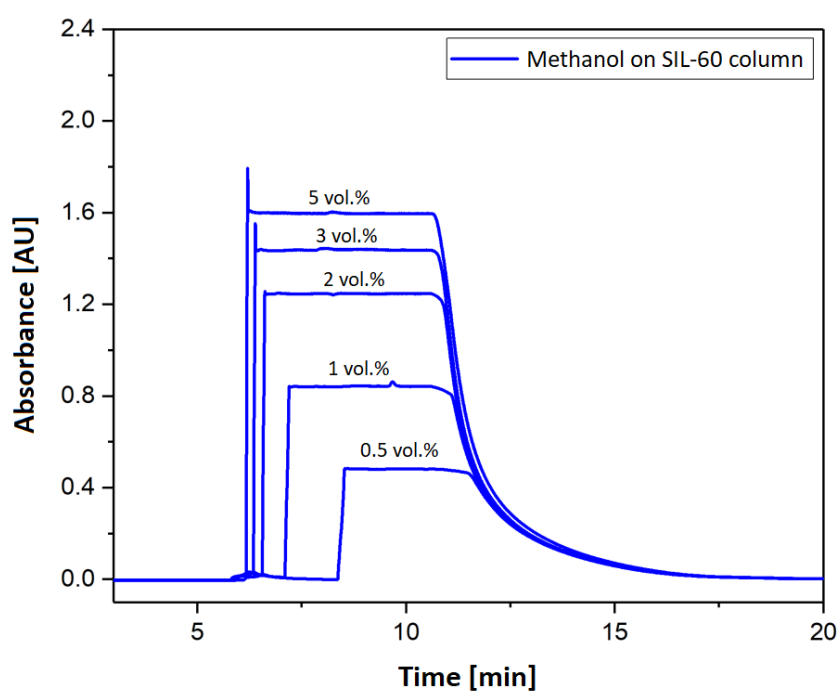


Figure 3.5: An example of breakthrough curves of a stepwise frontal analysis of methanol on SIL-60 column. (SFC condition: 200 bar, 40 °C, flow rate 2.0 mL/min, UV 200 nm).

Step series method

Measurements with step series method was conducted to confirm some of the results obtained using staircase method. The experimental conditions of the step series method were the same as those of staircase method, except the fraction of methanol was increased from 0 to the set value each time instead of from the set value of the previous step. Figure 3.5 presents the chromatogram of a step series frontal analysis on the SIL-60 column.

3.3.3 Determination of crucial parameters

To calculate the amount of methanol adsorbed on the stationary phase q based on the mass balance equation Eq. 16, parameters, including the plant hold-up volume $V_{M,p}$, the total porosity ε_{tot} , the breakthrough time t_{BT} and the average flow rate \dot{V}_{avg} were to be determined.

a. Determination of $V_{M,p}$

$V_{M,p}$ is the plant hold-up volume excluding the column. It was determined by measuring the hold-up time $t_{M,p}$. The column was bypassed by connecting the inlet and outlet capillaries directly. N_2O was used as the tracer as described in section 3.2.3. The plant hold-up volume was calculated by:

$$V_{M,p} = t_{M,p} \cdot \dot{V}_{avg} \quad \text{Eq. 17}$$

\dot{V}_{avg} is the average volumetric flow rate regarding to the density difference at the inlet and outlet of the column. The calculation of \dot{V}_{avg} is described in a later section d. Determination of \dot{V}_{avg} .

b. Determination of ε_{tot}

The total porosity of the column (ε_{tot}) is the sum of the external and internal porosity of the adsorbent [88], which can be calculated as:

$$\varepsilon_{tot} = \frac{V_{M,c}}{V_c} = \frac{V_{M,c}}{\pi r_c^2 L_c} \quad \text{Eq. 18}$$

where V_c is the volume of an empty column calculated with its geometry, i.e., the column inner radius, r_c and the column length, L_c . The column hold-up volume $V_{M,c}$ was calculated by subtracting the plant hold-up volume $V_{M,p}$ from the total hold up volume $V_{M,tot}$:

$$V_{M,c} = V_{M,tot} - V_{M,p} \quad \text{Eq. 19}$$

Where the total hold-up volume $V_{M,tot}$ was determined from the hold-up time when a column is installed:

$$V_{M,tot} = t_M \cdot \dot{V}_{avg} \quad \text{Eq. 20}$$

The column hold-up volumes and porosities of the columns in this work were summarized in Table 3.4.

Table 3.4: Column volumes and total porosities (measured at 30 °C).

Column	SIL-60	SIL-100	SIL-300	SIL-Aerogel
V_c [mL]	0.831	0.831	0.831	0.831
$V_{M,c}$ [mL]	0.690	0.676	0.663	0.624
ε_t [-]	0.831	0.814	0.798	0.751

c. Determination of t_{BT}

The n th breakthrough time $t_{BT,n}$ was determined with the integration method [89] as follows:

$$t_{BT,n} = \frac{\int_{t_{start,n}}^{t_{end,n}} (c - c_n) dt}{c_{n+1} - c_n} \quad \text{Eq. 21}$$

Here, $t_{start,n}$ and $t_{end,n}$ are the start time and end time of step n and c is the concentration of methanol at the column outlet measured by PDA detector.

d. Determination of \dot{V}_{avg}

Due to limitation that the SFC system applied for this work was not equipped with a volumetric flow meter at the inlet or outlet of the column, the average volumetric flow rate \dot{V}_{avg} was determined assuming a linear density profile. Figure 3.6 demonstrates the minor difference between a non-linear and linear density profile. Therefore, \dot{V}_{avg} was calculated as follows:

$$\dot{V}_{avg} = \frac{\dot{m}_{tot}}{\rho_{avg}} = \frac{\dot{m}_{tot}}{(\rho_{inlet} + \rho_{outlet})/2} \quad \text{Eq. 22}$$

Here, the total mass flow \dot{m}_{tot} is the sum of the mass flows of methanol $\dot{m}_{methanol}$ and CO₂ \dot{m}_{CO_2} , which were calculated from their volumetric flow rates recorded at the pump heads of the SFC system:

$$\dot{m}_{tot} = \dot{m}_{methanol} + \dot{m}_{CO_2} = \dot{V}_{methanol} \cdot \rho_{methanol} + \dot{V}_{CO_2} \rho_{CO_2} \quad \text{Eq. 23}$$

The densities of the methanol ($\rho_{methanol}$), CO₂ (ρ_{CO_2}) and the mixtures ($\rho_{inlet}, \rho_{outlet}$) were estimated by the software REFPROP 9.1 (Brief introduction in Appendix 12.1 Introduction to REFPROP) with the input of the temperature, pressure and mass fractions:

$$\rho_{methanol} = \rho(T_{methanol}, p_{methanol}) \quad \text{Eq. 24}$$

$$\rho_{CO_2} = \rho(T_{CO_2}, p_{CO_2}) \quad \text{Eq. 25}$$

$$\rho_{inlet} = \rho(T_{column}, p_{inlet}, w_{methanol}) \quad \text{Eq. 26}$$

$$\rho_{outlet} = \rho(T_{column}, p_{outlet}, w_{methanol}) \quad \text{Eq. 27}$$

T_{CO_2} was recorded at the CO₂ pump heads. Since the methanol pump heads were not equipped with a thermometer, room temperatures were applied for $T_{methanol}$. Both $p_{methanol}$ and p_{CO_2} were recorded at the pump heads respectively. Column

temperatures (T_{column}), column inlet pressures (p_{inlet}) and system back pressures (p_{outlet}) were recorded to determine the inlet and outlet densities, ρ_{inlet} and ρ_{inlet} . Mass fractions of methanol $w_{methanol}$ were calculated from mass flow rates:

$$w_{methanol} = \frac{\dot{m}_{methanol}}{\dot{m}_{tot}} \quad \text{Eq. 28}$$

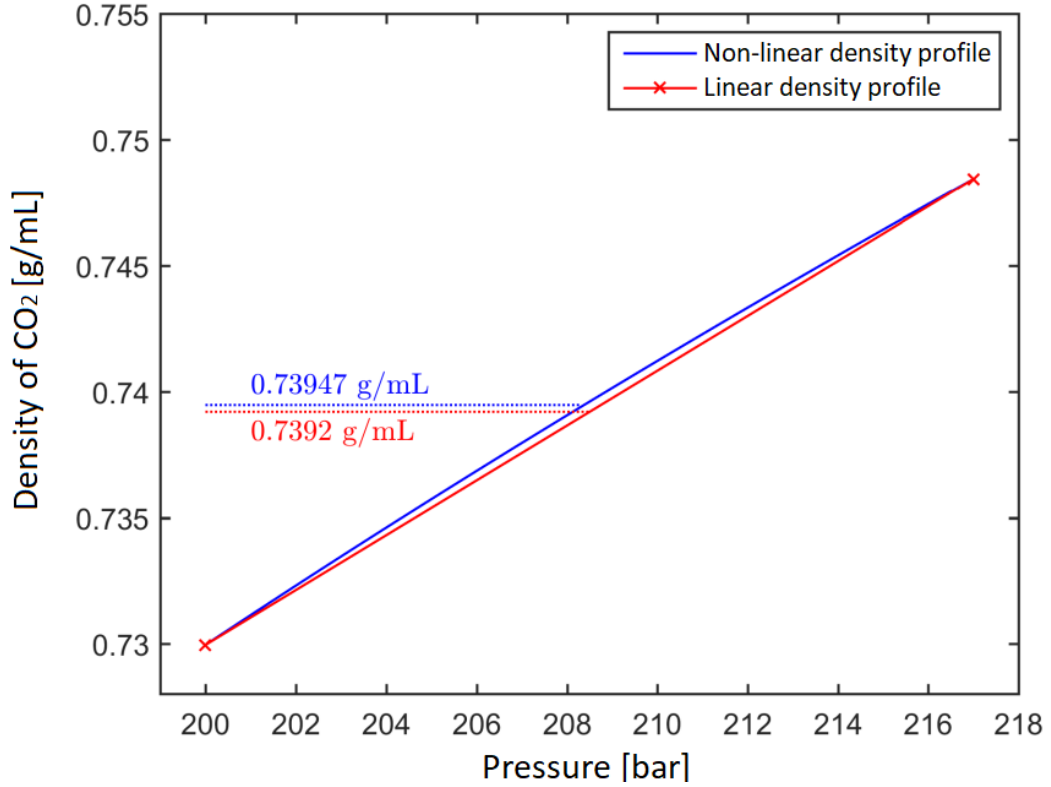


Figure 3.6: Density profile between column inlet and outlet of the SIL-60 column at 60 °C with 100% CO₂ as mobile phase. The x-axis presents the local pressure the column. As the back pressure was applied the density profile ended at 200 bar. The total pressure drops along the columns were observed to be no more than 18 bar.

Results and Discussion

4 Methodological Aspects

In this work, inverse SFC was applied to characterize the surface of stationary phases from chromatographic retention data. Special attention was given to following experimental aspects to ensure valid measurements: (i) reliable measurements of hold-up time; (ii) working region at single phase and (iii) reproducibility of retention factors. In the following sections, each of these aspects are addressed.

4.1 Measurement of t_M

Injections of five tracers, namely hexane, acetone, methanol, ethanol and methanolic solution of N_2O , were performed to identify the component with the lowest retention time (mobile phase composition: sc- CO_2 /methanol). Each injection was repeated at least twice. Although above 5 vol.% methanol in sc- CO_2 the retention time for all the tracers is close to each other, the situation is drastically different below 1 vol.% methanol as shown in Figure 4.1. As expected, the retention time does not depend on the modifier concentration only for chemically least interacting hexane and N_2O . Thus, these two can be utilized for the determination of the hold-up time. N_2O in methanol showed however a better peak shape (an example is given in Figure 4.2). Moreover, its retention time was found to be independent from the nature of the modifier when hexane, isopropanol and ethanol were used instead of methanol, seen in Figure 4.3. Thus, nitrous oxide in methanol was used throughout this work to record the hold-up times, t_M .

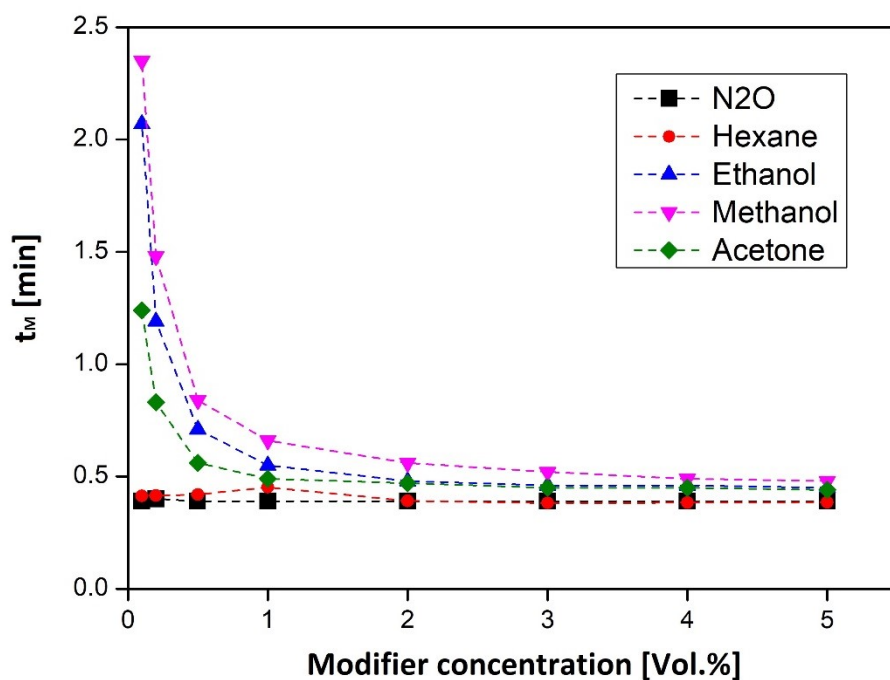


Figure 4.1: Retention time of commonly used hold-up tracers on SIL-100 [90]. SFC conditions: 200 bar, 40 °C, injection volume 2 μ L, flow rate 2 mL/min. The dashed lines were plotted to guide the eye.

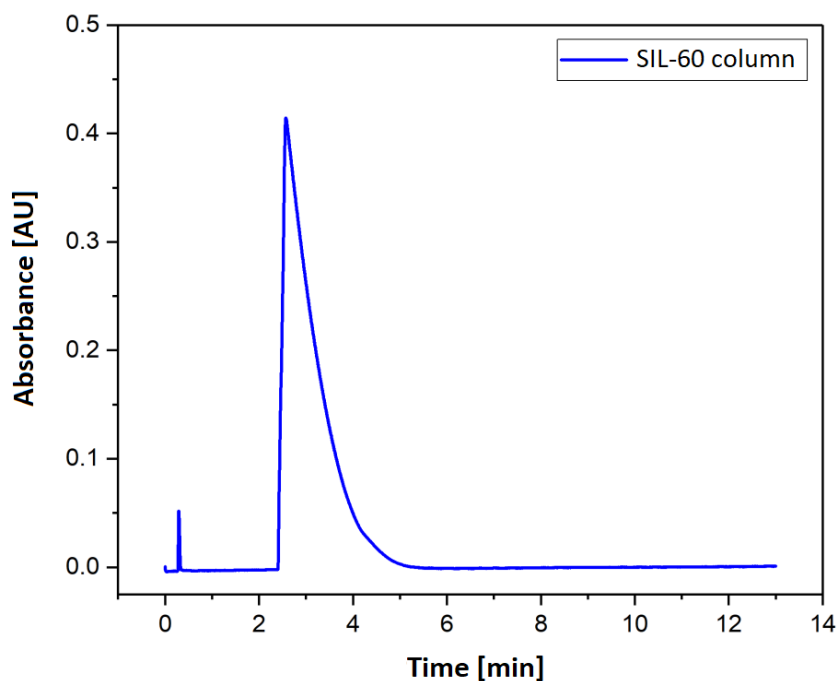


Figure 4.2: Chromatogram recorded on injection of a 2 μ L sample of N₂O/methanol solution on the SIL-60 column. The first peak corresponds to N₂O, the second one is the elution peak of methanol, which exhibits strong tailing on silica gel stationary phase. (SFC condition: 200 bar, 60 °C, injection volume 2 μ L, flow rate 2.0 mL/min, 100% CO₂, UV 195 nm).

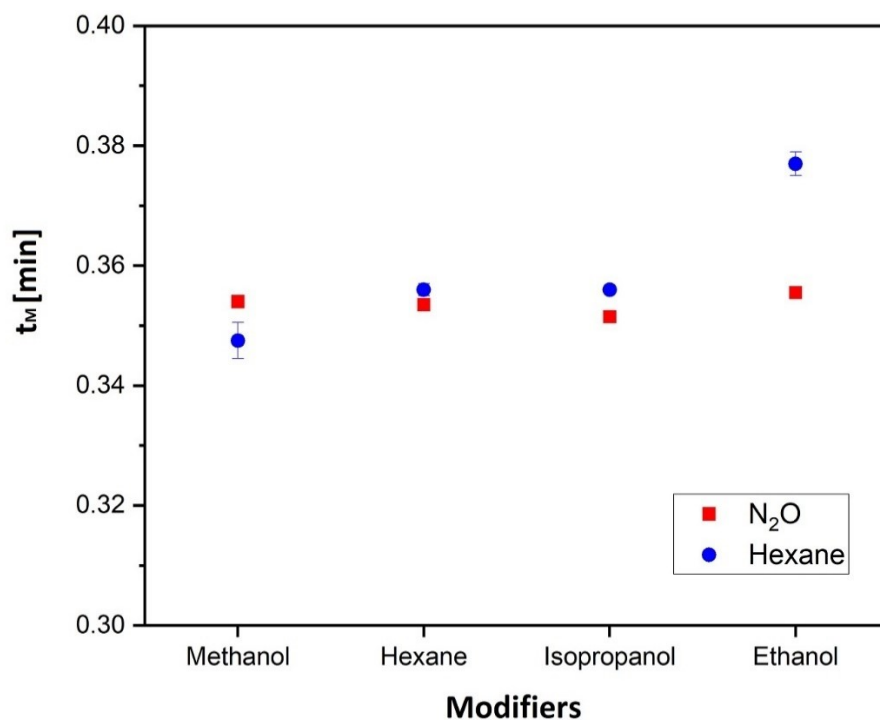


Figure 4.3: Retention time of nitrous oxide and hexane for four different modifiers, 5 vol.% in CO₂. Stationary phase: SIL-100; chromatographic conditions: 200 bar, 40 °C, injection volume 2 µL, flow rate 2 mL/min.

4.2 Working region

In supercritical fluid chromatography, carbon dioxide is the most widely used fluid due to its low critical temperature (T_c) and pressure (p_c) of 30.98 °C and 73.77 bar [24], respectively. Due to the limited solvation power of neat CO₂, most analyses of polar solutes are carried out with a mixture of CO₂ and modifier, which is referred to as the modifier. The addition of modifier favors the solute solubility in the mobile phase, however, it leads to the shift of the critical values (pressure and temperature) of the mixture. In case of methanol, it has a critical temperature of 239.6 °C and a critical pressure of 81.20 bar [91]. The addition of methanol to CO₂ leads to gradual increase of critical temperature of the binary mixture with methanol fraction from 0 to 100%. While the critical pressure at first increases, then decreases with the methanol fraction, reaching a maximum value at around 35 to 40% methanol, as is shown in Figure 4.4. For example, the critical temperature of the mixture reaches 135 °C when mass fraction of methanol is 30% [15], whereas the critical pressure increases to 168 bar.

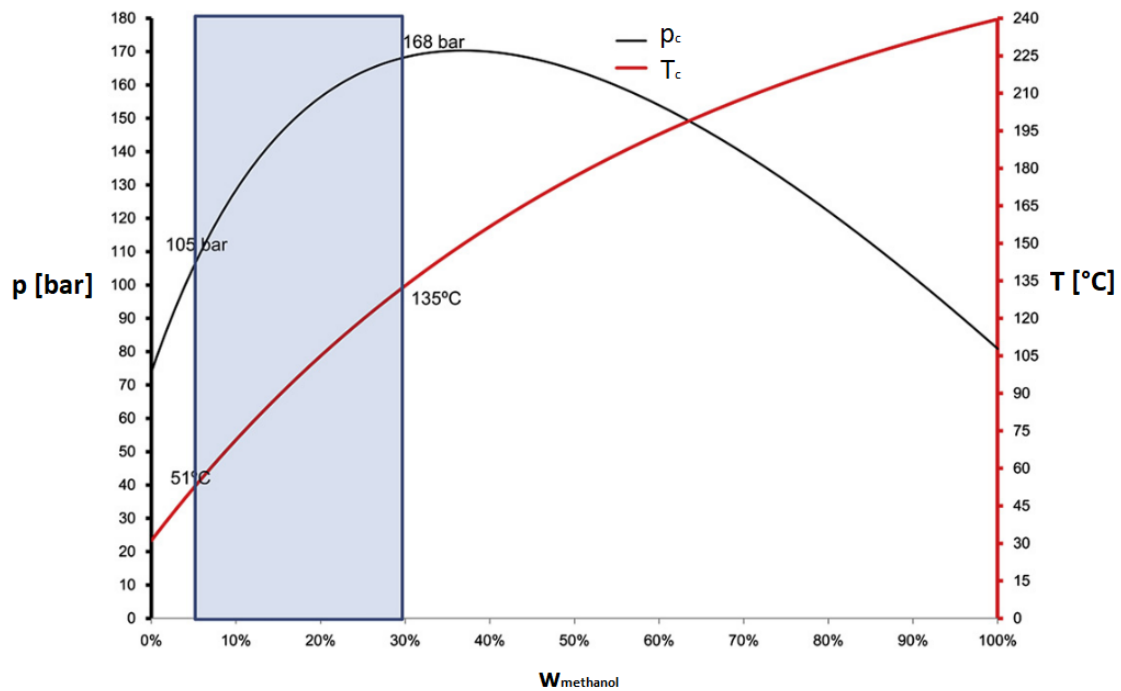


Figure 4.4: Relationship between the calculated critical pressure (P_c), temperature (T_c), and mass fraction of methanol (w_{methanol}) of a CO_2 /methanol mixture [17]. The critical temperature keeps on increasing from 0 to 100% methanol, while critical pressure first increases then decreases with increase of methanol percentage reaching a maximum at around 35-40% methanol. The box shows a typical experimental range of methanol as modifier (5-30%). Figure obtained from Saito [15].

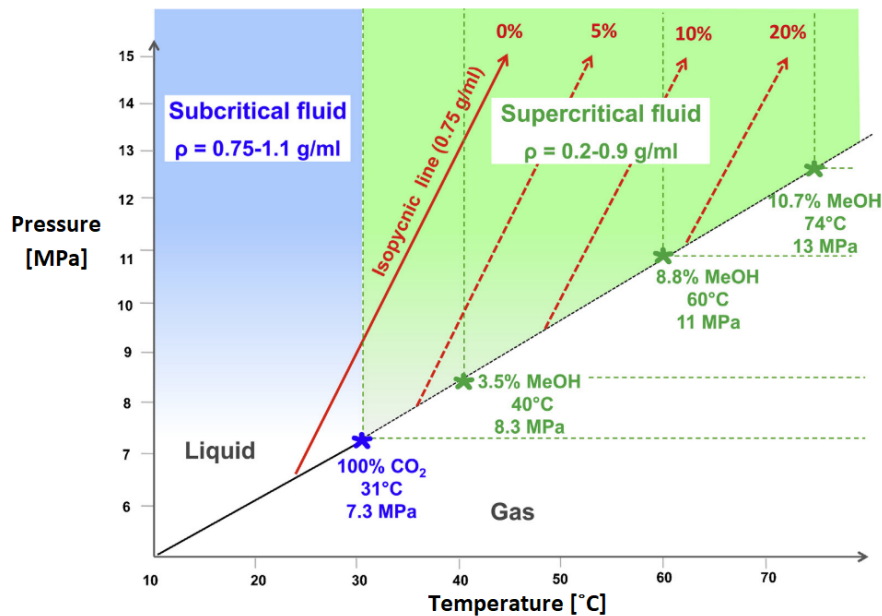


Figure 4.5: A $p - T$ phase diagram of pure CO_2 (in blue) or CO_2 /methanol mixture at different proportions (in green). Isopycnic lines (equal density) at $\rho = 0.75\text{g/mL}$ of CO_2 or mixture of CO_2 -methanol at different compositions were shown. Critical temperature (T_c) and critical pressure (p_c) values were denoted under each composition. Figure obtained from Lesellier et al. [17].

In practice, such a high temperature condition (i.e. $T > T_c$) is usually not full-filled, as the column temperature is set much lower than the critical temperature. Thus, strictly speaking, the mobile phase is actually not in the “supercritical” state but the “subcritical” state [17]. The pure CO₂ or CO₂ with a low fraction of methanol can be supercritical, but a slight higher fraction of methanol in the CO₂ can lead to the transition from super- to subcritical conditions [92], shown in Figure 4.5. If the mixture of CO₂ and methanol is in subcritical condition, phase separation could possibly happen, especially when working pressure is low. One phase contains predominantly methanol with a little CO₂ while the other phase is predominantly CO₂ containing a little methanol. One phase tends to be denser than the other [92]. Phase separation in SFC is generally not desirable, as it leads to broadened, split, and irregular peaks, also excessive noise on the baseline and irreproducible retention [93].

To keep the mixture single-phase and avoid phase separation, chromatographers usually maintained the system pressure sufficiently high [28]. In short, the mobile phase is a liquid (subcritical) or supercritical mixture of CO₂ and methanol. The transition from super- to subcritical region is not accompanied by a phase transition when the operating pressure is sufficiently high [92]. For example, a pressure in excess of approximately 156 bar, produces a one-phase mixture for temperature (T) ≤ 100 °C over the entire composition range for CO₂/methanol mixtures. For example, to ensure a single liquid phase at 25 °C, the minimum operating pressure is as low as 63.8 bar [28].

In this study, the column temperature was in the range from 30 to 60 °C, the column back pressure was maintained at 120 to 240 bar and the mole fractions of methanol in the mobile phase ($x_{methanol}$) vary from 0 to 0.33. In order to confirm whether the working region of this study is within the single-phase region, a figure which includes experimental conditions and phase transition information is used.

Figure 4.6 shows a three-dimensional phase diagram illustrating the single-phase region for the CO₂/methanol mixtures at 25 – 100 °C. The region above the surface is either a single-phase liquid or supercritical fluid, while below the surface, a two-phase liquid-vapor region and a single-phase vapor region at very low pressures are expected [28]. The surface was plotted from literature data of the $p - T - x_{CO_2}$ vapor-

liquid equilibrium [94], i.e., dew points, bubble points and critical points at different compositions. The equilibrium data were experimentally determined by slowly depressurizing the single-phase mixture at desired temperature, until a phase transition occurred. During the experiment, one can observe two different patterns of phase transition: at dew points, the dew was observed flowing down and the level of the lower phase increased, whereas at bubble point, bubbles were ascending and the level of the lower phase decreased [94]. The critical point was estimated using two adjacent dew and bubble points. As can be seen from the figure, the working region of experiments (red layers) is situated above the surface and thus in the single-phase region.

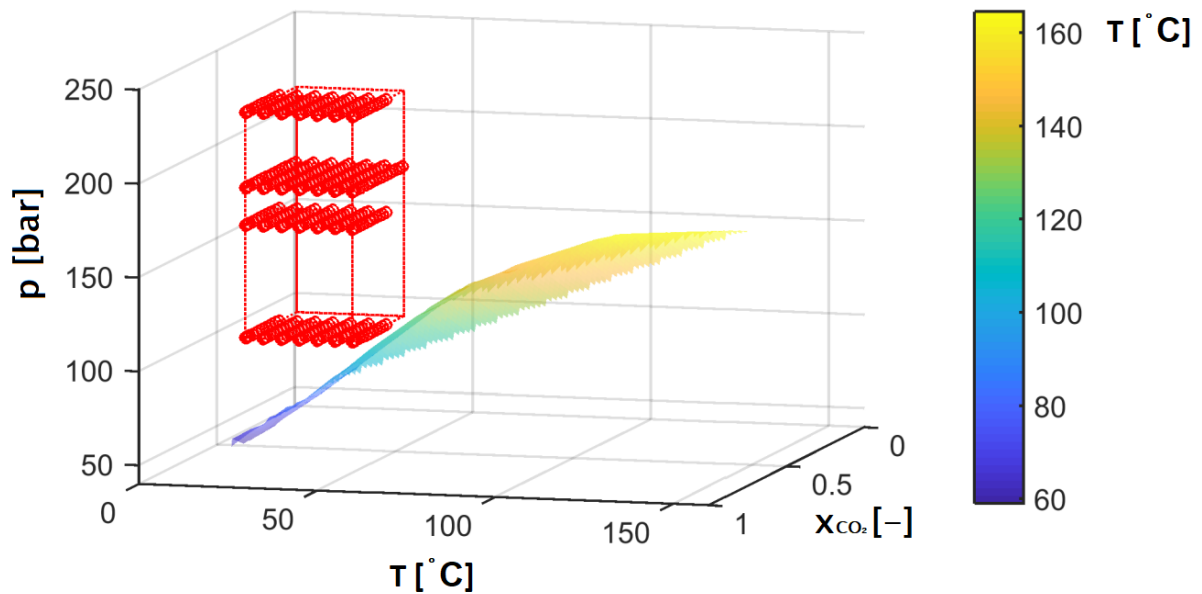


Figure 4.6: Three-dimensional plot of methanol/CO₂ vapor-liquid phase behaviors as a function of p - T - x_{CO_2} (CO₂ mole fraction). The region above the surface is the single phase. The working region of experiments (box in the figure) is situated above the surface and thus in the single-phase region. Figure plotted from data obtained by Yeo et al. [94].

4.3 Stability of columns

Another crucial aspect is the reproducibility of retention factors. For many custom packed columns, a drift of the retention factors was observed, which makes it almost impossible to accrue reliable data. However, the stabilization for 12 to 24 hours in CO₂ flow (200 bar, 40 °C, 2 mL/min) was found to remedy this problem. After this stabilization procedure, the retention of N₂O was further tracked in a temperature range from 40 to 85 °C over a period of 48 hours for each column. As illustrated in Figure 4.7, the retention times of N₂O, t_M , was measured at 40 °C at the beginning of the stability test. The t_M was measured again after the column temperature was raised to a higher temperature and stabilized for 4.5 hours and measured once more after the column temperature was changed back to 40 °C and stabilized for 4.5 hours. This procedure was repeated at 50 °C, 60 °C, 70 °C, 80 °C and 85 °C. No changes of the t_M at 40 °C were observed on both Kromasil and aerogel columns. Thus, the stabilization procedure was applied to all columns to guarantee reproducibility. Another observation from the stability test is that the t_M decreases as the temperature increases. This is because the decrease in density leads to the increase of the volumetric flow rate of CO₂, \dot{V}_{CO_2} . \dot{V}_{CO_2} is constant at the CO₂ pump head at a fixed temperature of 4 °C but increases in the column at increased temperatures.

Problems with reproducibility may arise not only from the changes in the packed bed but also due to chemical reaction between mobile and stationary phases. Although alcohols dissolved in sc-CO₂ are considered to be less reactive towards silanol groups than for instance towards silanes [95], reactions with alcohols take place in the gas phase [96]. Therefore, a special care should be taken to ensure chemical integrity of the surface throughout the characterization by inverse SFC.

Fourier transform infrared spectroscopy (FTIR) characterization of the stationary phases was performed to confirm if any chemical modification of the silicas take place over time. For that, samples of the stationary phase were taken every 30 minutes from the column intentionally operated at high temperatures (60 to 90 °C) and high modifier concentrations (10 and 20 vol.%). Only minor changes were

detected at characteristic 1381 and 2980 cm^{-1} wavelengths confirming chemical stability against high modifier concentration (seen in Figure 4.8).

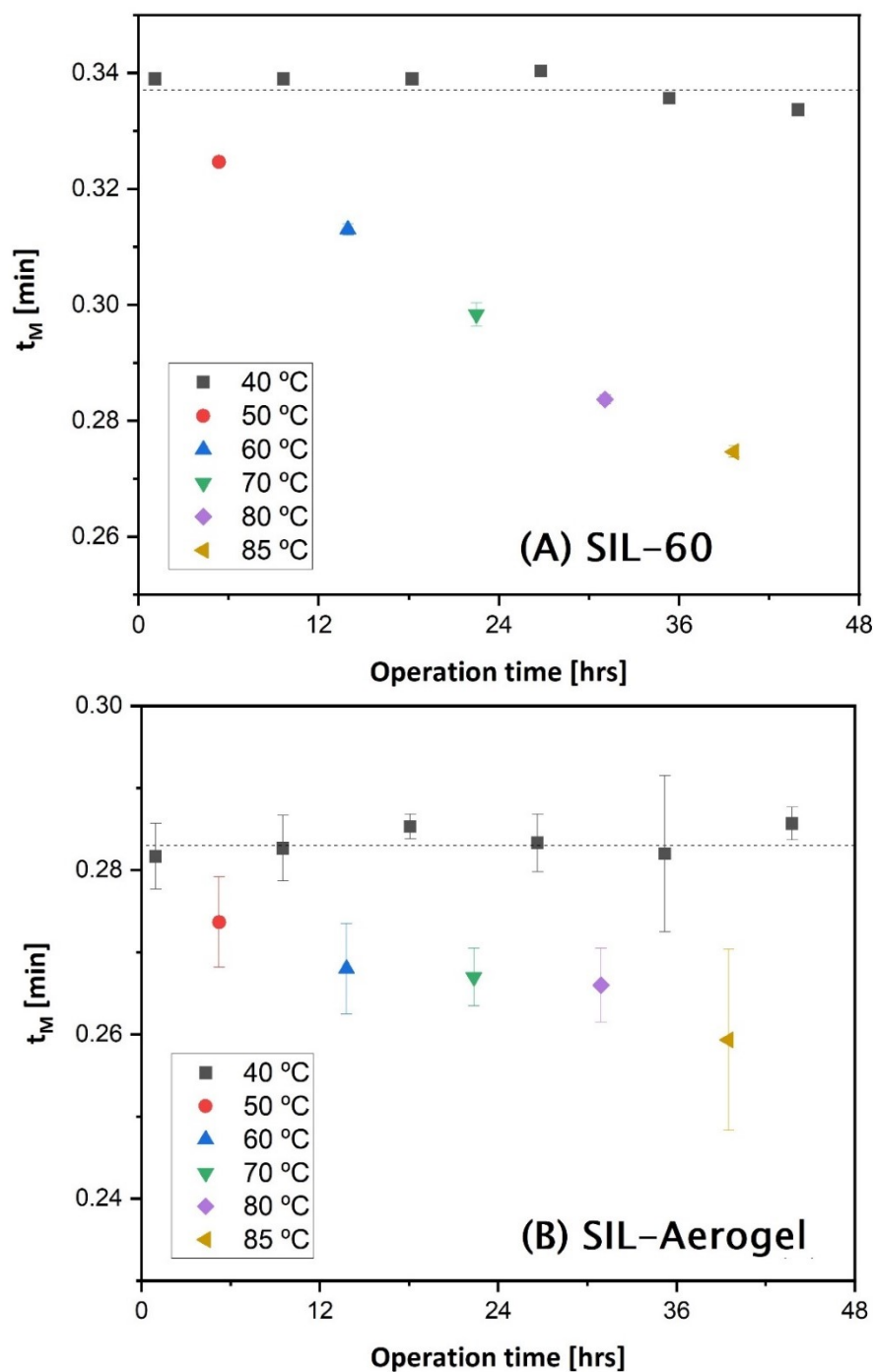


Figure 4.7: Retention time of nitrous oxide at various temperatures. The column was stabilized at each temperature for 4 hours and a half. Within this time, 3 measurements were carried out for each temperature in order to see the stability of the column at a certain temperature. Stationary phases: (A)SIL-60, (B)SIL-Aerogel; chromatographic conditions: 200 bar, 10 vol.% methanol, injection volume 2 μL , flow rate 2 mL/min.

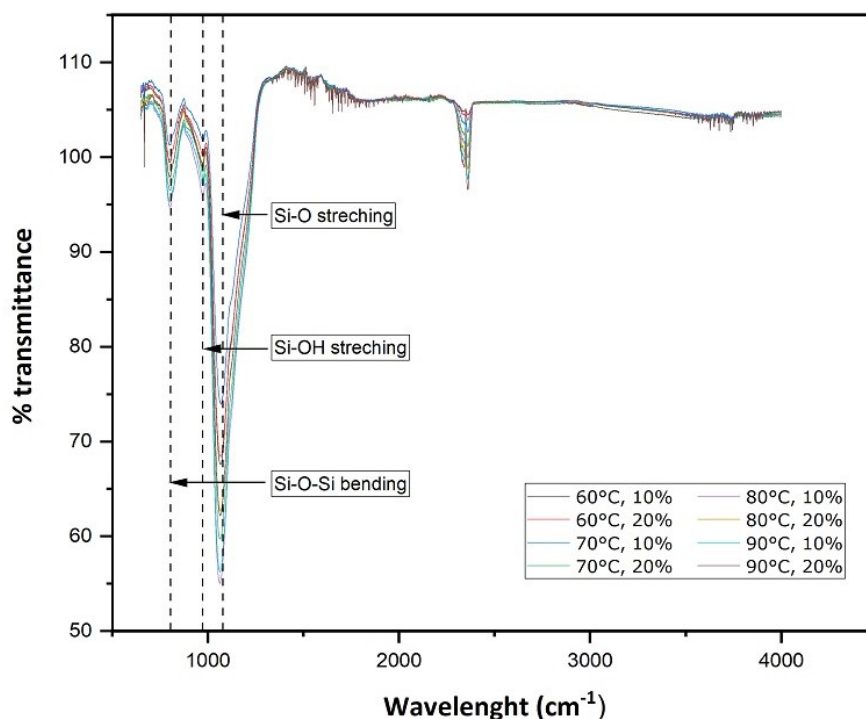


Figure 4.8: FTIR spectra of SIL-60 treated at 60 to 90 °C and 10 and 20 vol.% methanol in sc-CO₂ (200 bar, flow rate 2 mL/min). The column was stabilized for 30 minutes at each condition before taking the sample. The peaks at 810 cm⁻¹, 960 cm⁻¹ and 1100 cm⁻¹ are ascribed to Si-O-Si bending, Si-OH stretching and Si-O stretching vibration respectively. The affected peaks at 2400 cm⁻¹ are most probably influenced by the measurement technique, which is the degree of compression of the solid sample.

5 Analysis of Modifier Adsorption

Modifier adsorption and covering the active sites on the stationary phase is one of the major factors influencing the retention of any molecules on the stationary phases. Methanol was applied as the modifier throughout this study. Thus, the study on methanol adsorption is discussed in this chapter.

5.1 Isotherm models

5.1.1 Experimental

Adsorption isotherms were measured by frontal analysis in this work. Detailed procedures are described in section 3.3. The experimental data of methanol on four silica filled columns were preliminarily fitted with three different adsorption isotherm models: the Langmuir model, the extended liquid-solid BET model and the bi-Langmuir model. An example of the goodness of fit of the three models to the experimental data can be found in Figure 5.1.

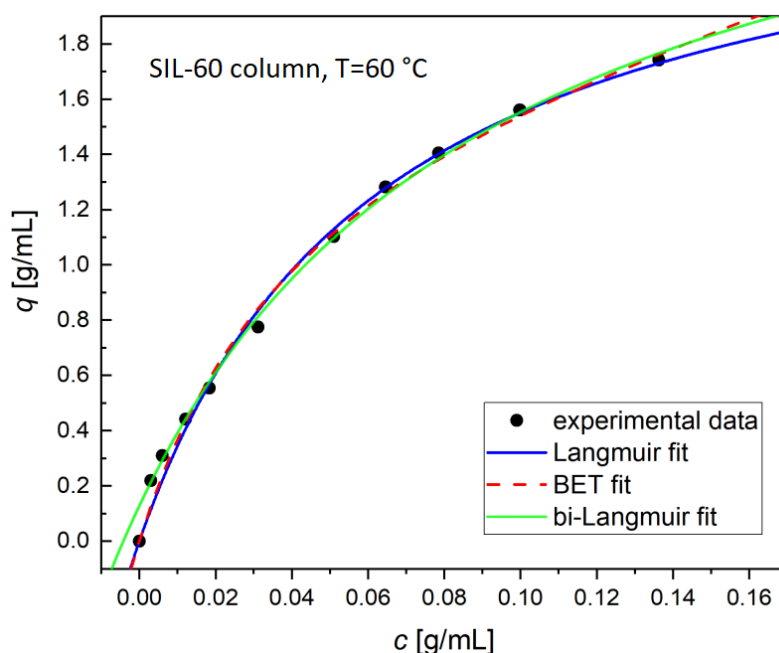


Figure 5.1: Experimental data fitted to the Langmuir, BET and bi-Langmuir model. (Chromatographic condition: stationary phase, silica gel K60 column; mobile phase, CO₂ – methanol, methanol: 0-20% (v/v); column temperature: 60 °C; nominal flow rate, 2.0 mL/min).

As demonstrated in the example, the goodness of fitting with all three models are acceptable. The adj. R^2 s are always higher than 0.99. However, comparing to Langmuir model which has 2 fitting parameters, BET has three and bi-Langmuir has four. To avoid introducing too many fitting parameters, Langmuir model was selected to be further applied for retention model development, details seen in chapter 6.2. The fitting parameters and adj. R^2 s by BET and bi-Langmuir models can be found in Appendix 12.4.

The Langmuir model is the most developed and widely used adsorption isotherm model. It is for homogeneous surfaces on which there are no significant adsorbate-adsorbate interactions. It is given by,

$$q_{mod} = \frac{q_{max}K_{eq,L}C_{mod}}{1 + K_{eq,L}C_{mod}} \quad \text{Eq. 29}$$

where q_{max} represents the maximum amount of modifier molecules adsorbed to the unit volume of the stationary phase (specific saturation capacity, g/mL). Parameter $K_{eq,L}$ (mL/g) is the adsorption equilibrium constant on the solid surface.

Guiochon et al. [87] has pointed out that the Langmuir isotherm equation is derived under the assumption of low mole fraction of the solute ($x_{solute} \ll 1$). To keep the model valid, the equation should be applied at low surface coverage ($\theta < 0.1$). However, most experimental measurements of adsorption isotherms should be carried out at concentration large enough to determine the parameter $K_{eq,L}$ with sufficient accuracy. Further, it is very often observed in practice that, in a wide range of concentrations, the experimental adsorption data are still in good agreement with the Langmuir isotherm. They suggested that the Langmuir model remained a first-choice empirical equation to fit experimental isotherm data, while no physical interpretation of the values for the saturation capacity (q_{max}) should be made.

Applying the Langmuir model to all four silica matrices produces physically reasonable parameters, with high adj. R^2 s. In other words, all isotherms on the four columns are approximately Langmuirian. For silica gel SIL-60 and SIL-100, the adj. R^2 s are higher than 0.97 and 0.98, respectively. The model fits better on the silica SIL-

300 and SIL-Aerogel, having adj. R^2 s higher than 0.99. The fitted parameters of methanol on the four columns can be found in Table 5.1 to Table 5.4.

Table 5.1: Fitted Langmuir parameters to the adsorption isotherm data points of methanol on SIL-60.

$T [^{\circ}\text{C}]$	$q_{\max} [\text{g/mL}]$	$K_{eq,L} [\text{mL/g}]$	Adj. R^2	RSS
30	1.50 ± 0.11	17.4 ± 3.0	0.9778	2.0×10^{-2}
35	1.63 ± 0.11	17.7 ± 2.9	0.9801	2.1×10^{-2}
40	1.74 ± 0.13	16.5 ± 2.7	0.9815	2.2×10^{-2}
45	1.84 ± 0.15	15.3 ± 2.6	0.9811	2.4×10^{-2}
50	2.03 ± 0.15	16.1 ± 2.5	0.9835	2.6×10^{-2}
55	2.34 ± 0.16	14.7 ± 2.1	0.9873	2.5×10^{-2}
60	2.54 ± 0.15	15.7 ± 2.0	0.9897	2.5×10^{-2}

Table 5.2: Fitted Langmuir parameters to the adsorption isotherm data points of methanol on SIL-100.

$T [^{\circ}\text{C}]$	$q_{\max} [\text{g/mL}]$	$K_{eq,L} [\text{mL/g}]$	Adj. R^2	RSS
30	1.30 ± 0.09	12.1 ± 1.7	0.9887	7.7×10^{-3}
35	1.36 ± 0.09	11.3 ± 1.5	0.9897	7.2×10^{-3}
40	1.38 ± 0.09	11.2 ± 1.5	0.9898	7.3×10^{-3}
45	1.43 ± 0.09	12.0 ± 1.6	0.9904	7.6×10^{-3}
50	1.53 ± 0.09	11.3 ± 1.3	0.9931	6.1×10^{-3}
55	1.60 ± 0.09	11.3 ± 1.3	0.9938	5.9×10^{-3}
60	1.87 ± 0.11	10.2 ± 1.2	0.9943	6.9×10^{-3}

Table 5.3: Fitted Langmuir parameters to the adsorption isotherm data points of methanol on SIL-300.

$T [^{\circ}\text{C}]$	$q_{\max} [\text{g/mL}]$	$K_{eq,L} [\text{mL/g}]$	Adj.R ²	RSS
30	1.54 ± 0.12	4.61 ± 0.54	0.9971	1.3×10^{-3}
35	1.63 ± 0.14	5.06 ± 0.68	0.9958	2.1×10^{-3}
40	1.62 ± 0.14	5.30 ± 0.68	0.9960	2.1×10^{-3}
45	1.89 ± 0.16	4.47 ± 0.56	0.9971	1.7×10^{-3}
50	1.96 ± 0.17	4.46 ± 0.57	0.9970	1.9×10^{-3}
55	2.01 ± 0.16	4.58 ± 0.53	0.9976	1.6×10^{-3}
60	1.84 ± 0.14	5.51 ± 0.64	0.9970	2.2×10^{-4}

Table 5.4: Fitted Langmuir parameters to the adsorption isotherm data points of methanol on SIL-Aerogel.

$T [^{\circ}\text{C}]$	$q_{\max} [\text{g/mL}]$	$K_{eq,L} [\text{mL/g}]$	Adj.R ²	RSS
30	2.25 ± 0.15	7.78 ± 0.90	0.9949	7.8×10^{-3}
35	2.40 ± 0.16	7.25 ± 0.81	0.9956	7.7×10^{-4}
40	2.49 ± 0.16	7.07 ± 0.77	0.9961	7.2×10^{-4}
45	2.63 ± 0.17	6.63 ± 0.70	0.9966	6.4×10^{-4}
50	2.59 ± 0.16	7.01 ± 0.71	0.9968	5.5×10^{-3}
55	2.72 ± 0.16	6.75 ± 0.67	0.9971	5.2×10^{-3}
60	2.78 ± 0.16	6.87 ± 0.66	0.9973	5.1×10^{-3}

Generally, the q_{\max} increases with increasing temperature, while $K_{eq,L}$ decreases with increasing temperature. The former can be explained by the lower solvation power of CO₂, whereas the latter is because the higher temperature does not favor the exothermic processes of adsorption.

It should be noted that in reality the assumptions of the Langmuir model are not always fulfilled, i.e., there are significant adsorbate-adsorbate or adsorbate-solvent

interactions, or the surface is not homogeneous and has different types of absorptive sites.

5.1.2 Comparison with literature

Not much literature was published on the adsorption of methanol on silica gel in sc-CO₂. Kern et al. reported the results for the same stationary phase SIL-100 at almost the same pressure and temperature but measured by a different method and equipment [97]. It determined the adsorption isotherm of methanol using frontal analysis by characteristic points (FACP) method on a different SFC system. For the convenience of comparison, the value of loading at methanol concentration 0.032 g/mL in “mmol/mg” was converted to a value in “g/mL” with the mass and porosity of SIL-100 and marked by dashed lines in Figure 5.2. It is found that the loading determined in this work is larger than from Kern et al. Although the adsorption isotherm should be independent of the method and equipment taken, it is hard to achieve same values when the system is very different, and it is difficult to argue which one is more accurate. Looking at Eq. 16, several critical parameters require precise measurements for an accurate analysis. One of the parameters is the total porosity, ε_{tot} . The ε_{tot} of SIL-100 column in this work is 0.814 while it is 0.775 by Kern et al. The difference is small and is unlikely to be the cause of the big deviation on loadings. Another two critical parameters are the flow rate, \dot{V}_{avg} , and the concentration of methanol, c_n . They are both calculated from the volumetric flow rate of the two pumps: the CO₂ pump, and the methanol pump. There is no secondary confirmation of the flow rate of both pumps other than the set values of the pump. The difference between the actual and set values was neglected in this study based on the result of another study with the same model of equipment by Forss et al. [83]. It was shown that the modifier fraction differences were below 1.3 %. However, there can be differences between individual equipment and the only way to confirm it is to incorporate a mass flow meter, which should be considered in the future work.

Results from two other literatures are also shown in Figure 5.2, in which experiments were performed in different pressure conditions but with same model of equipment as this study. Study from Vajda et al. [98], (c) in Figure 5.2, shows the adsorption isotherm of methanol determined using the same method (frontal analysis) and same

equipment (Waters UPC² supercritical fluid chromatograph), but at a lower pressure (145 bar). However, the study applied a commercial silica-packed column, 6 mm × 100 mm Waters Viridis SFC column. Although the particle size and the specific surface area of the silica packed in this column is very similar to SIL-100, we know little of its surface chemistry. Although we cannot directly compare the result from this work to that of Vajda et al. due to the lack of information of the silica, we see the two results are in the same magnitude. Similar situation applies to the other study from the same group, Vajda et al. [99], (d) in Figure 5.2.

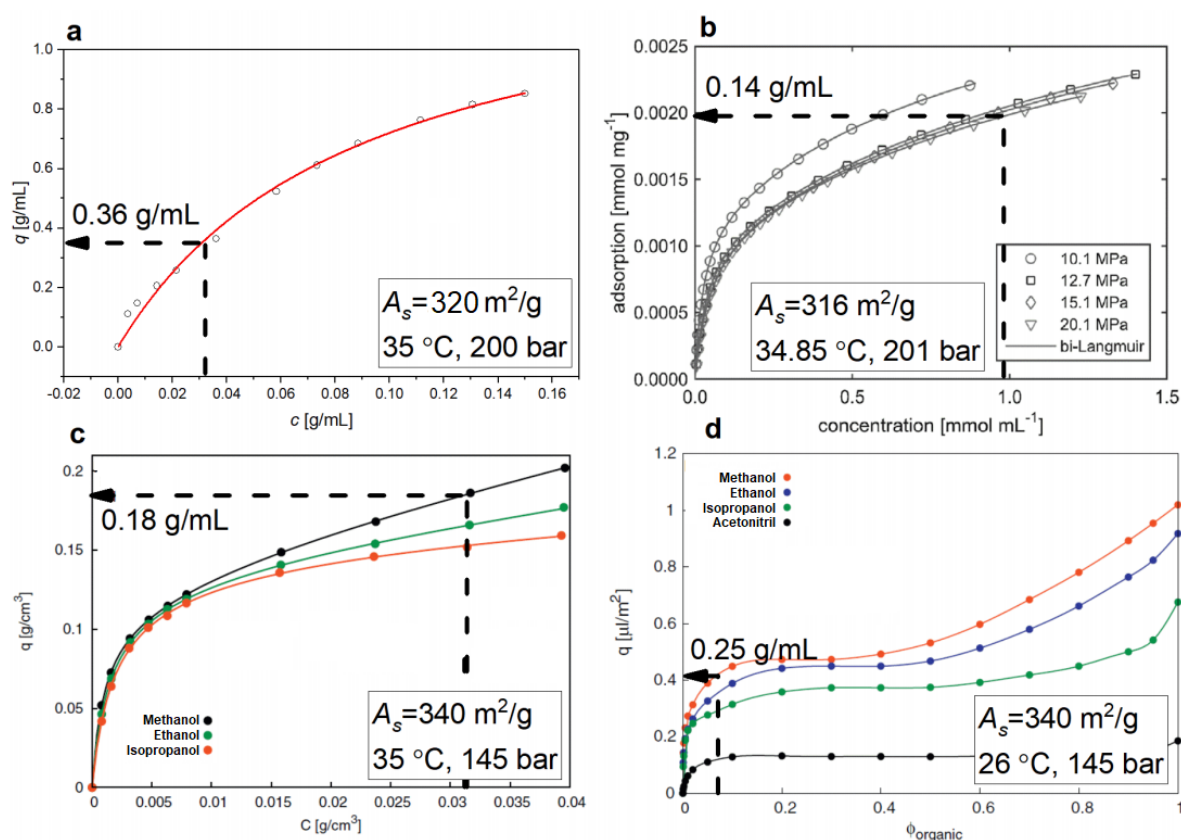


Figure 5.2: Comparison of the methanol adsorption on silica gel in (a) this study with (b) Kern et al. [97] (same stationary phase, same T and p , different method and different equipment), (c) Vajda et al. [98] (different T and p , same method and same equipment) and (d) Vajda et al. [99] (different conditions, different method and same equipment). The values of loading marked by dashed lines are at the methanol concentration of 0.032 g/mL in liquid phase.

5.2 Temperature and pressure influence

5.2.1 Temperature

As shown in Figure 5.3, the loading of methanol (q) on the stationary phase increases with increasing concentration of methanol (c) in the mobile phase. In the entire methanol concentration range investigated, the isotherms on four silica matrices are all concave, which indicates that the amount of methanol adsorbed at equilibrium (q) increases less rapidly than the concentration in the mobile phase (c). Besides, the loading of methanol was found to increase with increasing temperature, which can be explained based on solvation power of the supercritical CO_2 .

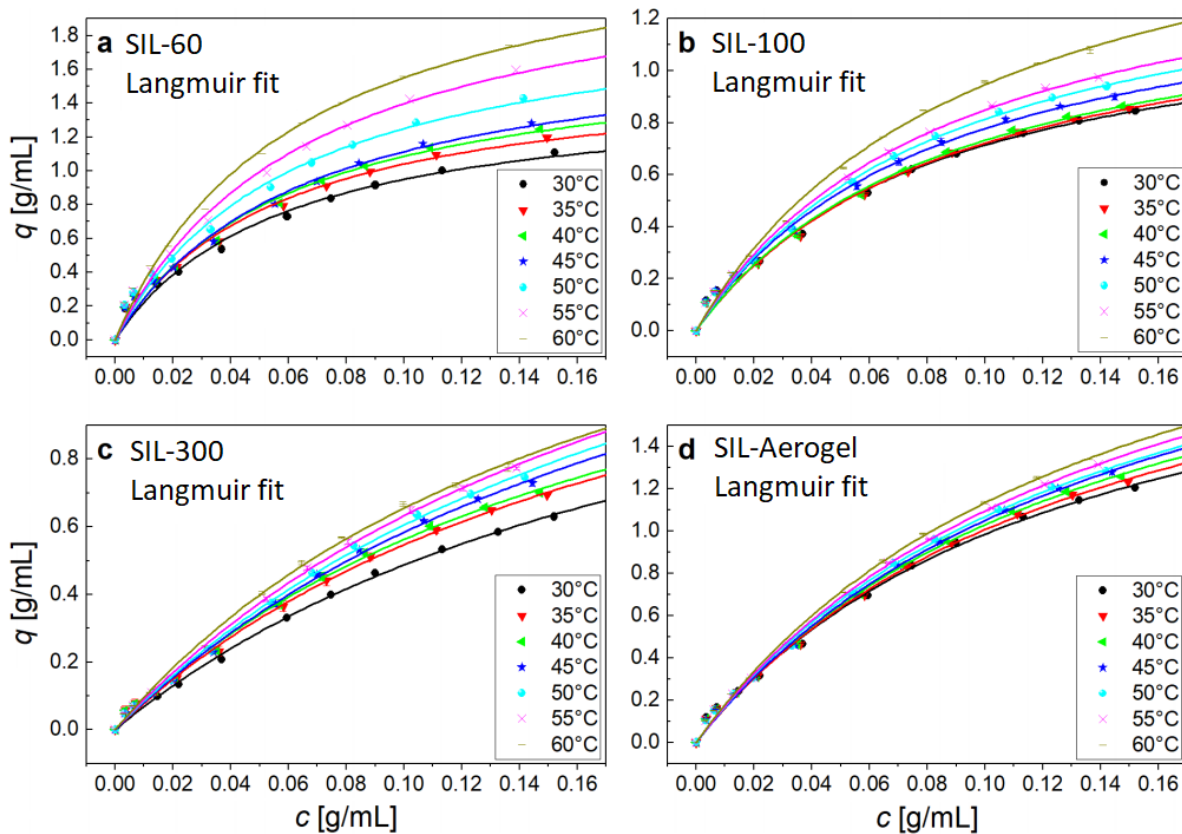


Figure 5.3: Adsorption isotherms of methanol on four silica matrices at temperature from 30 to 60°C, under a column back pressure of 200 bar.

The solvation power (or solubilizing power, elution power) of a supercritical fluid is related to its capacity for specific intermolecular interactions and its density [100]. It can be expressed in terms of the Hildebrand solubility parameter (δ), which is defined

as the square root of cohesive energy density, i.e., the energy content of the fluid per unit volume relative to the ideal gas state,

$$\delta = \sqrt{-\frac{E_{co}}{v}} \quad \text{Eq. 30}$$

where, E_{co} is the cohesive energy for 1 mol molecules of the fluid, it is a negative quantity as the energy is needed to be transferred from a real fluid into an ideal gas [101]. The “ $-E$ ” is the molar heat of vaporization to a gas at zero pressure, and v is the molar volume [102].

The temperature effect of the loading of methanol on the stationary phase in SFC should be complex, which is the compromise results of three competing phenomena: the solvation power of CO₂, the volatility of the solute (methanol, in this case) and the adsorption ability of the stationary phase surface). As the temperature increases, the density of CO₂ decreases. The lower fluid density results in a lower solvation power. Whereas the volatility of solute increases as temperature increases and the amount of solute dissolved increases when its vapor pressure is increased [100]. Regarding the adsorption ability of the stationary phase, it is assumed to decrease with increasing temperature, because of the exothermic nature of the adsorption. Higher temperature does not favor such an exothermic process. In conclusion, regarding the change of volatility of solute and adsorption ability of surface, a lower temperature is favored for achieving a higher loading. In contrary, regarding the change of solvation power, a higher temperature is favored for a higher loading.

As shown in Figure 5.3, higher loadings have been observed at higher temperature, based on what has been discussed, we can say that the solvation power of CO₂ is the predominant factor affecting the loading of methanol. Figure 5.4 shows the dependence of the Hildebrand solubility parameter (δ) on temperature and pressure for supercritical CO₂. Over the temperature and pressure ranges of this study (30 – 60 °C, 120 – 240 bar, or 118 – 237 atm, respectively), the parameter of CO₂ decreases with increasing temperature at a given pressure, indicating a lower solvation power. Hari Krishnan et al. [103] has analyzed the adsorption of ethyl benzene (C₈H₁₀) on activated carbon from supercritical CO₂ by frontal analysis. They

also reported an increase in loading of ethyl benzene with increasing temperature (from 39.85 to 54.85 °C), at a back pressure of 130 bar. It was explained that at higher temperatures, lower solubility of ethyl benzene resulted in higher loading.

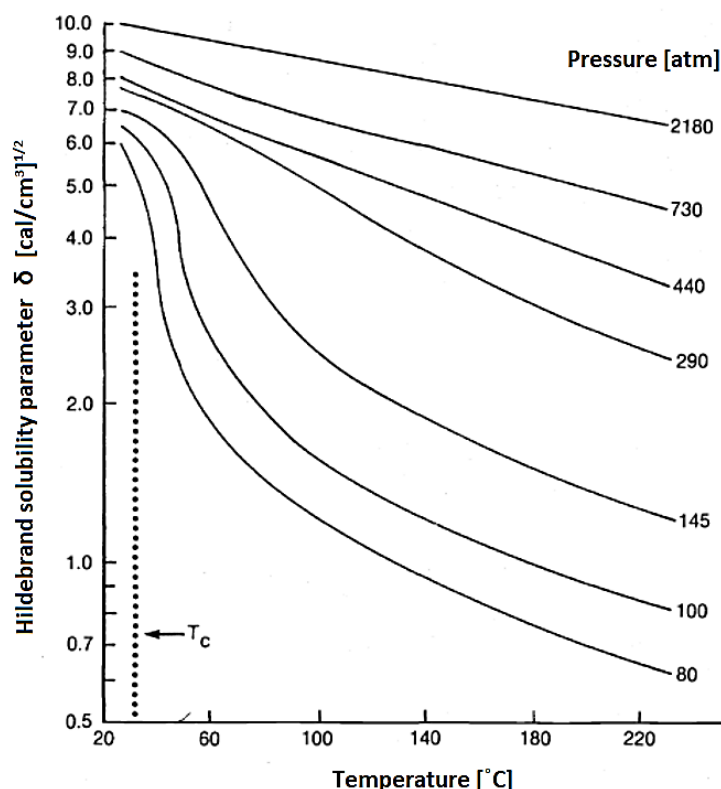


Figure 5.4: Effect of temperature and pressure on the Hildebrand solubility parameter (δ) for supercritical CO₂. The Hildebrand solubility parameter is an indicator of the solvation power of a fluid. A decrease of the parameter indicates a lower solvation power. Figure obtained from Robards et al.[100].

In Figure 5.5, the loading of methanol (q) is found to decrease with mobile phase density. The loading is more subject to the change with mobile phase density at high temperature. However, it is found that the density of mobile phase is not the only factor affecting the loading of methanol. At the same mobile phase density, the loading is still found to be higher at high temperature. The reason is to be clarified. It is noticed from Figure 5.4 that the Hildebrand solubility parameter (δ) decreases drastically at temperature a little higher than the critical temperature (T_c) of CO₂, it could be possible that the drastic decrease of the solvation power leads to a sudden increase in the loading in the temperature range investigated.

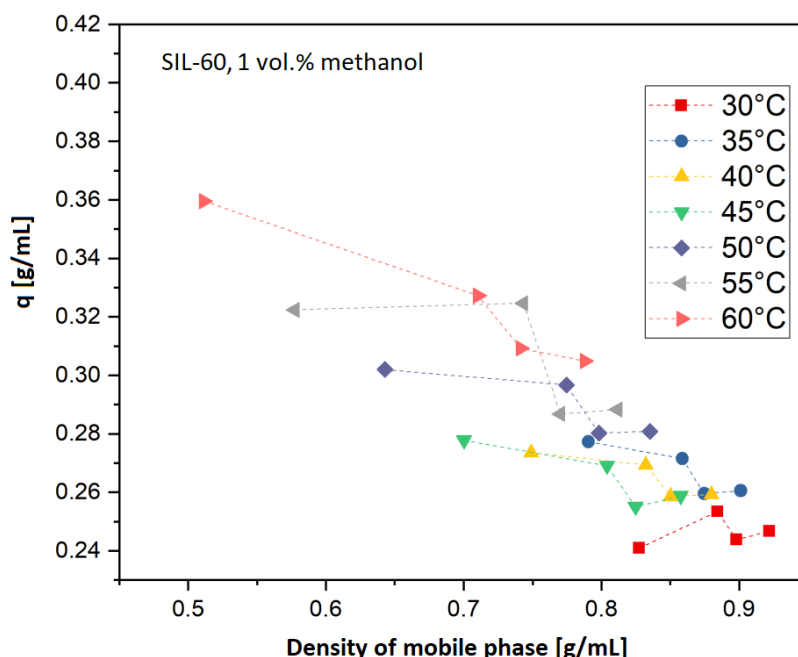


Figure 5.5: Loading of methanol at different densities of mobile phase. The density is varied by varying system back pressure (SFC conditions: flow rate 2 mL/min, methanol concentration at 1 vol.%, back pressure at 120, 180, 200 and 240 bar).

5.2.2 Pressure

As shown in Figure 5.6, the loading of methanol on the stationary phase (q) decreases with increasing column back pressure at a constant column temperature (T). It can be explained by that the fluid density, hence solvation power, increases at higher pressures. Figure 5.4 illustrates that the Hildebrand solubility parameter (δ) of CO_2 increases with increasing operating pressure.

Similar findings in other studies: Lochmüller et al. [104] determined the adsorption isotherms of ethyl acetate ($\text{C}_4\text{H}_8\text{O}_2$) modifier on bare silica stationary phase from supercritical CO_2 at 60 °C, using the peak maxima method. The loading of ethyl acetate stationary phase concentration) was observed to decrease with increasing column pressure from 138 to 276 bar (from 2000 to 4000 psi). Kern et al. [97] has measured the adsorption isotherms of methanol on bare silica stationary phase with the method of frontal analysis by characteristic points at 34.85 °C. The loading of methanol on the stationary phase was also found to decrease with increasing pressure from 101 to 201 bar.

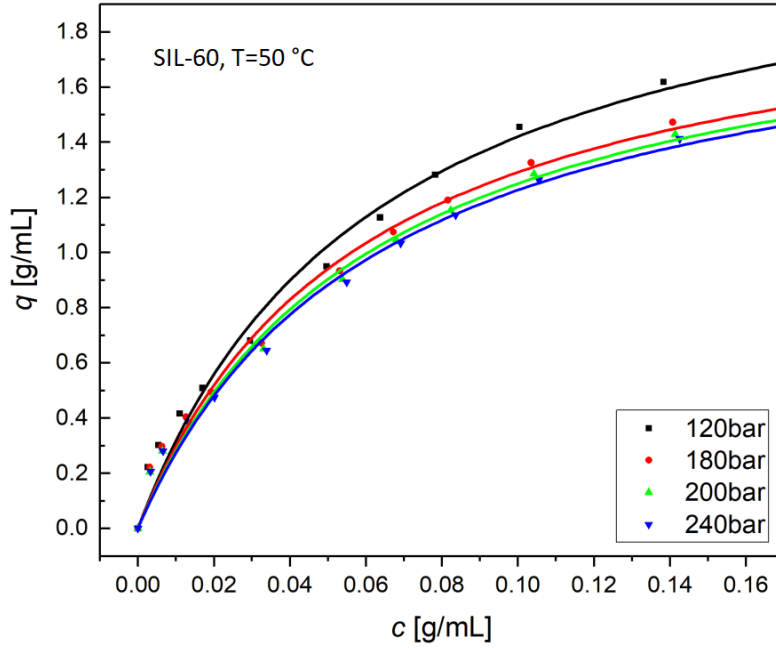


Figure 5.6: Adsorption isotherms of methanol at different column back pressure fitted by Langmuir isotherm. (SFC conditions: SIL-60 column, methanol concentration at 0-20 vol.%, column temperature 50 °C, flow rate 2 mL/min).

5.3 Surface coverage

According to the equation given by Vajda et al. [98], the loading of methanol, i.e., mass concentration of methanol on the stationary phase can be converted to a molar concentration referred to the unit surface area of the stationary phase ($\Gamma \left[\frac{\mu\text{mol}}{\text{m}^2} \right]$),

$$\Gamma \left[\frac{\mu\text{mol}}{\text{m}^2} \right] = \frac{q \text{ [g/mL]}}{M_{\text{modifier}} \text{ [g/mol]} \cdot A_s \text{ [m}^2 \text{ / mL]}} \cdot 10^6 \quad \text{Eq. 31}$$

where M_{modifier} is the molecular weight of the modifier, e.g., methanol. A_s is the specific surface area of the stationary phase. The surface concentrations of methanol Γ_{methanol} calculated based on this formula are given in Figure 5.7 at four different methanol concentrations (5, 10, 15, 20 vol.%) for four silica matrices: SIL-60, SIL-100, SIL-300 and SIL-Aerogel. The surface concentrations of the hydroxyl groups $\Gamma_{\text{-OH}}$, which act as the main active sites, were determined by the thermogravimetric analysis [105] and are shown in Table 5.5.

Table 5.5: Specific surface area (A_s) and surface concentration of hydroxyl groups (Γ_{-OH}) of four silica matrices: SIL-60, SIL-100, SIL-300 and SIL-Aerogel.

Matrix	$A_s[m^2/g]$	$\Gamma_{-OH}[\mu\text{mol}/m^2]$
SIL-60	540	17.8
SIL-100	320	22.2
SIL-300	110	244.5
SIL-Aerogel	858	9.6

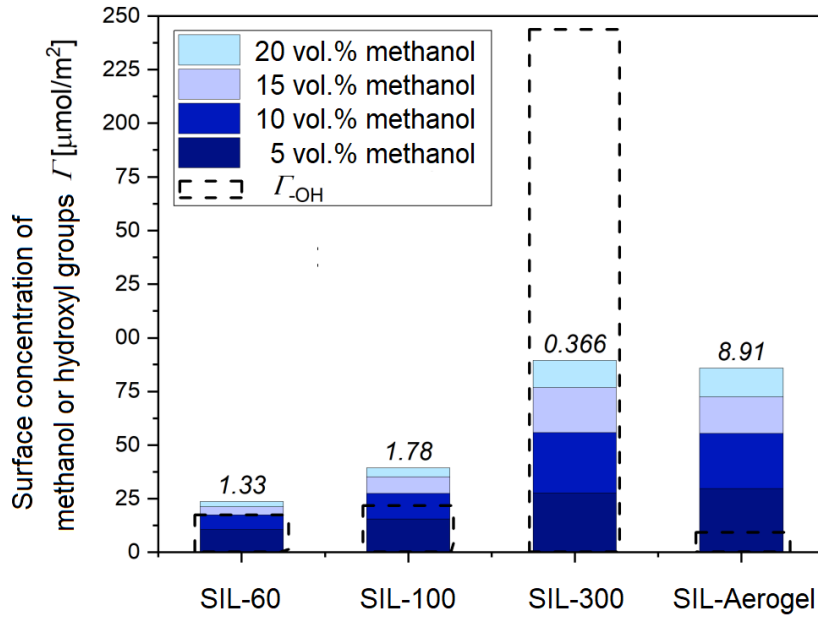


Figure 5.7: Surface concentration of methanol (Γ_{methanol}) and hydroxyl groups (Γ_{-OH}) on the four silica matrices: SIL-60, SIL100, SIL-300 and SIL-Aerogel. Numbers above the columns are the ratios of the surface concentration of methanol molecules (Γ_{methanol}) at 20 vol.% methanol to that of hydroxyl groups (Γ_{-OH}) on silica matrices.

In Figure 5.7, the surface concentration of methanol (Γ_{methanol}) increases for higher methanol concentration in the mobile phase, and the rate of increase slows down at higher concentration. The area at each 5% of methanol increased were different shades of blue. From the figure, the lighter blue area is smaller than the darker blue area, which means that the increase in surface concentration becomes smaller as the methanol concentration goes higher. It is within expectation considering the surface saturation. Based on the random site model [87,106], the molecules select locations on a uniform surface randomly. If a new molecule adsorbs on a trial position and it overlaps with a previously adsorbed molecule, it does not stick to the surface,

otherwise, it is adsorbed. An initially fresh surface can be covered by methanol molecules at a low concentration. The amount of molecules adsorption per unit change of concentration can drop rapidly with increasing surface coverage.

Figure 5.7 also shows that the ratio of surface concentration of methanol to that of hydroxyl groups ($\Gamma_{methanol} : \Gamma_{OH}$) is less than 1 at low fraction of methanol (5 vol.%) but exceeds one at higher methanol fraction (20 vol.%), in the cases of SIL-60 and SIL-100. This result implies monolayer adsorption of methanol molecules at low mobile phase methanol concentration, while double-layer or even multilayer adsorption happens at higher methanol concentration. For SIL-Aerogel, the ratio exceeds 1 at fraction of methanol at 5 vol.%, and continues to increase with methanol fraction, indicating the multilayer adsorption. As for the SIL-300, the ratio is much less than one in the mobile phase concentration range investigated, even at a high methanol fraction up to 20% (v/v), which indicates monolayer adsorption. This can be explained by the exclusion effects [87].

As shown in Figure 5.8, the smaller circles represent the configuration of molecules (assumed as hard spheres) of a certain diameter, while the larger circles represent the exclusion surface, i.e., the area that is inaccessible to the center of an additional sphere. The SIL-300 column has a lowest specific surface area (A_s) of 94 m²/g among three columns (Table 5.5), whereas a much higher surface concentration of hydroxyl groups (Γ_{OH}), up to 244.54 $\mu\text{mol}/\text{m}^2$. Consequently, the exclusion effect should be the most pronounced as the hydroxyl groups crowd together on the surface. The methanol molecules cannot cover the surface completely and only a fraction of the sites can be saturated. The exclusion effect may further hamper the formation of a second layer.

The results above suggest that the Langmuir isotherm model may be applied to the silica gel SIL-300 column, as the model assumes monolayer adsorption. On the other hand, the extended liquid-solid BET model may be better in describing the adsorption behavior on the SIL-60, SIL-100 and SIL-Aerogel since the model is based on the assumption of multilayer adsorption.

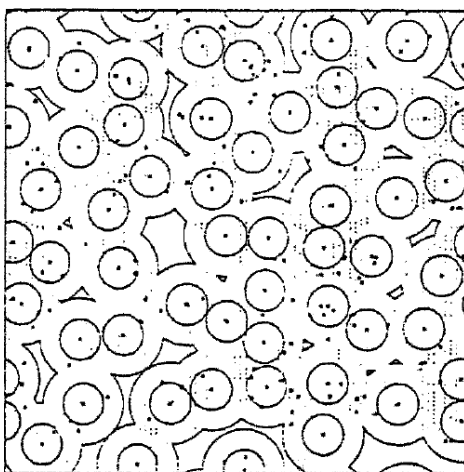


Figure 5.8: Coverage of a uniform surface by hard spheres. The circles show the foot- print of each adsorbed molecule; the area outside the circles is the excluded part of the surface. Figure obtained from [87].

6 Model Development

6.1 Linear solvation energy relationships

The linear solvation energy relationship, LSER, was used in this work to link measurable retention factors with the characteristics of the solute and those of the stationary phase. An introduction of LSER is given in 2.3.3. The most widely applied expression of the LSER model for SFC studies, where five characteristics of the solute and stationary phase are included, is given in Eq. 32.

$$\ln k = c + eE + sS + aA + bB + vV \quad \text{Eq. 32}$$

$$\ln k = c + eE + sS + aA + bB + vV + lL \quad \text{Eq. 33}$$

Each characteristic of any solute is represented by one Abraham descriptor. The introduction of the descriptors are written in section 2.3.3. In addition to this conventional set, a sixth descriptor L was also taken into consideration (Eq. 33). The descriptor L has been used in a recent work from Abraham and Acree to characterize solute-solvent interactions in liquid phases [107]. It is derived from the partition coefficient of compounds between gaseous phase and hexadecane, which indicates the strength of non-specific van der Waals interactions. In literature, the solute descriptor set $\{E, S, A, B, V\}$ was usually applied for gas chromatography while $\{E, S, A, B, L\}$ was for liquid chromatography. However, since supercritical CO_2 possesses properties of both gas and liquid, a set $\{E, S, A, B, V, L\}$ was used in order to take consideration of all major interactions. In this way, the contribution of non-specific cavity formation and van der Waals interactions are complemented. The same methodology was applied in the Goss-modified Abraham models [108], where both V and L appear in one model. The disadvantage of this approach is that it is not possible to distinguish the two contributions represented by V and L from each other due to the high correlation between them [109]. The six solute descriptors $\{E, S, A, B, V, L\}$ of the 17 compounds applied in this study were determined with the Absolv Webboxes program, based on ADME Boxes version 3.5 (Pharma Algorithms, ACD Labs, Toronto, Canada) and shown in Table 6.1. The set of the system constants $\{d = e, s, a, b, v, l\}$ that characterizes the solid phase is conventionally

obtained at fixed operation conditions by regression analysis according to Eq. 33. The logarithm of a retention factor was used as a dependent variable for each regression and the solute descriptors were used as independent variables.

The key factors to apply LSER successfully are reliable data acquisition and robust statistics. In this section, the details of model construction and validation focusing on these two factors are explained step by step. The related considerations and problems are also discussed.

Table 6.1: Solute descriptors used for the LSER analysis [110].

Solute	E	S	A	B	V	L
Toluene	0.58	0.63	0	0.12	0.8573	3.430
Benzene	0.56	0.69	0	0.12	0.7164	2.958
Caffeine	1.48	1.90	0	1.27	1.3632	7.793
Benzoic Acid	0.75	1.08	0.57	0.44	0.9317	4.533
Phenol	0.78	0.90	0.50	0.39	0.7751	3.777
Vanillin	1.02	1.46	0.44	0.76	1.1313	5.860
Naphthalene	1.27	1.02	0	0.17	1.0854	5.332
Anthracene	1.99	1.34	0	0.23	1.4544	7.706
p-Nitrotoluene	0.85	1.20	0	0.21	1.0315	4.911
Nitrobenzene	0.83	1.26	0	0.21	0.8906	4.439
Anisole	0.62	0.79	0	0.33	0.9160	3.803
p-Cresol	0.81	0.85	0.50	0.39	0.9160	4.248
o-Nitrophenol	0.96	1.24	0.11	0.35	0.9493	4.769
Butyl benzoate	0.64	1.05	0	0.46	1.4953	6.022
Ethyl benzoate	0.64	1.04	0	0.45	1.2135	5.033
Pyridine	0.60	0.82	0	0.40	0.6753	3.071
Nicotinamide	1.04	1.68	0.49	0.94	0.9317	5.515

6.1.1 Data acquisition and evaluation

To obtain the retention factors, 17 solutes were injected at various experimental conditions by changing pressure, temperature, and mobile phase composition. Each injection was repeated at least twice. The retention data generated from the injections of 17 solutes at one fixed experimental condition was defined as one data set. Each data set provides a set of dependent variables for one regression. Overall, by varying conditions, 80 data sets were obtained for four stationary phases. One special case was that due to the extreme strong retention of pyridine and nicotinamide on SIL-Aerogel, their precise retention times were not possible to be extracted. Thus, data sets containing 15 solutes were applied for the case of SIL-Aerogel. Preliminary experiments also showed that some polar solutes tend to deviate from linearity suggested by the LSER model. Although the calculation of Mahalanobis' distance (see Appendix 12.2), did not reveal outliers, the regression residuals were shown to be not normally distributed and thus the assumption for ordinary least square regression was violated. Therefore, robust regression was performed using Huber's t estimator with the median absolute deviation scaling (using statsmodels module, version 0.8.0 for Python version 2.7.13). The Huber's estimator introduces a sublinear function that is applied to the least-squares estimation to make the regression less sensitive to heavy-tailed errors and outliers [111].

The data sets for the four non-modified silica stationary phases (SIL-60, SIL-100, SIL-300 and SIL-Aerogel) were applied to develop and validate the robust LSER models. The validated models were further applied to other stationary phases.

6.1.2 Model screening

In the conventional LSER model, significant correlation across the solute descriptors $\{E, S, A, B, V\}$ of the chosen solutes should be avoided to prevent the multicollinearity problem, which results in high standard errors and thus underestimates the statistical significance of the independent descriptors [112].

Significant correlations between the descriptors were found (correlation matrix is presented in Table 6.2). Such correlations in the LSER analysis are reported by

many authors, even for larger sets of solutes indicating that caution must be taken when the LSER model is used [113–115].

Table 6.2: Correlation matrix (Pearson) of the solute descriptors from Table 6.1.

	E	S	A	B	V	L
E	1					
S	0.651	1				
A	−0.058	0.143	1			
B	0.294	0.785	0.318	1		
V	0.593	0.527	−0.249	0.341	1	
L	0.831	0.807	−0.071	0.557	0.893	1

In this work, a system constant resulted from regression is considered statistically not significant if its p-value is larger than 0.05. Based on this criterion, when applying all six descriptors $\{E, S, A, B, V, L\}$ in a model, at least one system constant in each data set was found not significant, which was caused by multicollinearities. The non-significant constants should be eliminated from the analysis. Thus, LSER models with reduced number of descriptors were constructed. These models are composed of a minimal number of significant constants and are called minimal model in the following discussion. Furthermore, the solute descriptors are restricted to be identical across the process parameters and stationary phases.

The minimal models were selected by a screening process. In the screening process, all possible combinations (pairs, triplets and so on) of the six descriptors from the set $\{E, S, A, B, V, L\}$ were applied as independent variable sets in the robust regression procedure described in the previous subsection. Each combination resulted in one set of system constants. The p-values of all resulted system constant sets were examined. In the end, only one model with descriptor A and S fulfilled the criterion for all stationary phases at any experimental conditions, which was that both system constants had p-values smaller than 0.05. The model is written as:

$$\ln k = c + aA + sS \quad \text{Eq. 34}$$

Retention factors calculated by the minimal (AS) model are plotted in Figure 6.1 vs. experimental data (different concentrations of methanol are shown with different symbols).

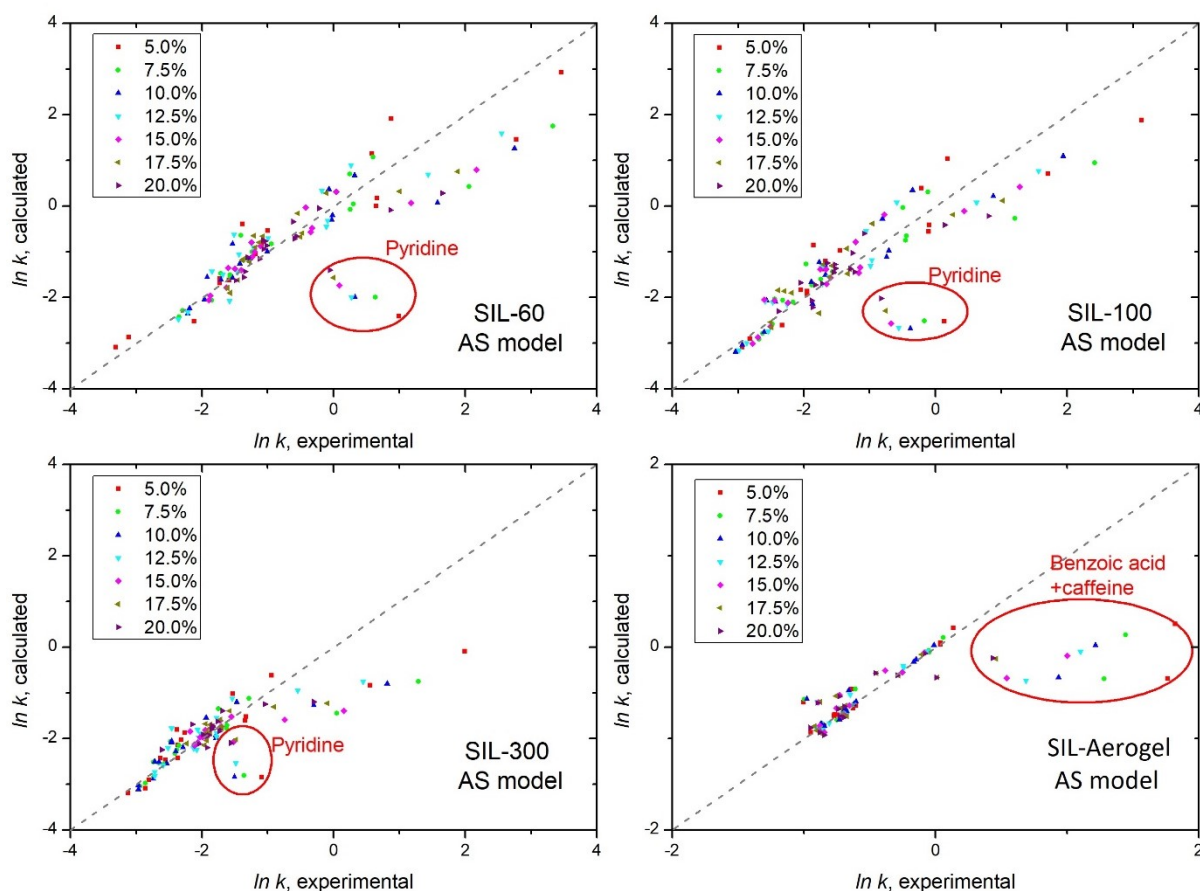


Figure 6.1: Natural logarithms of retention factors for four different columns calculated with the minimal (AS, Eq. 34) model vs. experimental values [90]. SFC conditions: 200 bar, 35 °C, injection volume 2 μ L, flow rate 2 mL/min, modifier (methanol) concentration at 5 to 20 vol.%. Dotted line is the line of the best fit.

It was also observed in this analysis that for each stationary phase a specific model with more than two statistically significant system constants (p-value < 0.05) can be identified: Eq. 35 to Eq. 37. These models were found to be valid for the varying process parameters.

$$\text{SIL-60, SIL-100:} \quad \ln k = c + aA + bB + vV + lL \quad \text{Eq. 35}$$

$$\text{SIL-300:} \quad \ln k = c + bB + vV + lL \quad \text{Eq. 36}$$

$$\text{SIL-Aerogel:} \quad \ln k = c + eE + aA + vV + lL \quad \text{Eq. 37}$$

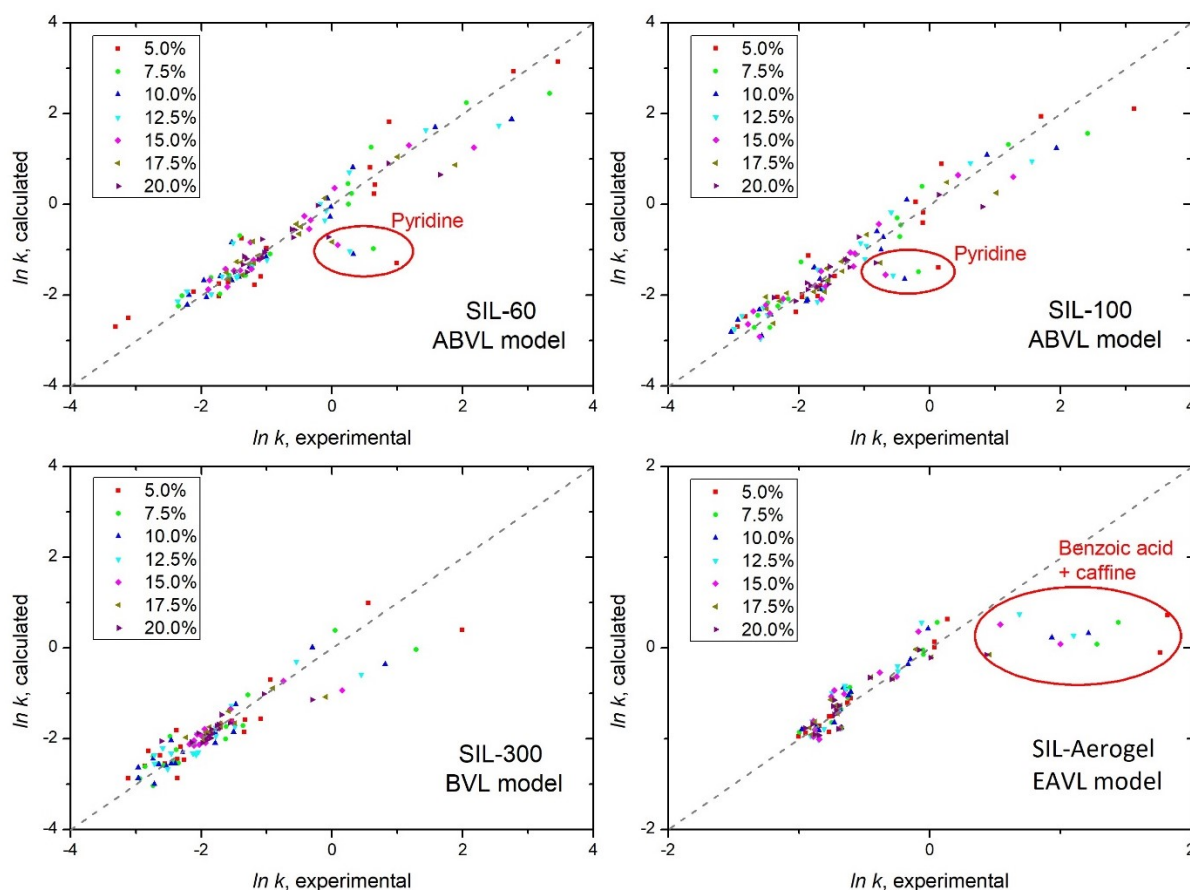


Figure 6.2: Natural logarithms of retention factors for four different columns calculated with the specific models Eq. 35 - Eq. 37 vs. experimental values [90]. SFC conditions: 200 bar, 35 °C, injection volume 2 μ L, flow rate 2 mL/min, modifier (methanol) concentration at 5 to 20 vol.%. Dotted line is the line of the best fit.

These models are referred to as ABVL, BVL and EAVL models for short in this work. Figure 6.2 shows the quality of prediction for these specific models. It is interesting to note that despite chemical similarities, only two materials, SIL-60 and SIL- 100, could be characterized with the same set of system constants, $\{a, b, v, l\}$, which contains both H-bond donor and acceptor ability. Only H-bond acceptance ability b was found to be significant for the phase SIL-300, in contrast to silica aerogel, for which H-bond donation ability a of the surface was statistically significant. Two system constants, v and l , that are associated with dispersion interactions and the gas to hexadecane partition, are common for all silicas. These models have similarities with the Goss-modified Abraham model where both descriptors V and L present [108]. It should be noted that the delineating of the contributions from cavity formation and van der Waals energy is not possible any more [109].

6.1.3 Evaluation of the models

Two observations can be made from Figure 6.1 and Figure 6.2. First, few polar compounds (pyridine for SIL-60, SIL-100 and SIL-300; benzoic acid and caffeine for SIL-Aerogel) significantly deviate from the minimal AS model with a moderate improvement when specific models are employed. Second, the larger the retention factor of a solute, the more pronounced deviations from the LSER models were observed. Since a higher retention is associated with a higher degree of solute/solid interactions, it is evident that the LSER model has a limited applicability for solutes strongly interacting with silica. Important practical aspect is that the ordinary least square multiple linear regression could not be applied due to the not normal distribution of the regression residuals, justifying the choice of the robust regression. One solution for a better fitting is to add extra terms in the model accounting for ionic interactions. Studies have shown that there are certain difficulties using LSER model constructed by only 'neural' descriptor set $\{E, S, A, B, V\}$ to describe the retention of ionisable compounds on stationary phases with high amount of surface silanol groups due to their strong electrostatic interactions [84]. However, there are not generally accepted descriptors in literature for such purpose so far for SFC, thus it is beyond the scope of this work.

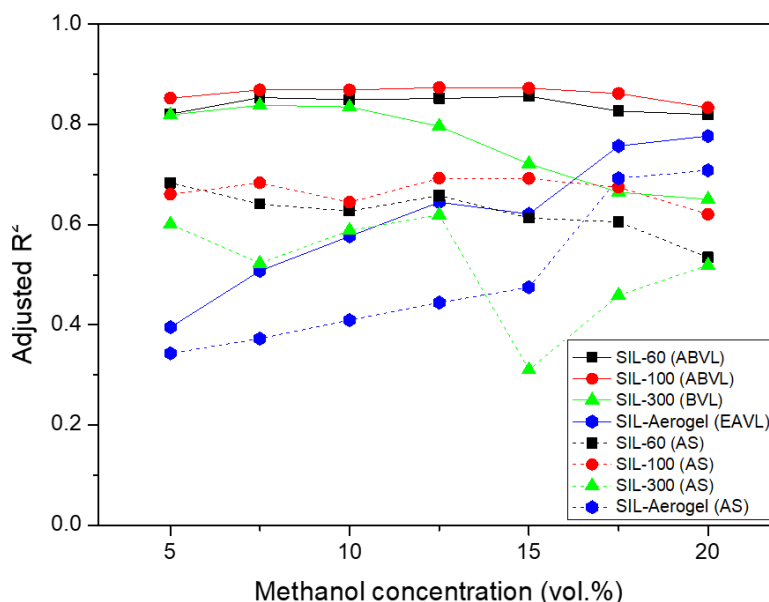


Figure 6.3: Influence of the concentration of modifier on the goodness of fit. SFC conditions: 200 bar, 35 °C, injection volume 2 µL, flow rate 2 mL/min.

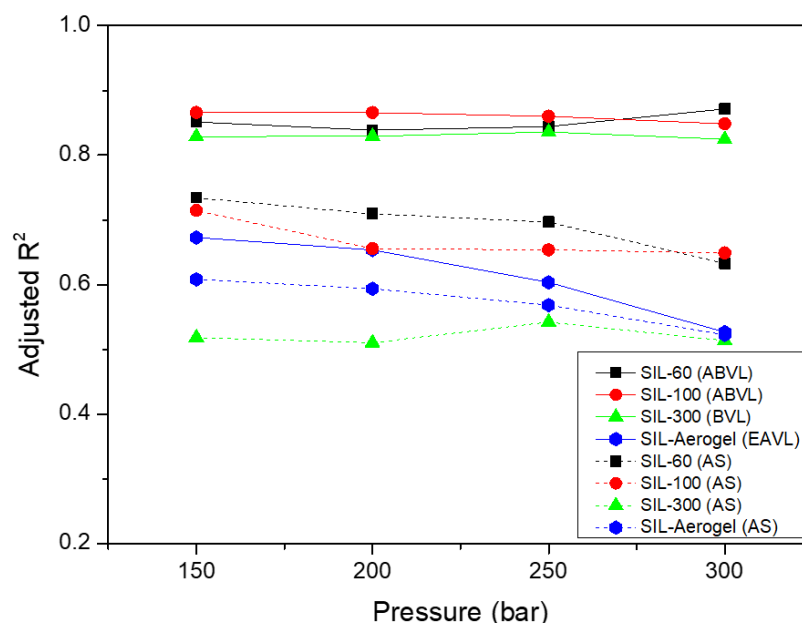


Figure 6.4: Influence of the pressure of modifier on the goodness of fit. SFC conditions: 35°C, 10 vol.% methanol, injection volume 2 μ L, flow rate 2mL/min.

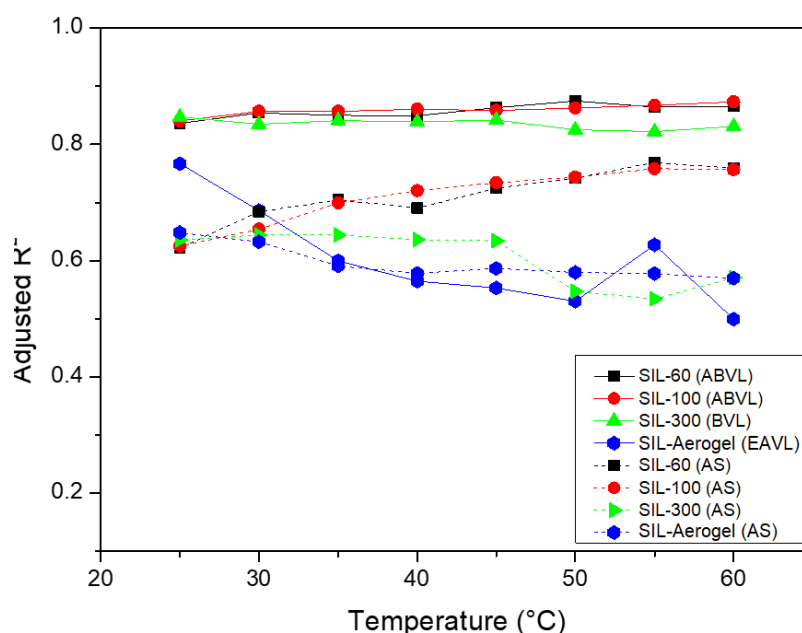


Figure 6.5: Influence of temperature on the goodness of fit. SFC conditions: 200 bar, 5 vol.% methanol, injection volume 2 μ L, flow rate 2 mL/min.

The goodness of fit (adjusted R^2) was also evaluated for the minimal and the specific models at various process parameters. By increasing the modifier concentration from 3 to 20 vol.%, the adjusted R^2 of the AS model for SIL-60 and SIL-100 decreases from 0.66 - 0.68 to 0.53 - 0.62. More pronounced decrease (from 0.64 to 0.52) was observed for SIL-300 while a much better performance was found at higher modifier concentration for silica aerogel (from 0.31 to 0.71) at the same conditions. Both

pressure and temperature have a minor effect on the adjusted R^2 of the minimal AS and the specific models with only one exception: the EAVL model for aerogel performs better at lowest temperature and pressure studied (150 bar and 25 °C), see in Figure 6.3, Figure 6.4 and Figure 6.5 for details. A possible reason for the relatively low quality of the fitting could be the intrinsic features of the LSER model. The solvation parameters applied in the model were originally derived to describe transfer properties between bulk liquid phases and have certain limitations in the case of heterogeneous silica surface where site-specific interactions play an important role [116].

In conclusion, based on the observations and discussions above, both minimal and specific model provides acceptable results for further analysis and are not strongly influenced by operation conditions. The minimal model gives possibilities to compare across all stationary phases, however, by scarifying a certain level of the goodness of fit. Therefore, both of minimal and specific models are applied compensatively for the studies on the solute/solid interactions in this work.

6.2 Retention models

A retention model of chromatography relates the retention factor k of solutes to certain characteristics of the operation system. With a valid retention model the quantification of the interactions between solutes and solid phase by supercritical fluid chromatography (SFC) becomes possible. As introduced in section 2.3.3, there are two prominent classes of retention models reported for SFC: the solvation parameter model and the mixed retention model. The former, which was further developed in chapter 6.1, focuses on the interaction types and strengths, while in this chapter, the latter will be further expanded to give a more comprehensive picture of the interactions. Different from LSER, this class of models should relate the retention factor k to operating conditions such as pressure, temperature, and composition of the mobile phase. Once such a model is obtained, the retention factor can then be related to the distribution coefficient of a solute between mobile phase and stationary phases, Eq. 38, and other thermodynamic quantities [19].

$$k = D \cdot \beta = \frac{c_s}{c_m} \cdot \beta \quad \text{Eq. 38}$$

Here D is the distribution coefficient, c_s and c_m are the concentrations of a solute in stationary and mobile phase and β is the ratio of stationary to mobile phase volumes [29].

It has been confirmed by many previous studies that the modifier concentration c_{mod} has a major effect on the retention of solutes in SFC [35,117–121]. In the current work, two classes of retention models were built based on different assumptions stressing on this effect. With a retention model in hand, which is valid at zero modifier concentration, the theoretical retention factor in pure sc-CO₂, k_0 , can be then extracted from experimental retention data.

6.2.1 Dual influential model (DIM)

The first class of models is based on the idea that modifier influences the solute retention both in the mobile and stationary phases. It is assumed that the ratio of the solute concentration in the mobile phase with modifier c_m over the corresponding

concentration without modifier is proportional to the modifier concentration c_{mod} , Eq. 39. Likewise, the solute concentration in the stationary phase is increased proportional to the modifier loading in the stationary phase, Eq. 40. The loading is assumed to be independent on the presence of the solute and is a function of pressure and temperature of the mobile phase. This class of models is referred to as dual influential models (DIM). Eq. 39 and Eq. 40 are suggested in the spirit of Setschenow equation for salting out effect and log-linear model for solubility in mixed solvents [122]:

$$\lg \frac{c_m}{c_{m,0}} = a c_{mod} \quad \text{Eq. 39}$$

$$\lg \frac{c_s}{c_{s,0}} = b q_{mod} \quad \text{Eq. 40}$$

where $c_{m,0}$ and $c_{s,0}$ are the concentrations of a solute in mobile and stationary phase at zero modifier concentration, c_{mod} is the modifier concentrations in mobile phase, q_{mod} is the loading (mg/mL) of modifier on stationary phase by adsorption and both a and b are empirical parameters (mL/g) that can be regarded as a strength of the modifier effect on the mobile and stationary phases, respectively. When the absolute values of a and b are large, the solute concentrations are more sensitive to small changes of modifier concentration. The values of a and b depend on the nature of solute, mobile and stationary phase and the operational conditions (temperature, pressure).

If now assume the simplest case, namely a linear isotherm for the modifier adsorption equilibrium, gives Eq. 41,

$$q_{mod} = K_{eq,lin} c_{mod} \quad \text{Eq. 41}$$

where $K_{eq,lin}$ is the equilibrium constant of a linear adsorption model. Eq. 38 – Eq. 41 can be rearranged into the following expression for the retention factors k at the modifier concentration c_{mod} and k_0 is the retention factor at $c_{mod} = 0$:

$$\lg k = \lg k_0 - A c_{mod} \quad \text{Eq. 42}$$

where $A = a - bK_{eq,lin}$. The constant A is the overall strength of modifier effect, which accounts for the change in the retention factor from its value k_0 under modifier-free conditions.

Another natural extension is to plug a non-linear adsorption isotherm in the retention model. Several previous works have demonstrated that the adsorption of individual organic solvents in supercritical CO₂ follows Langmuir type isotherm models [97,123–126].

In this study, it is also demonstrated that Langmuir isotherm, Eq. 43, provides an acceptable fit to the experimental data for methanol on silica-based materials (5.1 Isotherm models).

$$q_{mod} = \frac{q_{max}K_{eq,L}c_{mod}}{1 + K_{eq,L}c_{mod}} \quad \text{Eq. 43}$$

The fractional surface coverage θ of the stationary phase by modifier molecules is given as:

$$\theta = \frac{q_{mod}}{q_{max}} = \frac{K_{eq,L}c_{mod}}{1 + K_{eq,L}c_{mod}} \quad \text{Eq. 44}$$

Here $K_{eq,L}$ is the Langmuir equilibrium constant (mg/mL) and q_{max} is the maximum modifier loading (mg/mL) at monolayer coverage. Several $K_{eq,L}$ values were measured as a part of the study (Table 5.1 to Table 5.4).

Eq. 44 together with Eq. 38 - Eq. 40 results in the retention model given by Eq. 45.

$$\lg k = \lg k_0 + B\theta - ac_{mod} \quad \text{Eq. 45}$$

$$\lg k = \lg k_0 + B \frac{K_{eq,L}c_{mod}}{1 + K_{eq,L}c_{mod}} - ac_{mod} \quad \text{Eq. 46}$$

where, $B = bq_{max}$. Eq. 46 gives a concentration-explicit form of Eq. 45 and will be tested for the ability to estimate k_0 values along with linear-DIM model, Eq. 42.

6.2.2 Mixed-retention model (MRM)

Another class of retention models was developed and studied, which is based on the following assumption: the solute retention is due to independent adsorption on two types of active sites of the stationary phase, free adsorption sites as well as the active sites covered by adsorbed modifier, seen in Figure 6.6. Such models are called as mixed retention models (MRM). Experimentally observed retention is a joint effect of the retentions due to both sites.

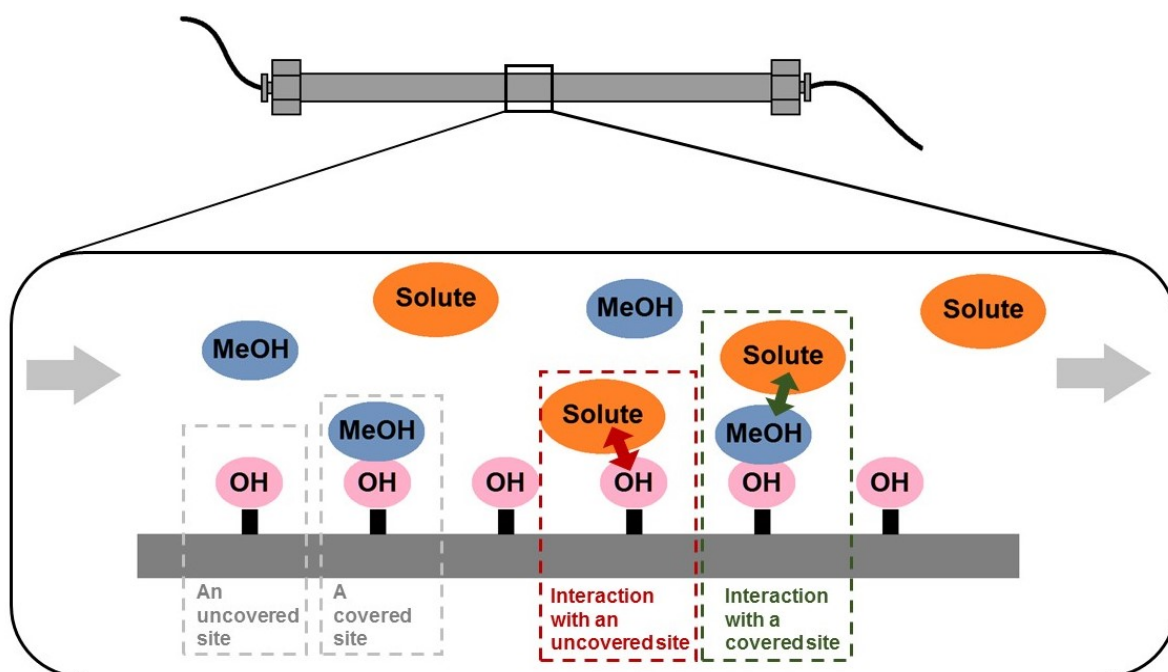


Figure 6.6: A schematic diagram of the mixed retention mechanism in a silica packed column [127]. The interaction in the green dashed line contributes to k_c in Eq. 47 and the interaction in red dashed line contributes to k_0 .

For plain silica, the adsorption sites are silanol groups and methanol molecules adsorbed on the silanols. Since the fraction of the methanol-covered sites is identical to the modifier surface coverage, θ , the retention factor can be expressed by a weighted sum of the retention factor at zero modifier concentration, k_0 , and the retention factor for completely covered surface, k_c (subscript c stands for covered):

$$k = k_0(1 - \theta) + k_c\theta \quad \text{Eq. 47}$$

If rearrange Eq. 47, a linear relation between k and θ is seen:

$$k = (k_c - k_0)\theta + k_0 \quad \text{Eq. 48}$$

However, according to the collected experimental data of k and θ in this work, the linear relationship does not hold for the whole range of modifier concentration. Details will be given later in section 6.2.5. Testing various modifications of Eq. 48 that better fit experimental data, an empirical parameter M is introduced to outweigh the influence of covered active sites: by introducing the term $M c_{mod}$ to the denominator, the influence of modifier on retention factor reduces at higher modifier concentration. The extended MRM is given by:

$$k = \frac{k_0(1 - \theta) + k_c(1 + M)\theta}{1 + M c_{mod}} \quad \text{Eq. 49}$$

The terms $(1 + M)$ in the numerator and M in the denominator are introduced to make the original model by Eq. 47 a special case of the extended model if $M = 0$.

The MRM given by Eq. 49 can also be written in a concentration-explicit form by substitution of a certain adsorption isotherm $\theta = f(c_{mod})$. For example, for the Langmuir isotherm the following equation is obtained:

$$k = \frac{k_0 + K_{eq,L} k_c (1 + M) c_{mod}}{(1 + K_{eq,L} c_{mod})(1 + M c_{mod})} \quad \text{Eq. 50}$$

6.2.3 Summary of DIM and MRM

As explained in the previous two sections, two classes of retention models were developed, DIMs and MRMs. Each class contains several models, derived with different isotherm types or extended versions. Furthermore, even with the same model, fits can be performed using different input data arrangements and lead to significantly different results. To keep the text clearer, the following notation is introduced: the name of each method contains three parts: 1) either a DIM or MRM, 2) either linear (Lin) or Langmuir isotherm (Lan), and 3) the symbols of input data. Table 6.3 and Table 6.4 gives an overview of the employed methods.

All regressions (linear and nonlinear) were performed in Origin 8.5.1 though chi-square minimization with a tolerance of 10^{-9} , where statistical weighting method was applied.

Table 6.3: Description of employed methods: each method is a combination of a model (DIM or MRM), adsorption isotherm and a set of fitted parameters [127].

Method	Equation used	Input data	Fitted parameters
DIM-Lin-kc	$\lg k = \lg k_0 - Ac_{mod}$	k, c_{mod}	A, k_0
DIM-Lan-kcK	$\lg k = \lg k_0 + B \frac{K_{eq,L} c_{mod}}{1 + K_{eq,L} c_{mod}} - ac_{mod}$	$k, c_{mod}, K_{eq,L}$	B, a, k_0
DIM-Lan-kc	$\lg k = \lg k_0 + B \frac{K_{eq,L} c_{mod}}{1 + K_{eq,L} c_{mod}} - ac_{mod}$	k, c_{mod}	$B, a, k_0, K_{eq,L}$
DIM-Lan-kcK'	$\lg k = \lg k_0 + B \frac{K_{eq,L}^{corr} c_{mod}}{1 + K_{eq,L}^{corr} c_{mod}} - ac_{mod}$	$k, c_{mod}, K_{eq,L}^{corr}$	B, a, k_0
MRM-Lan-kcK	$k = \frac{k_0 + K_{eq,L} k_c (1 + M) c_{mod}}{(1 + K_{eq,L} c_{mod})(1 + M c_{mod})}$	$k, c_{mod}, K_{eq,L}$	k_0, k_c, M
MRM-Lan-kcKM	$k = \frac{k_0 + K_{eq,L} k_c (1 + M) c_{mod}}{(1 + K_{eq,L} \cdot c_{mod})(1 + M c_{mod})}$	$k, c_{mod}, K_{eq,L}, M$	k_0, k_c

Table 6.4: Comparison of methods based on DIMs an MRMs [127].

Method	Number of fitting parameter	Range of R^2	Experimental efforts
DIM-Lin-kc	2 (A and k_0)	0.74 – 0.94	Low
DIM-Lan-kcK	3 (B , α , and k_0)	0.83 – 1.00	High
DIM-Lan-kc	4 (B , α , k_0 and $K_{eq,L}$)	0.87 – 1.00	Low
DIM-Lan-kcK'	3 (B , α , and k_0)	0.84 – 1.00	Low
MRM-Lan-kcK	3 (k_0 , k_c , M)	(0.86)* – 1.00	High
MRM-Lan-kcKM	2 (k_0 , k_c)	0.69 – 1.00	Low

* 0.86 is the lowest R^2 among successful fitting. However, several fittings failed by this method.

6.2.4 Evaluation of DIM

In this section, the DIMs based on linear and Langmuir isotherms were compared by analyzing the results of the fittings to experimental data. The appropriate method to proceed the regression analysis according to different situations will be suggested after the comparison and discussion.

Model assuming linear isotherms for modifier adsorption

For method DIM-Lin-kc, Eq. 42 is applied for data fitting. Eq. 42 was derived based on the assumption that the loading of modifier in stationary phase is proportional to the modifier concentration in the mobile phase. This assumption was applied as first attempt intended to obtain a simplest model with the least number of fitting parameters, although it is known that methanol adsorption on porous silica in sc-CO₂ does not follow a linear isotherm across the whole range of methanol fraction [128].

The results of the fitting for retention factors of phenol on silicas are demonstrated in Figure 6.7 and for other solutes on SIL-60 are in Figure 6.8. The model fittings were all successful in the sense that either the chi-square tolerance was reached or the chi-square no longer changed. The adjusted R^2 (adj. R^2) for all cases were in the

range of 0.74-0.94 and the relative standard errors (RSEs) of the fitting parameter A and k_0 were in the range of 7 - 16%. However, it can be observed from the figures that the model fittings diverge from the experimental data at low concentrations of methanol. This leads to the underestimations of the k_0 values (y-intercept) in all cases regardless of physical properties of stationary phase (Figure 6.7) and the solute nature (Figure 6.8). These observations point to inadequacy of the model assumptions: as expected, the use of linear isotherms to describe the modifier adsorption on porous silica materials is an oversimplification and cannot be recommended for estimation of k_0 .

Note that Eq. 42 derived in this work have certain similarity to the common retention model for reversed phase chromatography, where the logarithm of the retention factor of a solute is linearly related to the organic solvent fraction and the intercept is the logarithm of the retention factor in pure water as mobile phase [58]. This simple model was found to be not accurate enough for certain systems. Efforts were made to improve the model by introducing quadratic terms to the right-hand side [129]. Another natural way is, however, to apply non-linear adsorption isotherms.

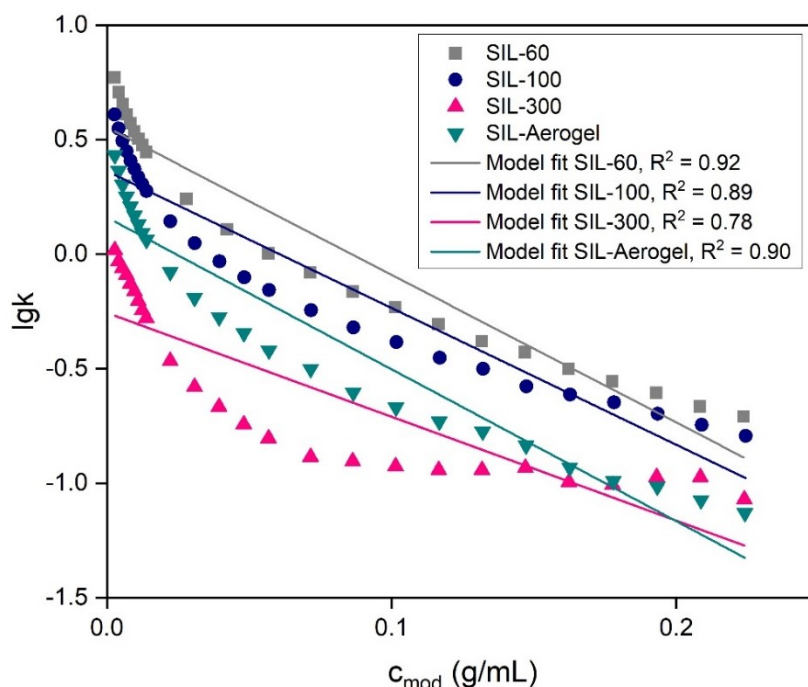


Figure 6.7: Retention factors of phenol on different silicas and model fittings according to DIM-Lin-kc [127]. SFC conditions: 200 bar, 40 °C, injection volume 2 μ L, flow rate 2 mL/min.

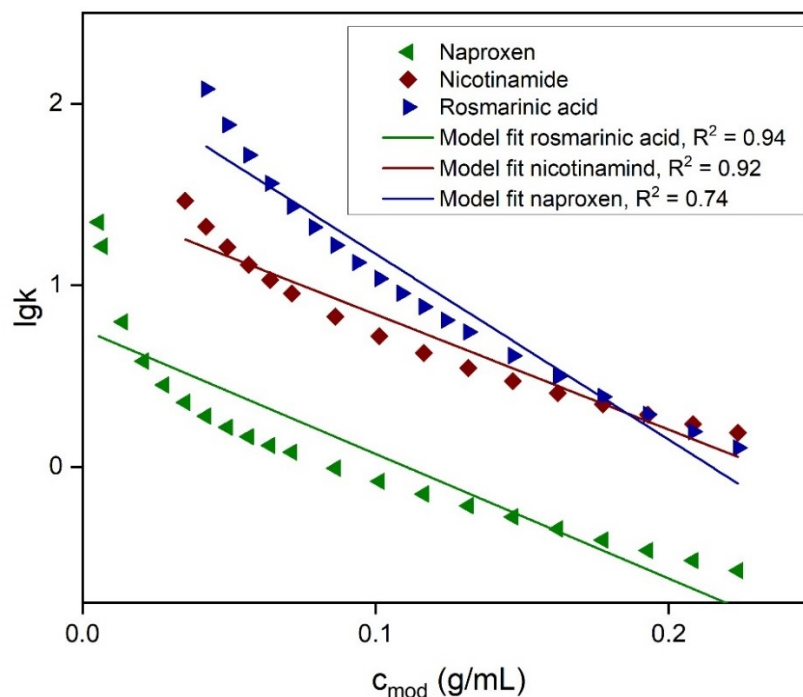


Figure 6.8: Retention factors of various solutes on SIL-60 and model fittings according to DIM-Lin-kc [127]. SFC conditions: 200 bar, 40 °C, injection volume 2 μ L, flow rate 2 mL/min.

Models assuming Langmuir isotherms for modifier adsorption

As mentioned in 6.2.1, Langmuir isotherm was adopted for constructing retention models to describe the modifier adsorption in this work. Three methods based on Langmuir isotherm to analyze the retention data were established. Together with the linear-isotherm-based method discussed in the previous section, in total four methods based on DIMs were studied. Estimated k_0 and adj. R^2 for the four methods are listed in Table 6.5. All experimental data were obtained at 40 °C, 200 bar. The method DIM-Lan-kcK' employs a corrected $K_{eq,L}^{corr}$ as input instead of measured $K_{eq,L}$. This method was established after analyzing the results from the first three methods and is described in the following passages.

In the aim of selecting the best method, three aspects were considered: (1) experimental efforts, (2) goodness of fitting, and (3) number of fitting parameters or problem of overfitting.

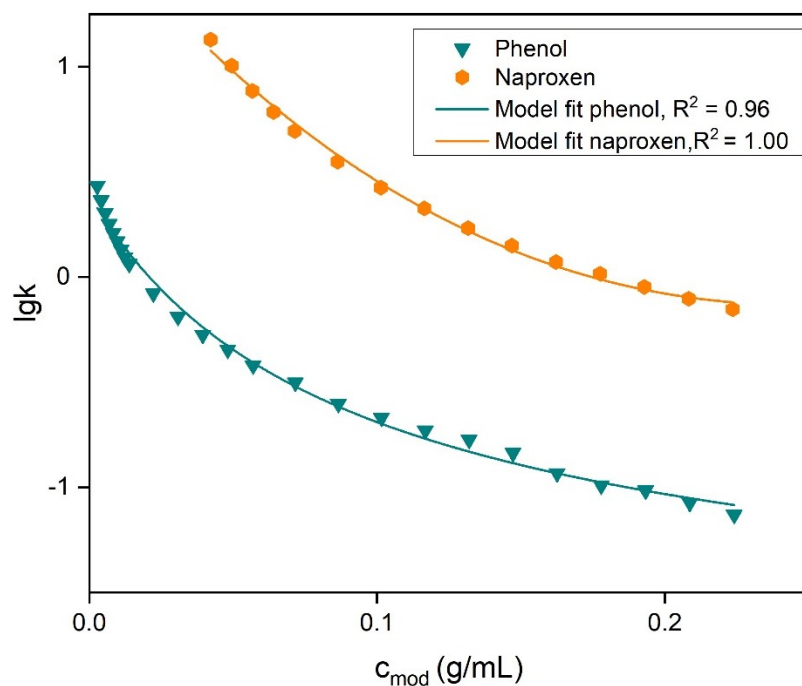


Figure 6.9: Retention factors of phenol and naproxen on SIL-Aerogel and model fittings according to DIM-Lan-kcK' [127]. SFC conditions: 200 bar, 40 °C, injection volume 2 μ L, flow rate 2 mL /min.

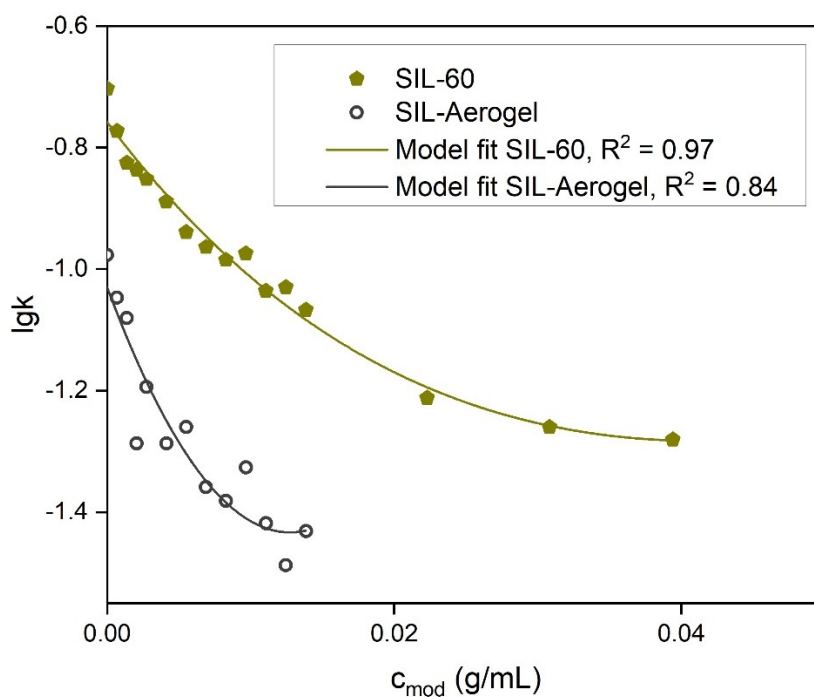


Figure 6.10: Retention factors of toluene on SIL-60 and SIL-Aerogel and model fittings according to method DIM-Lan-kcK' [127]. SFC conditions: 200 bar, 40 °C, injection volume 2 μ L, flow rate 2 mL/min.

The DIM-Lan-kcK method relies on experimentally measured $K_{eq,L}$ as input data for fitting, thus kept a small number of fitting parameters to avoid overfitting. However, measurements of $K_{eq,L}$ require intensive efforts considering both time and equipment upgrade [124,125]. In the method DIM-Lan-kc it was attempted to avoid such troublesome experimental measurements by making $K_{eq,L}$ a fitting parameter. The fitted $K_{eq,L}$ values were found to be significantly larger than the measured ones. In addition, the equilibrium constants should remain nearly constant for each stationary phase at a constant temperature regardless of the used solutes. Contrary to this, the fitted values of $K_{eq,L}$ obtained for different solutes deviate largely for SIL-60 and SIL-Aerogel (data not shown).

It is surmised that overfitting of the retention data is a possible reason. Nevertheless, it is observed that the fitted $K_{eq,L}$ values obtained in the DIM-Lan-kc method for phenol correlate well with the experimentally measured $K_{eq,L}$ values. Thus, the $K'_{eq,L}$ obtained from the DIM-Lan-kc method should be first corrected by multiplying by an empirical factor, F . This value is named $K_{eq,L}^{corr}$:

$$K_{eq,L}^{corr} = FK'_{eq,L} \quad \text{Eq. 51}$$

In the DIM-Lan-kcK' method, the corrected adsorption constant from Eq. 51 was employed to solve the overfitting problem of the DIM-Lan-kc method. An estimation for the correction factor F was made through a paired t-test (see details in Appendix, 12.6) and found to be 0.19. The value of k_0 estimated by the DIM-Lan-kcK' method is close (55 - 133%, Table 6.5) to those from the method DIM-Lan-kcK where experimental values of $K_{eq,L}$ are used.

Compared to linear adsorption isotherm, the use of Langmuir isotherms showed a significant better correlation, as expected due to a greater number of fitting parameters in the latter case. However, although DIM-Lan-kc method had one more fitting parameter than DIM-Lan-kcK and DIM-Lan-kcK', the adj. R^2 did not show a visible increase. Another observation regarding the goodness of fitting is that the regression for toluene always results in smallest adj. R^2 . Toluene was selected as it is the only solute, for which k_0 could be measured experimentally due to its low affinity to silica. However, because of the same reason, retention times of toluene are

close to the hold-up time, resulting in large uncertainties of the retention factor. Therefore, the low adj. R^2 for toluene should not be interpreted as a failure of the model.

To summarize, the DIM-Lin-kc method is not recommended in any case because of the worst goodness of fitting. Having the same level of the goodness of fitting, the DIM-Lan-kcK' method shows significant advantages compared to DIM-Lan-kcK for less experimental efforts and to DIM-Lan-kc for less risk of overfitting (Figure 6.9 and Figure 6.10).

Based on the above results, several issues shall be addressed when applying the DIMs for estimating k_0 from retention data in the presence of a modifier. First of all, when the methanol adsorption isotherm on the to-be-tested stationary phase in supercritical CO₂ is available at the required temperature and pressure, the method DIM-Lan-kcK can be applied with the measured $K_{eq,L}$ for the most reliable estimation. However, in most cases adsorption isotherms are not available. If so, phenol should be injected into the column as a model solute at various methanol concentration. The $K_{eq,L}$ can be obtained afterwards by regression using DIM-Lan-kc on the retention data of phenol. Value of $K_{eq,L}^{corr}$ can be then calculated by multiplying by the correction factor F . DIM-Lan-kcK' can be finally applied for estimation of k_0 of any solutes on the stationary phase of this column using the $K_{eq,L}^{corr}$.

6.2.5 Evaluation of MRM

According to the original MRM, Eq. 47, the retention factor k varies linearly with surface coverage θ :

$$k = (k_c - k_0)\theta + k_0 \quad \text{Eq. 48}$$

As seen in the k vs. θ plot (Figure 6.11), the experimental data does not show linear correlations among any solute/stationary phase pairs. Only the data points of each solute/stationary phase pair at relatively lower modifier concentration can be treated as a linear function. The reason might be that the assumption of single layer adsorption to apply Langmuir isotherm does not hold true. Studies have demonstrated the adsorption of alcohols on silica materials could exhibit multilayer

behavior above a certain concentration [128,130,131]. If this is the case, two issues should be considered. Firstly, the calculated θ values are only hypothetical and do not have any physical meaning. Secondly, the proposed model, Eq. 48, is based on the theory that when methanol is adsorbed as a single layer, the solute molecules are attracted to the methanol molecules which leads to k_c . However, when multilayer adsorption appears, the affinity between the solute and adsorbed methanol changes which leads to a different k'_c . In this case, k'_c depends on the modifier concentration, and the model assumptions break down. Because of these reasons, an advanced model Eq. 50 with an empirical factor M was suggested. As discussed above for the DIMs, when the experimental value of $K_{eq,L}$ is not available, an estimated value can be taken. The results from regression by MRM-Lan-kcK and MRM-Lan-kcKM methods are given in Table 6.6.

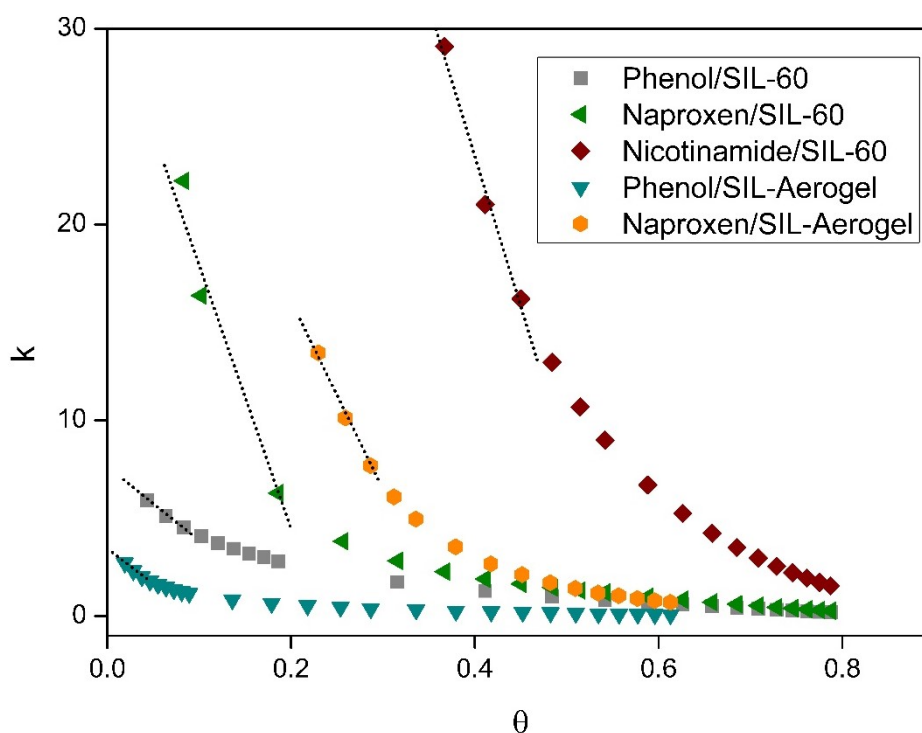


Figure 6.11: Retention factors of various solutes on SIL-60 and SIL-Aerogel [127]. SFC conditions: 200 bar, 40 °C, injection volume 2 μ L, flow rate 2 mL/min, modifier (methanol) fraction at 0.1–30 vol.%. The dashed straight lines were plotted to guide the eyes at low coverages.

It is observed that when Eq. 50 was applied using the experimental measured $K_{eq,L}$ (MRM-Lan-kcK), the data could not be regressed and the parameters did not

converge. The suspected reason was over-parameterization, which leads to deterioration of estimation accuracy and the resulted estimations and errors were unreliable. However, the fitting worked in all cases for phenol and toluene as solutes and the estimated k_0 values were always comparable to those from DIM-Lan-kcK. The parameter M was found to lie in the range 100-200.

Although the retention factors of toluene and phenol are very different at zero modifier concentration, they have similar M values. It may surmise that M is not solute-dependent, but modifier-dependent. This is reasonable because M was introduced to correct the strength of the modifier influence at high modifier concentration where multilayer adsorption may take place and the influence of solutes shall be minimal. Therefore, to solve the overparameterization problem, M was fixed to 150 in all cases for the next method MRM-Lan-kcKM.

Unlike developing method DIM-Lan-kcK' based on the result from DIM-Lan-kc, it is not possible to treat the $K_{eq,L}$ as a fitting parameter in the MRMs: it is not reasonable to add an extra fitting parameter to a model, which is already overparameterized. A rough estimation of $K_{eq,L} = 20 \text{ mL g}^{-1}$ can be suggested as a representative value across all studied silica materials. With these estimates for M and $K_{eq,L}$, the regressions were performed and the results show reasonable agreement (89 - 147%) with the method DIM-Lan-kcK (Table 6.5). One exception was the case of rosmarinic acid, which has an exceptionally high affinity to silica. In this case, the estimations of k_0 by MRM are not reliable. For the second strongest retained solute, nicotinamide, the DIM-Lan and MRM-Lan methods give consistent estimations (304 ± 16 and 277 ± 10 , respectively) even when arbitrary selected parameters $K_{eq,L}$ and M were taken.

To summarize, if $K_{eq,L}$ is not available, the method MRM-Lan-kcKM is recommended; it provides satisfying estimations close to DIM-Lan-kcK without over-parameterization.

Table 6.5: Regression results for DIMs [127]

Stationary phase	Solute	DIM-Lin-kc		DIM-Lan-kcK			DIM-Lan-kc			DIM-Lan-kcK'			$\frac{k_0^{(DIM-Lan-kcK')}}{k_0^{(DIM-Lan-kcK)}}$
		k_0	R ²	k_0	$K_{eq,L}$	R ²	k_0	$K_{eq,L}$	R ²	k_0	$K_{eq,L}^{corr}$	R ²	
SIL-60	Phenol	4.4±0.3	0.92	6.2±0.2		0.99	8.1±0.1	62±2	1.00	5.9±0.2		0.99	0.96
	Naproxen	25±5	0.74	36±4		0.93	330±19	170±4	1.00	32±4		0.91	0.91
	Nicotinamide	42±5	0.92	304±16	16.5	1.00	(1.4±0.2)×10 ³	40±3	1.00	219±14	11.7	1.00	0.72
	Rosmarinic acid	483±81	0.94	(1.02±0.08)×10 ⁴		1.00	(2.9±1.2)×10 ⁵	45±4	1.00	(5.6±0.4)×10 ³		1.00	0.55
	Toluene	0.2	0.89	0.2		0.97	0.2	308±131	0.98	0.2		0.97	1.00
SIL-100	Phenol	3.0±0.2	0.89	4.1±0.1	11.2	0.99	5.6±0.1	58±2	1.00	4.1±0.1	11.1	0.99	1.01
SIL-300	Phenol	0.9±0.1	0.78	1.1	5.3	0.97	1.4	24±3	1.00	1.1	4.6	0.97	0.99
SIL-Aerogel	Phenol	2.0±0.2	0.90	2.6±0.1		0.98	3.9±0.1	63±3	1.00	2.3±0.1		0.96	0.90
	Naproxen	96±23	0.93	139±8	7.1	1.00	641±178	26±3	1.00	185±10	11.9	1.00	1.33
	Toluene	0.1	0.74	0.1		0.83	0.1	433±487	0.87	0.1		0.84	1.05

Table 6.6: Regression results for MRMs [127].

Stationary phase	Solute	MRM-Lan-kcK				MRM-Lan-kcKM				$k_0^{(MRM-Lan-kcKM)} / k_0^{(DIM-Lan-kcK)}$
		k_0	M	$K_{eq,L}$	R^2	k_0	M	$K_{eq,L}$	R^2	
SIL-60	Phenol	7.6	113±13		1.00	8.3±0.1			1.00	1.35
	Naproxen	–	–		-	31.7			0.90	0.89
	Nicotinamide	–	–	16.5	-	277±10	150.0	20.0	0.99	0.91
	Rosmarinic acid	–	–		-	915±276			0.69	0.09
	Toluene	0.2	184±41		0.98	0.2			0.98	1.03
SIL-100	Phenol	5.4±0.2	135±9	11.2	1.00	5.6±0.1	150.0	20.0	1.00	1.39
SIL-300	Phenol	1.7±0.2	191±42	5.3	0.98	1.5±0.1	150.0	20.0	0.97	1.35
SIL-Aerogel	Phenol	3.8±0.1	152±10		1.00	3.78±0.04			1.00	1.47
	Naproxen	-	-	7.1	-	155±11	150.0	20.0	0.97	1.12
	Toluene	0.09±0.01	200±139		0.86	0.09±0.01			0.86	0.99

7 Modifier Effects on Solute-Matrix Interaction

Changes in the mobile phase composition are expected to have a profound effect on the intermolecular interactions between the solutes and the stationary phases. In this section, the influence of modifier concentration was evaluated on the system constants $\{e, s, a, b, v, l\}$ of the LSER minimal AS and specific ABVL, BVL and EAVL models. The choice of the significant constants is to a certain extent voluntary owing to the arbitrary choice of the p-values. Since the numerical values of the system constants do depend on whether other constants are included in the LSER model, the physical interpretation of the system constants become difficult while a comparative analysis is still possible.

The intermolecular interactions between the solutes and the stationary phases are affected strongly by the mobile phase composition. Such effect may arise not only due to changing composition of the mobile phase itself, but also because of the adsorption of the modifier on stationary phases [29]. A recent study by Glenne et al. [128] has distinguished these two effects on a silica column with a mixture of methanol and carbon dioxide as mobile phase. It proves that at a lower fraction of modifier the competitive adsorption between solvent and solute on active sites is the major effect whereas at higher fraction the modifier only influences the interactions due to changes in the mobile phase. However, the LSER model is not formulated so that to distinguish these two effects. Thus, in this work, the change of the values of system constants was considered as a result of the mixed mechanism of both effects.

As it was described in 6.1.2, the LSER-AS model was found to be universal for all silica based stationary phases considering the statistical significance of the system constants and acceptable predictability. First, the system constants a and s were evaluated for all stationary phases at different methanol concentrations (5–20 vol.% in increments of 2.5%). The temperature was set to 35 °C, the back pressure was 200 bar and the flow rate of the mobile phase was 2 mL/min. Results are presented in Figure 7.1 (the error bars represent the standard error of the system constants).

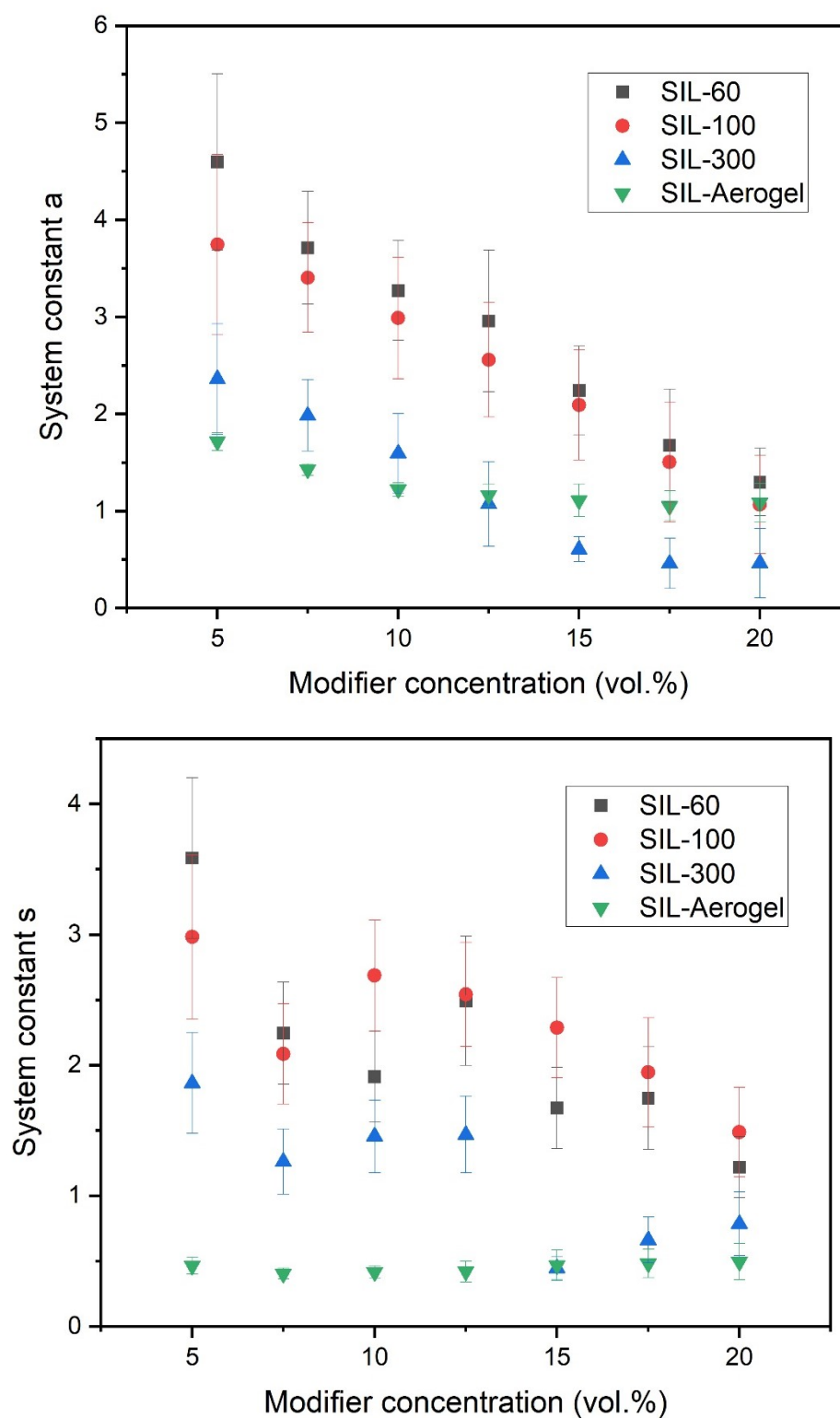


Figure 7.1: Comparison of *a* and *s* system constants from the AS model in SIL-60, SIL-100, SIL-300 and SIL-Aerogel stationary phase across different concentrations of modifier in mobile phase. SFC conditions: 200 bar, 35 °C, injection volume 2 μ L, flow rate 2mL/min, modifier concentration at 5 to 20 vol.%.

As it is shown, both system constants have positive values for the four stationary phases at all modifier concentration. The system constant a associated with the hydrogen bonding is always larger than the system constant s , which is related to the non-specific dipole-dipole interactions. An evident decreasing trend for both a and s was observed for SIL-60 as well as for other precipitated silicas, SIL-100 and SIL-300, whereas for SIL-Aerogel a less pronounced influence can be noticed. This trend can be explained by two factors: (i) the coverage of the stationary phase with the modifier (interaction between silanols and hydroxyl group of methanol), which weakens the possibility of the forming of hydrogen bonds between the solutes and the silica surface; (ii) associations of methanol around the solute molecules in the mobile phase preventing them from the interactions with the stationary phase. Whereas the modifier effects for SIL-60, SIL-100 and SIL-300 are of similar magnitude, SIL-Aerogel stands out with much smaller contribution from non-specific dipole-dipole interactions (system constant s) and a clear plateau for the hydrogen bonding (system constant a) reached at ~ 15 vol.% methanol. One possible explanation could be that silica aerogel has a higher adsorption capacity towards methanol or higher accessibility of the silanols groups for methanol when compared with conventional precipitated silica. Although detailed structural studies for silica aerogel are required to support this hypothesis, a higher accessibility of the NH_2 groups in chitosan aerogels compared to xerogels was reported [132].

As discussed previously, three specific and more accurate LSER models, Eq. 35, Eq. 36 and Eq. 37 were built. The influence of modifier is demonstrated in Figure 7.2, which shows the change of system constants from the specific models across stationary phases as a function of the methanol concentration. The main conclusion is that acid-basic interactions (a and b) dominate over all other types, even at high modifier concentrations. As it was discussed above, the interpretation of the downward trend for the system constants a and b may rely on the adsorption of the modifier on silanols that have both H-bond donation and acceptance ability. This should result in a “hydrophobization” of the surface. The trend for the system constant l further supports this reasoning (less preferable partitioning between gas and the “hydrophobized” surface), although the effect is small (Figure 7.2). Polarizability contribution from n and π electrons (system constant e) is only

significant and positive for SIL-aerogel and does not depend on the modifier concentration. Contribution of dispersion interactions (system constant v) is negative with highest standard errors making difficult to draw a firm conclusion whether a dependency on modifier concentration is present.

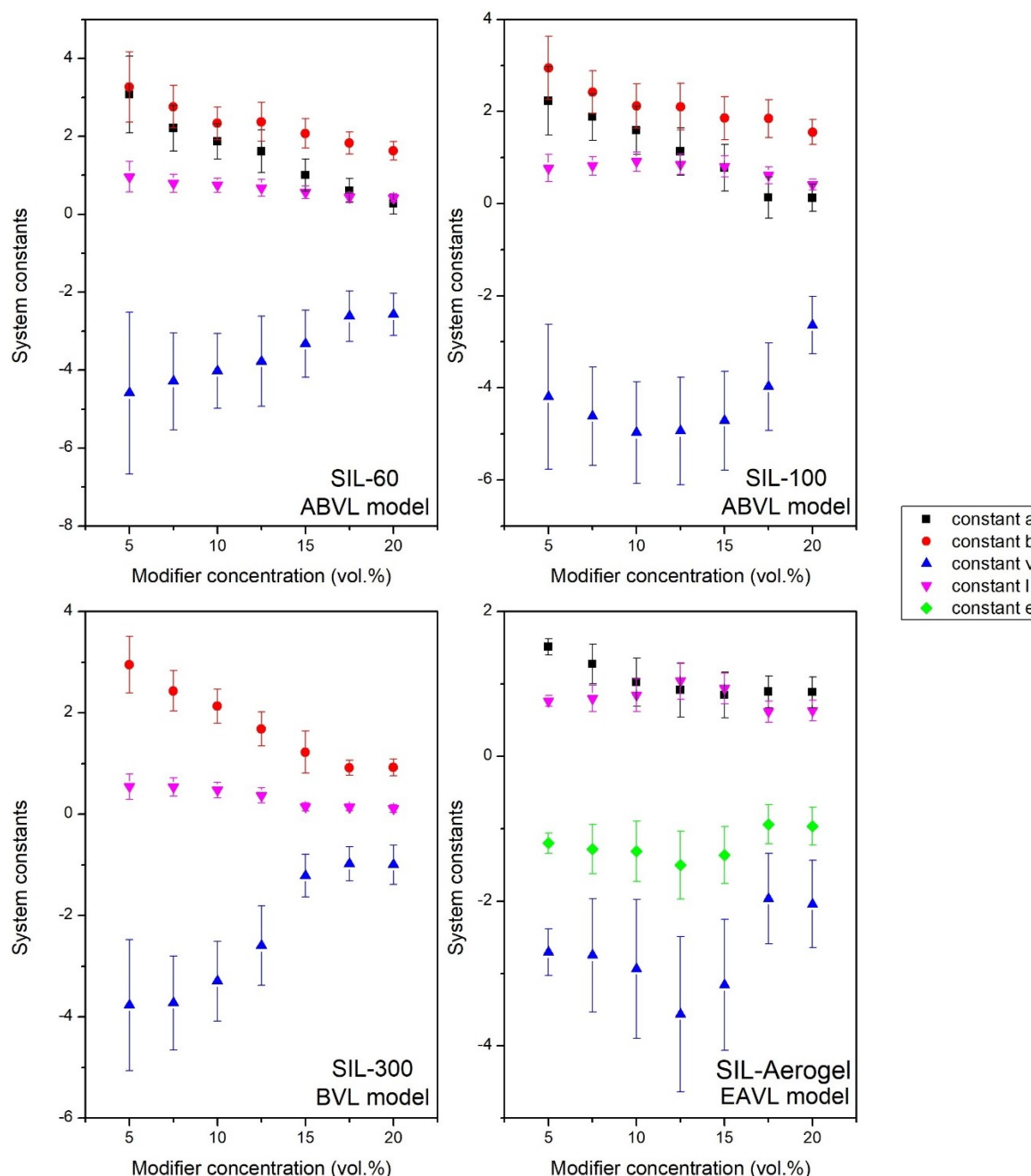


Figure 7.2: System constants from the specific models, Eq. 35, Eq. 36 and Eq. 37 for all silica materials at different modifier concentrations [90]. Error bars represent the standard error of the system constants. SFC conditions: 200 bar, 35 °C, injection volume 2 μ L, flow rate 2 mL/min, modifier (methanol) concentration at 5 to 20 vol.%.

8 Other Factors Influencing Interactions

The influence of pressure and temperature was evaluated on the system constants a and s of the minimal AS model on the first attempt. The temperature was increased from 25 to 60 °C with increments of 5 °C. The pressure was increased from 150 to 300 bar with increments of 50 bar. Results are presented in Figure 8.1.

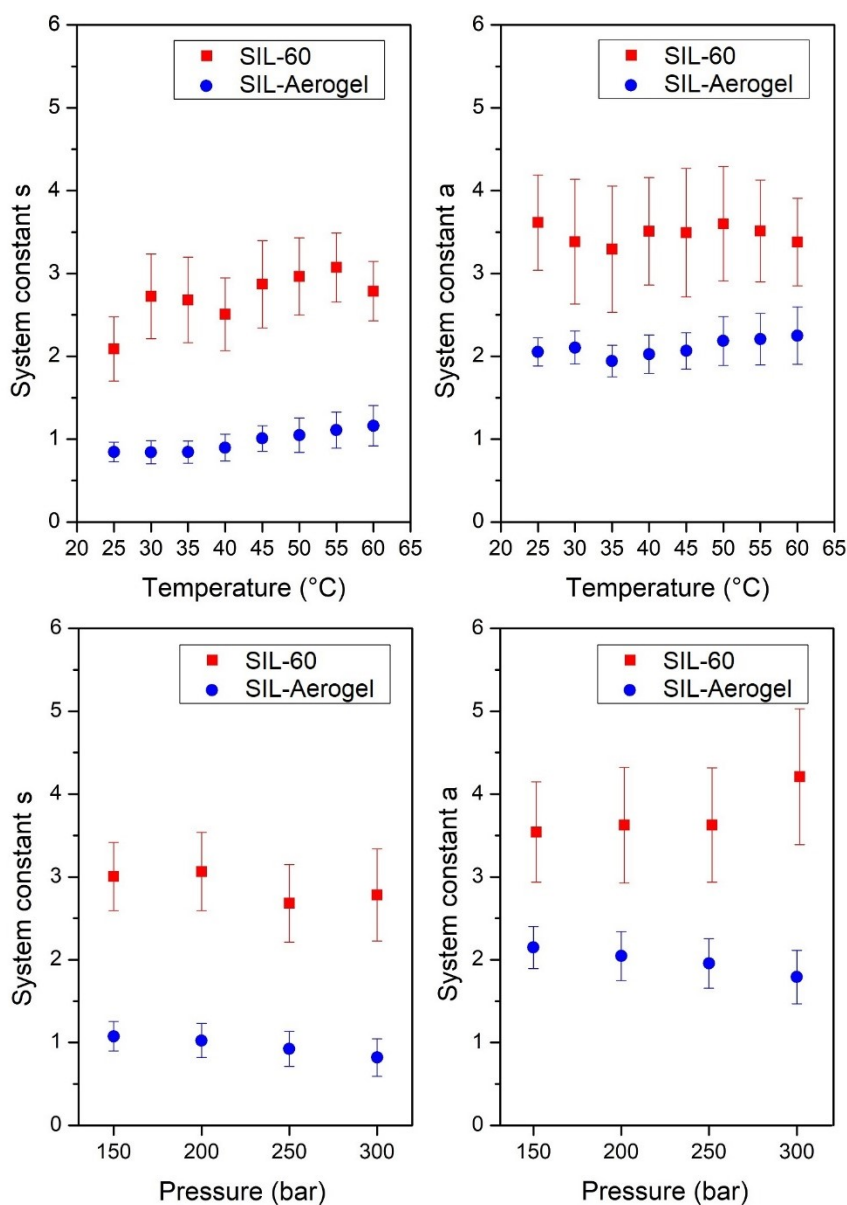
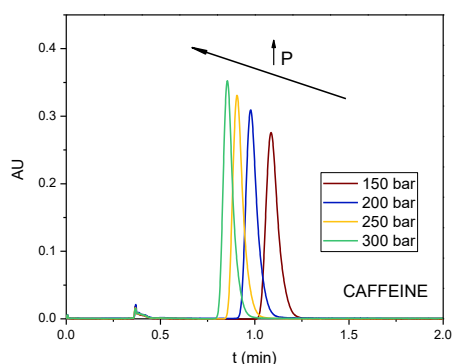


Figure 8.1: System constants a and s from the minimal AS model for SIL-60 and SIL-Aerogel stationary phases across different temperature and pressure [90]. Error bars represent the standard error of the system constants. SFC conditions for the top panel: 200 bar, 25 to 60 °C; for the bottom panel: 150 to 200 bar, 45 °C. Other conditions: flow rate 2 mL/min, modifier concentration at 10 vol.%, injection volume 2 μ L.

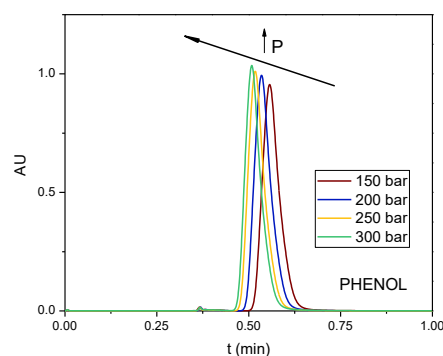
It was observed that neither pressure nor temperature has a significant effect on the system constants a and s . To better visualize the effect of temperature and pressure, it is useful to classify all solutes from Table 6.1 into three groups depending on their hydrogen bond (H-bond) donation or acceptance ability: weak H-bond donors/acceptors (small A and B), strong H-bond acceptors (small A , large B), strong H-bond acceptors and donors (A and B are both large). The following sections will discuss the temperature and pressure effect based on this classification.

Strongest H Bond Accept. analyte Strong H-Bond Donor/Accept. analytes

a) Caffeine



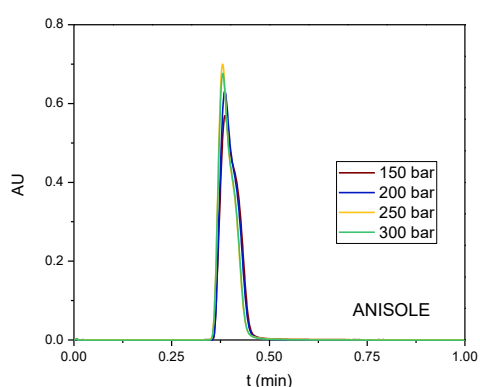
b) Phenol



Strong H-Bond Accept. analytes

Weak H-Bond Accept. analytes

c) Anisole



d) Toluene

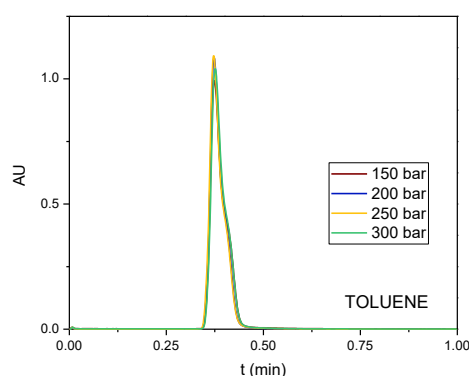


Figure 8.2: Influence of the pressure on the retention time and in the peak shape of the representative solutes. Stationary phase: SIL-100. SFC conditions: 35 °C, 10 vol.% methanol, injection volume 2 μ L, flow rate 2 mL/min.

Pressure

A decrease of the retention factor with increasing pressure was observed only for solutes with both strong H-bond donation and acceptance ability such as caffeine and phenol (Figure 8.2). Due to a small fraction of such solutes in the overall set, the variation of the system constants is expected to be small. Indeed, variations with pressure are within the range of the standard errors (Figure 8.1, bottom panel).

Temperature

More complex effects were observed when temperature was varied, which are the results of the combination of different mechanisms. First of all, the density and thus the solvation ability of the mobile phase decreases with increasing temperature. The retention factor of a solute shall increase due to this effect. Secondly, with further temperature increase the solubility of the solutes increases, which in turn may lead to the decrease of retention factors. Thirdly, the solute adsorption is an exothermic process and thus the retention factor shall decrease with rising temperature. Lastly, the competitive adsorption between modifier and solute molecules also has a drastic effect on retention.

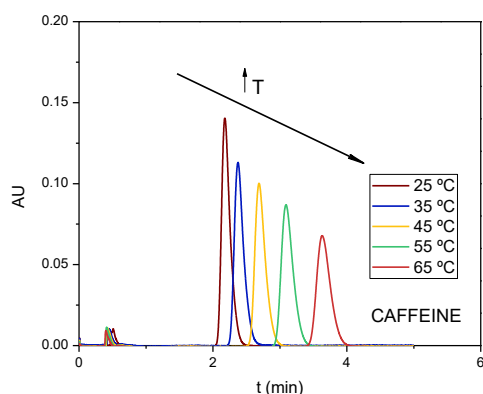
In this work the observation was that for weak H-bond donors/acceptors such as toluene the retention time shortens with rising temperature (Figure 8.3). This behavior may be attributed to the exothermic character of the solute adsorption (toluene and CO₂ are fully miscible at the operating conditions used so its solubility is “infinite” at any p,T employed). For solutes highly interacting with the stationary phases such as caffeine the opposite effect was observed: the retention time systematically increases with increasing temperature. The same trend has been observed by Blackwell and Stringham [119]. One possible explanation for this phenomenon is due to the competitive adsorption of the modifier. At lower temperatures adsorption of the solute takes place on the almost fully covered stationary phase (domination of the modifier adsorption). At a higher temperature the modifier desorbs leaving behind free (uncovered) silanols available for the interaction with the solute. This consideration assumes that the enthalpy of adsorption for the modifier is lower than for the solute and thus can be influenced by temperature to a larger degree. Furthermore, the

decrease of the solvation ability due to density drop when temperature increases may also contribute to this effect. Such oppositely directed temperature dependencies for the different solute classes most likely result in a certain compensation of the regressed system constants (Figure 8.1, upper panel) and thus in only a slight response to the temperature variation.

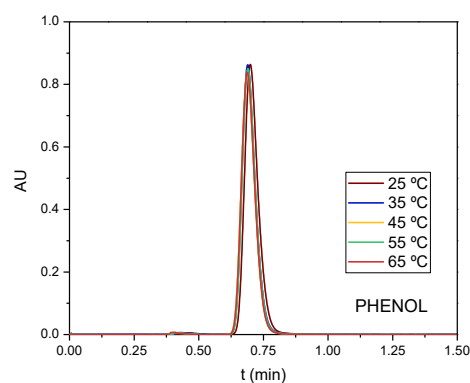
Strongest H Bond Accept. analyte

Strong H-Bond Donor/Accept. analytes

a) Caffeine



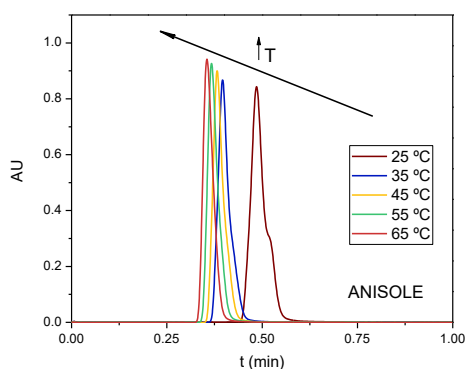
b) Phenol



Strong H-Bond Accept. analytes

Weak H-Bond Accept. analytes

c) Anisole



d) Toluene

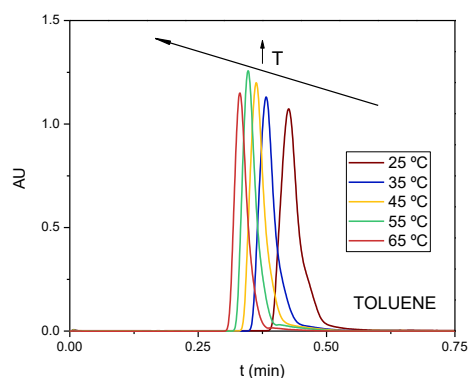


Figure 8.3: Influence of the temperature on the retention time and in the peak shape of the representative solutes. Stationary phase: SIL-100. SFC conditions: 200 bar, 5 vol.% methanol, injection volume 2 μ L, flow rate 2 mL/min.

The temperature dependence of adsorption in supercritical CO₂ was studied in many previous works [133–137]. However, all these works were done by varying

temperatures at a fixed pressure. No matter which solutes or stationary phases were studied, the same conclusion was drawn that the adsorbed amount increases with increasing temperature. This phenomenon was explained mainly by the density influence. With increasing temperature, the density and solvation power of CO₂ is lowered favoring solute adsorption on the solid surface.

A set of experiment was conducted aiming to eliminate this cause by fixing the density to a constant value (807 g/L). Four temperatures were investigated, and the back pressure of the system was adjusted accordingly. The concentration of the modifier was very low and considered having no influence on fluid density. The experimental data and the model fitting with MRM-Lan-kcKM method is given in Figure 8.4, while the estimated k_0 values using the methods DIM-Lan-kcK, DIM-Lan-kcK' and MRM-Lan-kcKM are presented in Figure 8.5. The estimated k_0 values from all three methods were constant considering the margin of error.

It was found that the k_0 decreases with increasing temperature. When temperature increases, the vapor pressure of ketoprofen increases and therefore, ketoprofen shows lower affinity to the stationary phase at higher temperatures. This behavior follows the general temperature dependence of adsorption in gases and liquids. It is also seen in Figure 8.4 that the four lines come closer at higher c_{mod} pointing to the fact that temperature has less influence at higher c_{mod} on the adsorption of solute to SIL-Aerogel. One explanation is that the higher modifier content leads to higher solubility of solutes in mobile phase which dominates over the temperature effect. Another explanation could be that the temperature influence on the adsorption of modifier and solute counteracts each other: at lower temperatures, the adsorption of both modifier and solute is higher. At the same time, since more modifier is adsorbed, it is covering larger surface and inhibiting the adsorption of the solute. This counteraction is more obvious at higher methanol concentration.

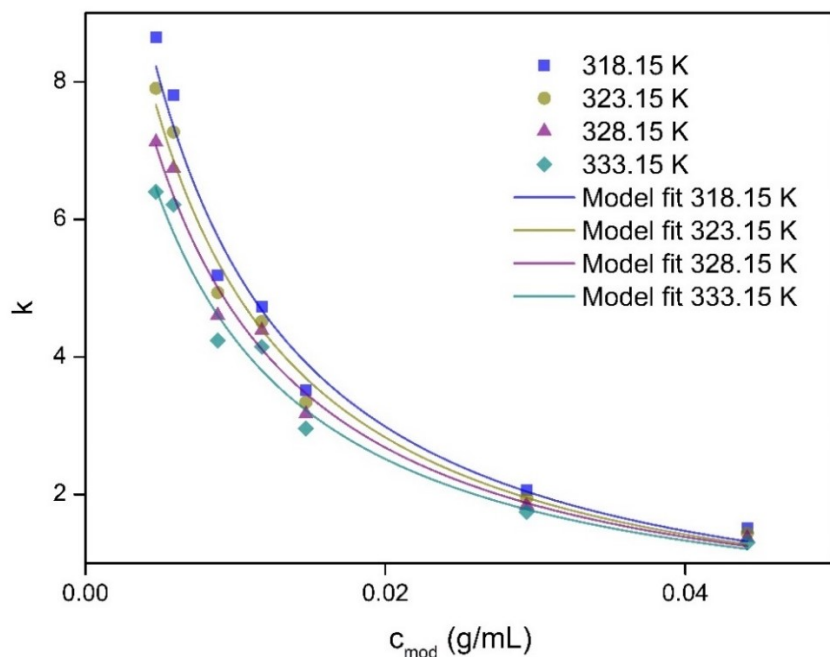


Figure 8.4: Retention factors of ketoprofen on SIL-Aerogel at different temperatures and model fitting according to MRM-Lan-kcKM [127]. SFC conditions: 191 bar for 318.15 K, 217 bar for 323.15 K, 242 bar for 328.15 K and 268 bar for 333.15 K, flow rate 2 mL/min, modifier (methanol) fraction at 0.8 to 7.5 vol.%.

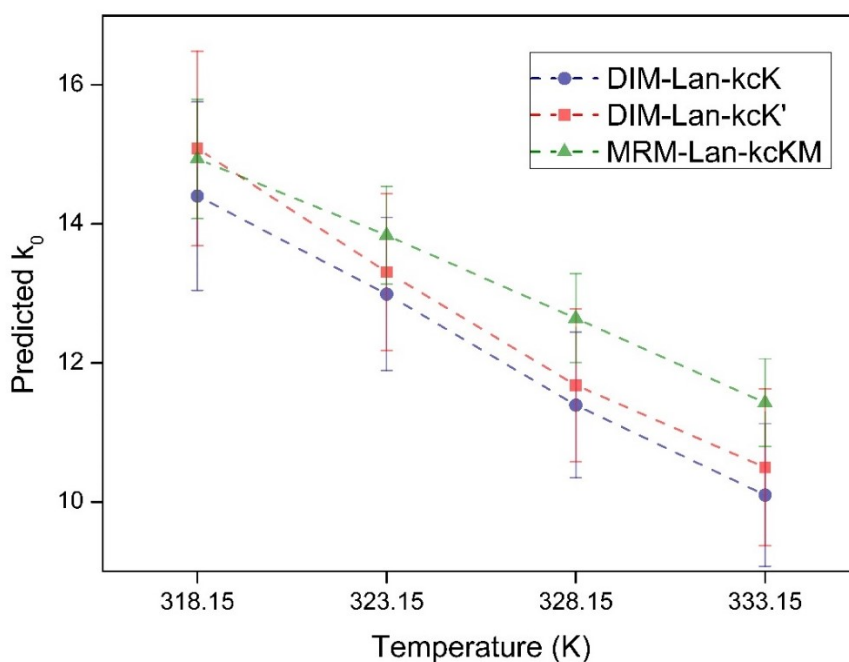


Figure 8.5: Estimated k_0 values of ketoprofen on SIL-Aerogel at different temperatures. Method DIM-Lan-kcK, DIM-Lan-kcK' and MRM-Lan-kcKM were applied following the procedure explained in chapter 6.2.

9 Transferability of the Free Energies

In view of chemical similarities of the examined silica materials it is interesting to study whether the free energies of adsorption ΔG and the corresponding adsorption equilibrium constants K_{eq} are transferable from one material to another. In other words, whether for two materials, X and Y , the Eq. 52 holds true at fixed temperature, pressure and modifier concentration (α and β are constants):

$$\ln K_{eq}(X) = \alpha \ln K_{eq}(Y) + \beta \quad \text{Eq. 52}$$

Eq. 52 for the adsorption constant can be rewritten for the retention factor k since these two quantities are directly proportional, $k = K_{eq}(V_S/V_M)$.

The transferability of the retention factors was indeed observed for all stationary phases. This phenomenon is demonstrated in Figure 9.1, when SIL-60 was chosen as reference material (material Y in terms of Eq. 52) at 200 bar, 40 °C, 10 vol.% methanol, and for the retention factors calculated from Eq. 35 to Eq. 37 by the LSER to minimize the influence of the outliers.

Once the transferability of the adsorption free energies is established, the retention factor and thus the adsorption constant for a given solute can be determined from a plot such as Figure 9.1. This can be helpful when a custom-packed column with a material of interest is characterized against a well-packed (e.g. commercial) column used as a reference.

The slope α in Eq. 52 is a comparative measure for the overall “strength” of the retention. For those materials which show $\alpha > 1$ the retention is systematically larger than for the reference material and vice versa. The value $\alpha = 1$ would correspond to the materials with identical retention characteristics. According to this view, silicas SIL-60 and SIL-100 are the most similar ones ($\alpha = 1.01 \pm 0.02$), whereas SIL-300 and SIL-Aerogel possess a lower retention strength ($\alpha = 0.62 \pm 0.05$ and $\alpha = 0.39 \pm 0.05$, respectively). However, more data are required to draw a firm conclusion whether the pore size influences the retention phenomena.

Based on the above results, the following protocol is suggested for prediction of adsorption constants on novel solid carriers in sc-CO₂-containing solutions. First, under fixed operating conditions (p , T , modifier concentration) inject the 17 probe molecules (Table 3.1Table 6.1) into a well-packed reference column and a column packed with a novel solid material. Second, construct the linear relationship between the $\ln K_{ads}$ values for the novel solid material and the reference material using Eq. 52 and determine the coefficients α and β . Finally, by injecting a solute of interest into the reference column, the adsorption constant of this solute on the novel solid material can be calculated. Therefore, experimental efforts can be significantly saved.

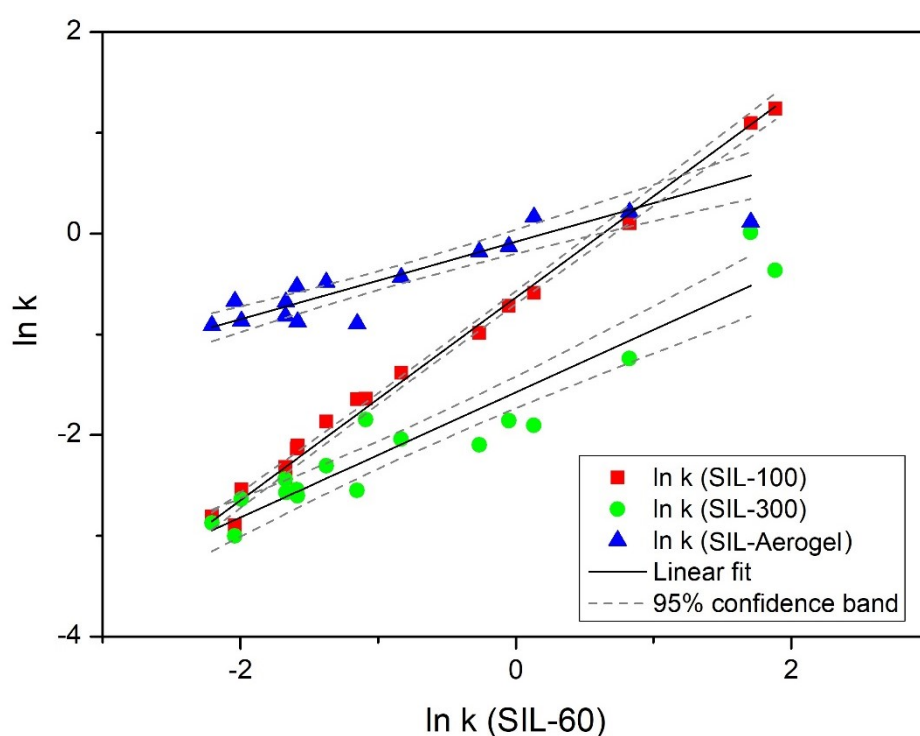


Figure 9.1: Transferability of the retention factors according to Eq. 52 [90]. Reference material: SIL-60, SFC conditions: 200 bar, 40 °C, 10 vol.% methanol, injection volume 2 μ L, flow rate 2 mL/min. Dashed lines indicate 95 % confidence bands.

10 Conclusions and Outlook

The goal of this work was to develop a fast and robust approach to quantify the interactions of organic solutes with porous solids in sc-CO₂. Inverse SFC was adopted for this purpose.

This work reports on experimental retention factors for moderately polar solutes on four silica-based porous matrices used as stationary phases in packed-column SFC. First of all, the experimental set-up was developed and validated to make sure the reliable measurements of retention factors by SFC. Methanolic solution of N₂O was selected as the tracer to determine the hold-up time based on its sharp and symmetric peak shape and retention time independence of modifier concentration. All experiment were designed to proceed at pressure 150 to 300 bar, temperature 25 to 60 °C and modifier (methanol) concentration 5 to 20 vol.% to ensure a single-phase working region based on phase equilibrium data from literature. A stabilization process was decided to apply on all columns and the reproducibility of retention factors on them was examined and confirmed.

Modifier adsorption on stationary phase is a major factor influencing the retention of solute on stationary phases and the adsorption equilibrium constant $K_{eq,L}$ is an essential parameter for retention model development. Thus, the adsorption isotherms of the modifier (methanol) on four silica stationary phases were measured by frontal analysis and fitted with different models to compare. The goodness of fitting with Langmuir, bi-Langmuir and BET models are all acceptable but Langmuir model was selected to calculate the equilibrium constant for retention models due to its smallest number of fitting parameters. The temperature and pressure effect of methanol loading on the stationary phase is found to be mainly a result of the change in solvation power of CO₂ which is correlated to the Hildebrand solubility parameter. By comparing the number of methanol molecules adsorbed and the hydroxyl group density on the stationary phase surfaces, multilayer adsorption is suggested on SIL-60, SIL-100 and SIL-Aerogel.

Two classes of retention models were developed with the goal to describe the solute-solid-interactions in sc-CO₂: LSER models and modifier-based retention models.

Two types of the LSER models were further identified: (i) the minimal model with two solute descriptors (dipolarity/polarizability and solute hydrogen-bonding acceptor ability) that is valid for all process parameters; (ii) the specific model for each particular silica. The goodness of fit of the minimal model is lower than the specific models. However, the minimal model gives possibilities to compare wider range of stationary phases.

Low polarity of pure sc-CO₂ makes elution of the solutes only possible if modifier (methanol) is added to the mobile phase. To extrapolate the retention factors into experimentally inaccessible modifier-free conditions, two classes of modifier-based empirical retention models were developed. The first class relies on log-linear relations for the equilibrium concentration of the solute in both mobile and stationary phases. The second class interprets the overall retention as a sum result of the retention on native and covered-by-modifier adsorption sites. To obtain analytical expressions for both classes, a functional form for adsorption isotherms of modifier on the porous matrix is required. It is demonstrated that linear adsorption isotherm is insufficient to describe experimental results. Langmuir isotherm yields qualitatively correct behaviour. To obtain quantitative agreement and to avoid overfitting of the models, suggestions are given in this work to estimate the adsorption coefficient of the modifier. An additional advantage is that the time-consuming prior determinations of adsorption isotherms of modifier can be avoided. The developed models were applied to the adsorption of a model drug, ketoprofen, on silica aerogel and deduce the retention factor in modifier-free conditions, k_0 , based on retention data obtained with modifier.

Regardless of which LSER model applied, the acid-basic interactions have a major contribution to the retention for all studied silicas. The intensity of these interactions decreases with increasing modifier concentration (methanol) in the mobile phase. The competitive adsorption of the modifier on silanol groups and the change of the solvation power of the mobile phase could both contribute to this phenomenon. Further insights of the temperature and pressure influences on interactions can be generated by grouping solutes based on their acid-basic interaction abilities and observing their response to changes. Temperature influence was also discussed with the help of the modifier-based retention models. The modifier-based retention models

were applied to the adsorption of a model drug, ketoprofen, at a constant mobile phase density for four temperatures and the retention factor in modifier-free conditions was deduced. A higher retention factor was observed at higher temperature which implies stronger affinity.

Finally, a way to plot retention factors of a pair of materials measured under constant pressure, temperature, and modifier concentration in logarithmic scale, where linear relationships were found between silicas was demonstrated. Thus, the transferability of the adsorption free energies and adsorption constants across four studied silica materials was illustrated.

To conclude, a framework to evaluate the interactions between various solutes and silica matrices by SFC was initiated. A simple experimental set-up with self-packed columns and a common analytical SFC system was proved to be robust. The major types of interactions can be identified by LSER; The critical parameter, k_0 , can be predicted quickly by the modifier-based models even without the time-consuming determination of adsorption equilibrium constants; The effects of temperature, pressure and modifier can be analyzed by applying both approaches which compensate each other.

There are several considerations for future work. The accuracy of the isotherm determination can be validated by adding mass flow meters to both the methanol and CO₂ pumps. However, the purpose of this work is to recommend a straightforward method for any laboratories for a fast analysis where modifications on the commercial SFC system is not favorable. Thus, a suggestion to future work is not to validate the SFC used in this work but to extend the validation to multiple commercial SFC systems in the market and provide an overview of the accuracy and the applicability of applying the method developed in this work. Due to the time and supply limitation, only 17 solutes were studied so far. Validation of the suggested procedures, especially applying the “transferability of the free energies” in chapter 9, requires an analysis with a wider range of solutes. Not only the solutes, but also the variety of solid matrices can also be expanded. The surface chemistry of SIL-60, SIL-100 and SIL-300 are very similar with free hydroxyl groups. Spherical end-capped silicas could be the next targets to broaden the application of the framework build by this study on the analysis of solute-solid-interactions in sc-CO₂.

11 References

- [1] A. Tabernero, S. Cardea, Supercritical carbon dioxide techniques for processing microbial exopolysaccharides used in biomedical applications, *Mater. Sci. Eng. C*. 112 (2020) 110940. <https://doi.org/10.1016/j.msec.2020.110940>.
- [2] W.C. Tsai, Y. Wang, Progress of supercritical fluid technology in polymerization and its applications in biomedical engineering, *Prog. Polym. Sci.* 98 (2019) 101161. <https://doi.org/10.1016/j.progpolymsci.2019.101161>.
- [3] R.K. Kankala, Y.S. Zhang, S. Bin Wang, C.H. Lee, A.Z. Chen, Supercritical Fluid Technology: An Emphasis on Drug Delivery and Related Biomedical Applications, *Adv. Healthc. Mater.* 6 (2017). <https://doi.org/10.1002/adhm.201700433>.
- [4] A.R.C. Duarte, J.F. Mano, R.L. Reis, Supercritical fluids in biomedical and tissue engineering applications: A review, *Int. Mater. Rev.* 54 (2009) 214–222. <https://doi.org/10.1179/174328009X411181>.
- [5] V.P. Costa, M.E.M. Braga, J.P. Guerra, A.R.C. Duarte, C.M.M. Duarte, E.O.B. Leite, M.H. Gil, H.C. de Sousa, Development of therapeutic contact lenses using a supercritical solvent impregnation method, *J. Supercrit. Fluids*. 52 (2010) 306–316. <https://doi.org/10.1016/j.supflu.2010.02.001>.
- [6] T. Gamse, R. Marr, C. Wolf, K. Lederer, Supercritical CO₂ impregnation of polyethylene components for medical purposes, *Hem. Ind.* 61 (2007) 229–232. <https://doi.org/10.2298/HEMIND0704229G>.
- [7] A.A. Barros, C. Oliveira, R.L. Reis, E. Lima, A.R.C. Duarte, Ketoprofen-eluting biodegradable ureteral stents by CO₂ impregnation: In vitro study, *Int. J. Pharm.* 495 (2015) 651–659. <https://doi.org/10.1016/j.ijpharm.2015.08.040>.
- [8] P. Gurikov, I. Smirnova, Amorphization of drugs by adsorptive precipitation from supercritical solutions: A review, *J. Supercrit. Fluids*. 132 (2018) 105–125. <https://doi.org/10.1016/j.supflu.2017.03.005>.
- [9] K.E. Laintz, C.M. Wai, C.R. Yonker, R.D. Smith, Solubility of fluorinated metal diethyldithiocarbamates in Supercritical carbon dioxide, *J. Supercrit. Fluids*. 4 (1991) 194–198. [https://doi.org/10.1016/0896-8446\(91\)90008-T](https://doi.org/10.1016/0896-8446(91)90008-T).

- [10] U. Kopcak, R.S. Mohamed, Caffeine solubility in supercritical carbon dioxide/co-solvent mixtures, *J. Supercrit. Fluids*. 34 (2005) 209–214. <https://doi.org/10.1016/j.supflu.2004.11.016>.
- [11] J.F. Brennecke, C.A. Eckert, Phase equilibria for supercritical fluid process design, *AIChE J.* 35 (1989) 1409–1427. <https://doi.org/10.1002/aic.690350902>.
- [12] V.S.S. Gonçalves, P. Gurikov, J. Poejo, A.A. Matias, S. Heinrich, C.M.M. Duarte, I. Smirnova, Alginate-based hybrid aerogel microparticles for mucosal drug delivery, *Eur. J. Pharm. Biopharm.* 107 (2016) 160–170. <https://doi.org/10.1016/j.ejpb.2016.07.003>.
- [13] E. Kiran, P.G. Debenedetti, C.J. Peters, *Supercritical Fluids: Fundamentals and Applications*, Kemer, Antalya, Turkey, 1998.
- [14] L.T. Taylor, Supercritical fluid chromatography for the 21st century, *J. Supercrit. Fluids*. 47 (2009) 566–573. <https://doi.org/10.1016/j.supflu.2008.09.012>.
- [15] M. Saito, History of supercritical fluid chromatography: Instrumental development, *J. Biosci. Bioeng.* 115 (2013) 590–599. <https://doi.org/10.1016/j.jbiosc.2012.12.008>.
- [16] M.C. Henry, C.R. Yonker, Supercritical fluid chromatography, pressurized liquid extraction, and supercritical fluid extraction, *Anal. Chem.* 78 (2006) 3909–3915. <https://doi.org/10.1021/ac0605703>.
- [17] E. Lesellier, C. West, The many faces of packed column supercritical fluid chromatography - A critical review, *J. Chromatogr. A*. 1382 (2015) 2–46. <https://doi.org/10.1016/j.chroma.2014.12.083>.
- [18] M. Roth, Diffusion and thermodynamic measurements by supercritical fluid chromatography, *J. Microcolumn Sep.* 3 (1991) 173–184. <https://doi.org/10.1002/mcs.1220030302>.
- [19] M. Roth, Determination of Thermodynamic Properties by Supercritical Fluid Chromatography, *J. Chromatogr. A*. 1037 (2004) 369–391. <https://doi.org/10.1016/j.chroma.2003.10.126>.
- [20] P.J. Schoenmakers, Supercritical-fluid chromatography: Open columns vs packed columns, *J. High Resolut. Chromatogr.* 11 (1988) 278–282.

<https://doi.org/10.1002/jhrc.1240110311>.

- [21] J.G.M. Janssen, Supercritical-fluid chromatography in packed and open-tubular columns, Technische Universiteit Eindhoven, Eindhoven, 1991.
<https://doi.org/10.6100/IR357895>.
- [22] T.A. Berger, Packed Column SFC, The Royal Society of Chemistry, Newark, Delaware, USA, 1995.
- [23] M. Caude, D. Thiébaud, Practical Supercritical Fluid Chromatography and Extraction, Harwood Academic Publishers, Amsterdam, The Netherlands, 1999.
- [24] R. Span, W. Wagner, A new equation of state for carbon dioxide covering the fluid region from the triple-point temperature to 1100 K at pressures up to 800 MPa, J. Phys. Chem. Ref. Data. 25 (1996) 1509–1596.
<https://doi.org/10.1063/1.555991>.
- [25] J.M. Levy, W.M. Ritchey, Investigations of the uses of modifiers in supercritical fluid chromatography, J. Chromatogr. Sci. 24 (1986) 242–248.
<https://doi.org/10.1093/chromsci/24.6.242>.
- [26] A.L. Blilie, T. Greibrokk, Modifier Effects on Retention and Peak Shape in Supercritical Fluid Chromatography, Anal. Chem. 57 (1985) 2239–2242.
<https://doi.org/10.1021/ac00289a015>.
- [27] P. Mourier, P. Sassiati, M. Caude, R. Rosset, Retention and selectivity in carbon dioxide supercritical fluid chromatography with various stationary phases, J. Chromatogr. 353 (1986) 61–75. [https://doi.org/10.1016/S0021-9673\(01\)87077-1](https://doi.org/10.1016/S0021-9673(01)87077-1).
- [28] T.S. Reighard, S.T. Lee, S. V. Olesik, Determination of methanol/CO₂ and acetonitrile/CO₂ vapor-liquid phase equilibria using a variable-volume view cell, Fluid Phase Equilib. 123 (1996) 215–230. [https://doi.org/10.1016/0378-3812\(96\)03063-4](https://doi.org/10.1016/0378-3812(96)03063-4).
- [29] H.G. Janssen, P.J. Schoenmakers, C.A. Cramers, Mobile and stationary phases for SFC: Effects of using modifiers, Mikrochim. Acta. 104 (1991) 337–351. <https://doi.org/10.1007/BF01245520>.
- [30] T.A. Berger, J.F. Deye, Composition and Density Effects Using

- Methanol/Carbon Dioxide in Packed Column Supercritical Fluid Chromatography, *Anal. Chem.* 62 (1990) 1181–1185.
<https://doi.org/10.1021/ac00210a017>.
- [31] J.G.M. Janssen, P.J. Schoenmakers, C.A. Cramers, A fundamental study of the effects of modifiers in supercritical fluid chromatography, *J. High Resolut. Chromatogr.* 12 (1989) 645–651. <https://doi.org/10.1002/jhrc.1240121003>.
- [32] J.F. Deye, T.A. Berger, A.G. Anderson, Nile Red as a Solvatochromic Dye for Measuring Solvent Strength in Normal Liquids and Mixtures of Normal Liquids with Supercritical and Near Critical Fluids, *Anal. Chem.* 62 (1990) 615–622.
<https://doi.org/10.1021/ac00205a015>.
- [33] G.S. Gurdial, S.J. Macnaughton, D.L. Tomasko, N.R. Foster, Influence of Chemical Modifiers on the Solubility of o- and m-Hydroxybenzoic Acid in Supercritical CO₂, *Ind. Eng. Chem. Res.* 32 (1993) 1488–1497.
<https://doi.org/10.1021/ie00019a024>.
- [34] K.M. Payne, B.J. Tarbet, J.S. Bradshaw, K.E. Markides, M.L. Lee, Simultaneous Deactivation and Coating of Porous Silica Particles for Microcolumn Supercritical Fluid Chromatography, *Anal. Chem.* 62 (1990) 1379–1384. <https://doi.org/10.1021/ac00213a006>.
- [35] W. Zou, J.G. Dorsey, T.L. Chester, Modifier effects on column efficiency in packed-column supercritical fluid chromatography, *Anal. Chem.* 72 (2000) 3620–3626. <https://doi.org/10.1021/ac991417u>.
- [36] C. West, E. Lesellier, Effects of modifiers in subcritical fluid chromatography on retention with porous graphitic carbon, *J. Chromatogr. A.* 1087 (2005) 64–76.
<https://doi.org/10.1016/j.chroma.2005.03.104>.
- [37] K.D. Bartle, A.A. Clifford, S.A. Jafar, Measurement of Solubility in Supercritical Fluids Using Chromatographic Retention: The Solubility of Fluorene, Phenanthrene, and Pyrene in Carbon Dioxide, *J. Chem. Eng. Data.* 35 (1990) 355–360. <https://doi.org/10.1021/je00061a037>.
- [38] K.D. Bartle, A.A. Clifford, S.A. Jafar, Relationship between retention of a solid solute in liquid and supercritical fluid chromatography and its solubility in the mobile phase, *J. Chem. Soc. Faraday Trans.* 86 (1990) 855–860.
<https://doi.org/10.1039/FT9908600855>.

- [39] K.D. Bartle, A.A. Clifford, S.A. Jafar, J.P. Kithinji, G.F. Shilstone, Use of chromatographic retention measurements to obtain solubilities in a liquid or supercritical fluid mobile phase, *J. Chromatogr.* 517 (1990) 459–476. [https://doi.org/10.1016/S0021-9673\(01\)95741-3](https://doi.org/10.1016/S0021-9673(01)95741-3).
- [40] C.M. Cowey, K.D. Bartle, M.D. Burford, A.A. Clifford, S. Zhu, N.G. Smart, N.D. Tinker, Solubility of Ferrocene and a Nickel Complex in Supercritical Fluids, *J. Chem. Eng. Data.* 40 (1995) 1217–1221. <https://doi.org/10.1021/je00022a015>.
- [41] K. Chandler, F.L.L. Pouillot, C.A. Eckert, Phase equilibria of alkanes in natural gas systems. 3. Alkanes in carbon dioxide, *J. Chem. Eng. Data.* 41 (1996) 6–10. <https://doi.org/10.1021/je950138a>.
- [42] J. -J Shim, K.P. Johnston, Molecular thermodynamics of solute-polymer-supercritical fluid systems, *AIChE J.* 37 (1991) 607–616. <https://doi.org/10.1002/aic.690370414>.
- [43] P.D. Condo, S.R. Sumpter, M.L. Lee, K.P. Johnston, Partition Coefficients and Polymer-Solute Interaction Parameters by Inverse Supercritical Fluid Chromatography, *Ind. Eng. Chem. Res.* 35 (1996) 1115–1123. <https://doi.org/https://doi.org/10.1021/ie950356x>.
- [44] N. Wang, K. Hattori, S. Takishima, H. Masuoka, Measurement and prediction of vapor-liquid equilibrium ratios for solutes at infinite dilution in CO₂+polyvinyl acetate system at high pressures, *Kagaku Kogaku Ronbunshu.* 17 (1991) 1138–1145. <https://doi.org/10.1252/kakoronbunshu.17.1138>.
- [45] J.J. Shim, Distribution of Solutes between Polymer and Supercritical Fluid by Inverse Supercritical Fluid Chromatography, *Korean J. Chem. Eng.* 19 (2002) 146–152. <https://doi.org/10.1007/BF02706888>.
- [46] J.J. Shim, K.P. Johnston, Phase equilibria, partial molar enthalpies, and partial molar volumes determined by supercritical fluid chromatography, *J. Phys. Chem.* 95 (1991) 353–360. <https://doi.org/10.1021/j100154a064>.
- [47] B. Spicka, A. Cortesi, M. Fermeglia, I. Kikic, Determination of partial molar volumes at infinite dilution using SFC technique, *J. Supercrit. Fluids.* 7 (1994) 171–176. [https://doi.org/10.1016/0896-8446\(94\)90022-1](https://doi.org/10.1016/0896-8446(94)90022-1).
- [48] Z.S. Gonenc, U. Akman, A.K. Sunol, Articles Solubility and Partial Molar Volumes of Naphthalene, Phenanthrene, Benzoic Acid, and 2-

- Methoxynaphthalene in Supercritical Carbon Dioxide, *J. Chem. Eng. Data.* 40 (1995) 799–804.
- [49] Z.S. Gonenc, U. Akman, A.K. Sunol, Solubility / retention relationships in supercritical-fluid chromatography, *Can. J. Chem. Eng.* 73 (1995) 267–271. <https://doi.org/10.1002/cjce.5450730217>.
- [50] Y.P. Jeon, M. Roth, Y.J. Kwon, Infinite-dilution partial molar properties of azulene and acenaphthylene in supercritical carbon dioxide, *J. Phys. Chem. B.* 103 (1999) 8132–8136. <https://doi.org/10.1021/jp991122k>.
- [51] Y.P. Jeon, M. Roth, Y.J. Kwon, Infinite-dilution partial molar properties of naphthalene and biphenyl in carbon dioxide from supercritical fluid chromatography: Composition effects in the stationary phase, *J. Phys. Chem. A.* 104 (2000) 5396–5400. <https://doi.org/10.1021/jp000416z>.
- [52] A. Cortesi, I. Kikic, B. Spicka, K. Magoulas, D. Tassios, Determination of Partial Molar Volumes at Infinite Dilution of Alcohols and Terpenes in Supercritical Carbon Dioxide, *J. Supercrit. Fluids.* 9 (1996) 141–145. [https://doi.org/10.1016/S0896-8446\(96\)90024-8](https://doi.org/10.1016/S0896-8446(96)90024-8).
- [53] T. Funazukuri, C.Y. Kong, S. Kagei, Infinite-Dilution Binary Diffusion Coefficient, Partition Ratio, and Partial Molar Volume for Ubiquinone CoQ10 in Supercritical Carbon Dioxide, *Ind. Eng. Chem. Res.* 41 (2002) 2812–2818. <https://doi.org/10.1021/ie0109096>.
- [54] T. Funazukuri, C.Y. Kong, S. Kagei, Binary diffusion coefficients, partition ratios and partial molar volumes at infinite dilution for b-carotene and a-tocopherol in supercritical carbon dioxide, *J. Supercrit. Fluids.* 27 (2003) 85–96. [https://doi.org/10.1016/S0896-8446\(02\)00209-7](https://doi.org/10.1016/S0896-8446(02)00209-7).
- [55] B.O. Brown, A.J. Kishbaugh, M.E. Paulaitis, Experimental Determination of Enhancement Factors from Supercritical-Fluid Chromatography, *Fluid Phase Equilib.* 36 (1987) 247–261. [https://doi.org/10.1016/0378-3812\(87\)85027-6](https://doi.org/10.1016/0378-3812(87)85027-6).
- [56] C.B. Kautz, U.H. Dahlmann, G.M. Schneider, Capacity ratios in supercritical fluid chromatography. Effect of mobile and stationary phases on hexasubstituted benzenes, *J. Chromatogr. A.* 776 (1997) 305–309. [https://doi.org/10.1016/S0021-9673\(97\)00456-1](https://doi.org/10.1016/S0021-9673(97)00456-1).
- [57] M. Roth, Partial molar properties from solute retention in supercritical fluid

- chromatography: thermodynamic framework, advantages, and limitations, *Fluid Phase Equilib.* 148 (1998) 189–199. [https://doi.org/10.1016/S0378-3812\(97\)00333-6](https://doi.org/10.1016/S0378-3812(97)00333-6).
- [58] L.R. Snyder, M.A. Quarry, Computer simulation in HPLC method development. reducing the error of predicted retention times, *J. Liq. Chromatogr.* 10 (1987) 1789–1820. <https://doi.org/10.1080/01483918708066799>.
- [59] P.J. Schoenmakers, H.A.H. Billiet, R. Tijssen, L. De Galan, GRADIENT SELECTION IN REVERSED-PHASE LIQUID CHROMATOGRAPHY, *J. Chromatogr.* 149 (1978) 519–537. [https://doi.org/https://doi.org/10.1016/S0021-9673\(00\)81008-0](https://doi.org/https://doi.org/10.1016/S0021-9673(00)81008-0).
- [60] A. Kaibara, C. Hohda, N. Hirata, M. Hirose, T. Nakagawa, Evaluation of Solute Hydrophobicity by Reversed-Phase High Performance Liquid Chromatography Using Aqueous Binary Mobile Phases, *Chromatographia.* 29 (1990) 275–288.
- [61] Y.W. Lee, K.H. Row, M.S. So, I.A. Polunina, A.V. Larin, Reversed-phase hplc retention of deoxyribonucleosides as a function of mobile phase composition, *J. Liq. Chromatogr.* 18 (1995) 3077–3089. <https://doi.org/10.1080/10826079508010434>.
- [62] A. Nahum, C. Horvath, Surface silanols in silica-bonded hydrocarbonaceous stationary phases: I. dual retention mechanism in reversed-phase chromatography, *J. Chromatogr.* 203 (1981) 53–63.
- [63] K. BIJ, C. Horvath, W.R. Melander, A. Nahum, Surface silanols in silica-bonded hydrocarbonaceous stationary phases: II. Irregular retention behavior and effect of silanol masking, *J. Chromatogr.* 203 (1981) 65–84.
- [64] E. Lesellier, K. Gurdale, A. Tchapla, Separation of cis/trans isomers of β -carotene by supercritical fluid chromatography, *J. Chromatogr. A.* 844 (1999) 307–320. [https://doi.org/10.1016/S0021-9673\(99\)00364-7](https://doi.org/10.1016/S0021-9673(99)00364-7).
- [65] T. Bamba, E. Fukusaki, S. Kajiyama, K. Ute, T. Kitayama, A. Kobayashi, High-resolution analysis of polyprenols by supercritical fluid chromatography, *J. Chromatogr. A.* 911 (2001) 113–117. [https://doi.org/10.1016/S0021-9673\(00\)01250-4](https://doi.org/10.1016/S0021-9673(00)01250-4).
- [66] E. Grushka, N. Grinberg, *Advances in Chromatography: Volume 48*, CRC Press, 2009.

- [67] M.H. Abraham, A. Ibrahim, A.M. Zissimos, Determination of sets of solute descriptors from chromatographic measurements, *J. Chromatogr. A.* 1037 (2004) 29–47. <https://doi.org/10.1016/j.chroma.2003.12.004>.
- [68] C. West, G. Guenegou, Y. Zhang, L. Morin-Allory, Insights into chiral recognition mechanisms in supercritical fluid chromatography. II. Factors contributing to enantiomer separation on tris-(3,5-dimethylphenylcarbamate) of amylose and cellulose stationary phases, *J. Chromatogr. A.* 1218 (2011) 2033–2057. <https://doi.org/10.1016/j.chroma.2010.11.085>.
- [69] D. Pyo, W.B. Li, M.L. Lee, J.D. Weckwerth, P.W. Carr, Addition of methanol to the mobile phase in packed capillary column supercritical fluid chromatography - Retention mechanisms from linear solvation energy relationships, *J. Chromatogr. A.* 15 (1996) 291–298. [https://doi.org/10.1016/S0021-9673\(96\)00554-7](https://doi.org/10.1016/S0021-9673(96)00554-7).
- [70] M. Alnaief, I. Smirnova, Effect of surface functionalization of silica aerogel on their adsorptive and release properties, *J. Non. Cryst. Solids.* 356 (2010) 1644–1649. <https://doi.org/10.1016/j.jnoncrysol.2010.06.027>.
- [71] P.B. Wagh, S. V. Ingale, Comparison of some physico-chemical properties of hydrophilic and hydrophobic silica aerogels, *Ceram. Int.* 28 (2002) 43–50. [https://doi.org/10.1016/S0272-8842\(01\)00056-6](https://doi.org/10.1016/S0272-8842(01)00056-6).
- [72] Z. Ulker, C. Erkey, An emerging platform for drug delivery: Aerogel based systems, *J. Control. Release.* 177 (2014) 51–63. <https://doi.org/10.1016/j.jconrel.2013.12.033>.
- [73] C.A. García-González, M. Alnaief, I. Smirnova, Polysaccharide-based aerogels - Promising biodegradable carriers for drug delivery systems, *Carbohydr. Polym.* 86 (2011) 1425–1438. <https://doi.org/10.1016/j.carbpol.2011.06.066>.
- [74] M. Schmidt, F. Schwertfeger, Applications for silica aerogel products, *J. Non. Cryst. Solids.* 225 (1998) 364–368. [https://doi.org/10.1016/S0022-3093\(98\)00054-4](https://doi.org/10.1016/S0022-3093(98)00054-4).
- [75] I. Smirnova, P. Gurikov, Aerogel production: Current status, research directions, and future opportunities, *J. Supercrit. Fluids.* 134 (2018) 228–233. <https://doi.org/10.1016/j.supflu.2017.12.037>.
- [76] L.T. Zhuravlev, The surface chemistry of amorphous silica. Zhuravlev model,

- Colloids Surfaces A Physicochem. Eng. Asp. 173 (2000) 1–38.
[https://doi.org/10.1016/S0927-7757\(00\)00556-2](https://doi.org/10.1016/S0927-7757(00)00556-2).
- [77] L. Corredor, B. Maini, M. Husein, Improving polymer flooding by addition of surface modified nanoparticles, Soc. Pet. Eng. - SPE Asia Pacific Oil Gas Conf. Exhib. 2018, APOGCE 2018. (2018). <https://doi.org/10.2118/192141-ms>.
- [78] I. Smirnova, P. Gurikov, Aerogels in Chemical Engineering: Strategies Toward Tailor-Made Aerogels, Annu. Rev. Chem. Biomol. Eng. 8 (2017) 307–334.
<https://doi.org/10.1146/annurev-chembioeng-060816-101458>.
- [79] D.M. Heaton, K.D. Bartle, A.A. Clifford, M.S. Klee, T.A. Berger, Retention Prediction Based on Molecular Interactions in Packed-Column Supercritical Fluid Chromatography, Anal. Chem. 66 (1994) 4253–4257.
<https://doi.org/10.1021/ac00095a021>.
- [80] P. Vajda, G. Guiochon, Determination of the column hold-up volume in supercritical fluid chromatography using nitrous-oxide, J. Chromatogr. A. 1309 (2013) 96–100. <https://doi.org/10.1016/j.chroma.2013.07.114>.
- [81] D. Åsberg, M. Enmark, J. Samuelsson, T. Fornstedt, Evaluation of co-solvent fraction, pressure and temperature effects in analytical and preparative supercritical fluid chromatography, J. Chromatogr. A. 1374 (2014) 254–260.
<https://doi.org/10.1016/j.chroma.2014.11.045>.
- [82] Empower 3, Waters Corporation, Massachusetts, USA, 2010.
- [83] E. Forss, D. Haupt, O. Ståhlberg, M. Enmark, J. Samuelsson, T. Fornstedt, Chemometric evaluation of the combined effect of temperature, pressure, and co-solvent fractions on the chiral separation of basic pharmaceuticals using actual vs set operational conditions, J. Chromatogr. A. 1499 (2017) 165–173.
<https://doi.org/10.1016/j.chroma.2017.03.077>.
- [84] C. West, E. Lemasson, S. Bertin, P. Hennig, E. Lesellier, An improved classification of stationary phases for ultra-high performance supercritical fluid chromatography, J. Chromatogr. A. 1440 (2016) 212–228.
<https://doi.org/10.1016/j.chroma.2016.02.052>.
- [85] K. Miyabe, Moment analysis of chromatographic behavior in reversed-phase liquid chromatography, J. Sep. Sci. 32 (2009) 757–770.
<https://doi.org/10.1002/jssc.200800607>.

- [86] B. Howard G, *Chromatography Fundamentals, Part VI: The Gaussian Distribution and Moment Analysis*, LCGC North Am. 37 (2019) 269–273.
- [87] G. Guiochon, A. Felinger, D.G. Shirazi, *Fundamentals of Preparative and Nonlinear Chromatography*, 2nd ed., 2006.
- [88] M. Al-Bokari, D. Cherrak, G. Guiochon, Determination of the porosities of monolithic columns by inverse size-exclusion chromatography, *J. Chromatogr. A.* 975 (2002) 275–284. [https://doi.org/10.1016/S0021-9673\(02\)01271-2](https://doi.org/10.1016/S0021-9673(02)01271-2).
- [89] J.A. Vente, H. Bosch, A.B. De Haan, P.J.T. Bussmann, Evaluation of sugar sorption isotherm measurement by frontal analysis under industrial processing conditions, *J. Chromatogr. A.* 1066 (2005) 71–79. <https://doi.org/10.1016/j.chroma.2004.12.071>.
- [90] M. Sun, S. Ruiz, M. Johannsen, I. Smirnova, P. Gurikov, Retention Characteristics of Silica Materials in Carbon Dioxide/Methanol Mixtures Studied by Inverse Supercritical Fluid Chromatography, *J. Chromatogr. A.* 1588 (2019) 127–136. <https://doi.org/10.1016/j.chroma.2018.12.053>.
- [91] A.R. Bazaev, I.M. Abdulagatov, E.A. Bazaev, A.A. Abdurashidova, A.E. Ramazanov, PVT measurements for pure methanol in the near-critical and supercritical regions, *J. Supercrit. Fluids.* 41 (2007) 217–226. <https://doi.org/10.1016/j.supflu.2006.09.012>.
- [92] T.A. Berger, Density of methanol-carbon dioxide mixtures at three temperatures: Comparison with vapor-liquid equilibria measurements and results obtained from chromatography, *J. High Resolut. Chromatogr.* 14 (1991) 312–316. <https://doi.org/10.1002/jhrc.1240140504>.
- [93] J.W. Ziegler, J.G. Dorsey, J.G. Dorsey, T.L. Chester, D.P. Innis, Estimation of Liquid—Vapor Critical Loci for CO₂-Solvent Mixtures Using a Peak-Shape Method, *Anal. Chem.* 67 (1995) 456–461. <https://doi.org/10.1021/ac00098a034>.
- [94] S.D. Yeo, S.J. Park, J.W. Kim, J.C. Kim, Critical Properties of Carbon Dioxide +Methanol, +Ethanol, +1-Propanol, and +1-Butanol, *J. Chem. Eng. Data.* 45 (2000) 932–935. <https://doi.org/10.1021/je000104p>.
- [95] D. Sanli, C. Erkey, Silylation from supercritical carbon dioxide: a powerful technique for modification of surfaces, *J. Mater. Sci.* 50 (2015) 7159–7181.

<https://doi.org/10.1007/s10853-015-9281-9>.

- [96] B.C. Bunker, D.M. Haaland, T.A. Michalske, W.L. Smith, Kinetics of dissociative chemisorption on strained edge-shared surface defects on dehydroxylated silica, *Surf. Sci.* 222 (1989) 95–118.
[https://doi.org/10.1016/0039-6028\(89\)90337-3](https://doi.org/10.1016/0039-6028(89)90337-3).
- [97] J. Kern, M. Johannsen, Modeling adsorption on energetically heterogeneous surfaces with an extended SAFT-VR approach, *J. Supercrit. Fluids.* 133 (2018) 70–76. <https://doi.org/10.1016/j.supflu.2017.07.014>.
- [98] P. Vajda, G. Guiochon, Modifier adsorption in supercritical fluid chromatography onto silica surface, *J. Chromatogr. A.* 1305 (2013) 293–299.
<https://doi.org/10.1016/j.chroma.2013.06.075>.
- [99] P. Vajda, G. Guiochon, Surface excess isotherms of organic solvent mixtures in a system made of liquid carbon dioxide and a silicagel surface, *J. Chromatogr. A.* 1308 (2013) 139–143.
<https://doi.org/10.1016/j.chroma.2013.07.113>.
- [100] K. Robards, P. Jackson, P. Haddad, *Principles and Practice of Modern Chromatographic Methods*, 1st Editio, 2012.
- [101] E. Grushka, P.R. Brown, J.C. Giddings, *Advances in Chromatography: Volume 30*, Taylor & Francis, 1989.
- [102] M.J. Kamlet, P.W. Carr, R.W. Taft, M.H. Abraham, Linear Solvation Energy Relationships. 13. Relationship between the Hildebrand Solubility Parameter, δH , and the Solvatochromic Parameter, π^* , *J. Am. Chem. Soc.* 103 (1981) 6062–6066. <https://doi.org/10.1021/ja00410a013>.
- [103] R. Harikrishnan, M.P. Srinivasan, C.B. Ching, Adsorption of ethyl benzene on activated carbon from supercritical CO₂, *AIChE J.* 44 (1998) 2620–2627.
<https://doi.org/10.1002/aic.690441205>.
- [104] C.H. Lochmüller, L.P. Mink, Adsorption isotherms of ethyl acetate modifier on silica from supercritical carbon dioxide, *J. Chromatogr. A.* 409 (1987) 55–60.
[https://doi.org/10.1016/S0021-9673\(01\)86782-0](https://doi.org/10.1016/S0021-9673(01)86782-0).
- [105] R. Mueller, H.K. Kammler, K. Wegner, S.E. Pratsinis, OH surface density of SiO₂ and TiO₂ by thermogravimetric analysis, *Langmuir.* 19 (2003) 160–165.

<https://doi.org/10.1021/la025785w>.

- [106] X. Jin, N.H.L. Wang, G. Tarjus, J. Talbot, Irreversible adsorption on nonuniform surfaces: The random site model, *J. Phys. Chem.* 97 (1993) 4256–4258. <https://doi.org/10.1021/j100119a003>.
- [107] M.H. Abraham, W.E. Acree, Descriptors for Pentane-2,4-dione and Its Derivatives, *J. Solution Chem.* 46 (2017) 1625–1638. <https://doi.org/10.1007/s10953-017-0667-y>.
- [108] K.U. Goss, Predicting the equilibrium partitioning of organic compounds using just one linear solvation energy relationship (LSER), *Fluid Phase Equilib.* 233 (2005) 19–22. <https://doi.org/10.1016/j.fluid.2005.04.006>.
- [109] C.F. Poole, T.C. Ariyasena, N. Lenca, Estimation of the environmental properties of compounds from chromatographic measurements and the solvation parameter model, *J. Chromatogr. A.* 1317 (2013) 85–104. <https://doi.org/10.1016/j.chroma.2013.05.045>.
- [110] C. West, E. Lesellier, Characterisation of stationary phases in supercritical fluid chromatography with the solvation parameter model. V. Elaboration of a reduced set of test solutes for rapid evaluation, *J. Chromatogr. A.* 1169 (2007) 205–219. <https://doi.org/10.1016/j.chroma.2007.09.011>.
- [111] S. Lambert-Lacroix, L. Zwald, Robust regression through the Huber's criterion and adaptive lasso penalty, *Electron. J. Stat.* 5 (2011) 1015–1053. <https://doi.org/10.1214/11-EJS635>.
- [112] S. Studzińska, B. Buszewski, Linear solvation energy relationships in the determination of specificity and selectivity of stationary phases, *Chromatographia.* 75 (2012) 1235–1246. <https://doi.org/10.1007/s10337-012-2310-9>.
- [113] H. Bui, T. Masquelin, T. Perun, T. Castle, J. Dage, M.S. Kuo, Investigation of retention behavior of drug molecules in supercritical fluid chromatography using linear solvation energy relationships, *J. Chromatogr. A.* 1206 (2008) 186–195. <https://doi.org/10.1016/j.chroma.2008.08.050>.
- [114] M. Vitha, P.W. Carr, The chemical interpretation and practice of linear solvation energy relationships in chromatography, *J. Chromatogr. A.* 1126 (2006) 143–194. <https://doi.org/10.1016/j.chroma.2006.06.074>.

- [115] C. West, Y. Zhang, L. Morin-Allory, Insights into chiral recognition mechanisms in supercritical fluid chromatography. I. Non-enantiospecific interactions contributing to the retention on tris-(3,5-dimethylphenylcarbamate) amylose and cellulose stationary phases, *J. Chromatogr. A.* 1218 (2011) 2019–2032. <https://doi.org/10.1016/j.chroma.2010.11.084>.
- [116] W. Kiridena, C.F. Poole, Influence of solute size and site-specific surface interactions on the prediction of retention in liquid chromatography using the solvation parameter model, *Analyst.* 123 (1998) 1265–1270. <https://doi.org/10.1039/a801231h>.
- [117] C. West, E. Lesellier, Effects of mobile phase composition on retention and selectivity in achiral supercritical fluid chromatography, *J. Chromatogr. A.* 1302 (2013) 152–162. <https://doi.org/10.1016/j.chroma.2013.06.003>.
- [118] M. Roth, Thermodynamics of Modifier Effects in Supercritical Fluid Chromatography, *J. Phys. Chem.* 100 (1996) 2372–2375. <https://doi.org/10.1021/jp952450x>.
- [119] J.A. Blackwell, R.W. Stringham, Characterization of Temperature Dependent Modifier Effects in SFC Using Linear Solvation Energy Relationships, *Chromatographia.* 46 (1997) 301–308. <https://doi.org/10.1007/BF02496323>.
- [120] M.H. Fatemi, H. Malekzadeh, H. Shamseddin, Prediction of supercritical fluid chromatographic retention factors at different percents of organic modifiers in mobile phase, *J. Sep. Sci.* 32 (2009) 653–659. <https://doi.org/10.1002/jssc.200800594>.
- [121] D. Bolten, M. Johannsen, Influence of 2-Propanol on Adsorption Equilibria of α - and δ -Tocopherol from Supercritical Carbon Dioxide on Silica Gel, *J. Chem. Eng. Data.* 51 (2006) 2132–2137.
- [122] J.W. Millard, F.A. Alvarez-Núñez, S.H. Yalkowsky, Solubilization by cosolvents: Establishing useful constants for the log-linear model, *Int. J. Pharm.* 245 (2002) 153–166. [https://doi.org/10.1016/S0378-5173\(02\)00334-4](https://doi.org/10.1016/S0378-5173(02)00334-4).
- [123] S. Ottiger, J. Kluge, A. Rajendran, M. Mazzotti, Enantioseparation of 1-phenyl-1-propanol on cellulose-derived chiral stationary phase by supercritical fluid chromatography II. Non-linear isotherm, *J. Chromatogr. A.* 1162 (2007) 74–82. <https://doi.org/10.1016/j.chroma.2007.01.115>.

- [124] M. Enmark, P. Forssén, J. Samuelsson, T. Fornstedt, Determination of adsorption isotherms in supercritical fluid chromatography, *J. Chromatogr. A.* 1312 (2013) 124–133. <https://doi.org/10.1016/j.chroma.2013.09.007>.
- [125] M. Enmark, J. Samuelsson, E. Forss, P. Forssén, T. Fornstedt, Investigation of plateau methods for adsorption isotherm determination in supercritical fluid chromatography, *J. Chromatogr. A.* 1354 (2014) 129–138. <https://doi.org/10.1016/j.chroma.2014.05.070>.
- [126] C. Wenda, A. Rajendran, Enantioseparation of flurbiprofen on amylose-derived chiral stationary phase by supercritical fluid chromatography, *J. Chromatogr. A.* 1216 (2009) 8750–8758. <https://doi.org/10.1016/j.chroma.2009.02.047>.
- [127] M. Sun, Z. Ülker, Z. Chen, S. Deeptanshu, M. Johannsen, C. Erkey, P. Gurikov, Development and Validation of Retention Models in Supercritical Fluid Chromatography for Impregnation Process Design, *Appl. Sci.* 11 (2021). <https://doi.org/10.3390/app11157106>.
- [128] E. Glenne, K. Öhlén, H. Leek, M. Klarqvist, J. Samuelsson, T. Fornstedt, A closer study of methanol adsorption and its impact on solute retentions in supercritical fluid chromatography, *J. Chromatogr. A.* 1442 (2016) 129–139. <https://doi.org/10.1016/j.chroma.2016.03.006>.
- [129] J. Ko, J.C. Ford, Comparison of selected retention models in reversed-phase liquid chromatography, *J. Chromatogr. A.* 913 (2001) 3–13.
- [130] C.F. Poole, N. Lenca, Applications of the solvation parameter model in reversed-phase liquid chromatography, *J. Chromatogr. A.* 1486 (2017) 2–19. <https://doi.org/10.1016/j.chroma.2016.05.099>.
- [131] P. Vajda, G. Guiochon, Effects of the back pressure and the temperature on the finite layer thickness of the adsorbed phase layer in supercritical fluid chromatography, *J. Chromatogr. A.* 1309 (2013) 41–47. <https://doi.org/10.1016/j.chroma.2013.08.028>.
- [132] R. Valentin, B. Bonelli, E. Garrone, F. Di Renzo, F. Quidnard, Accessibility of the functional group of chitosan aerogel probed by FT-IR-monitored deuteration, *Biomacromolecules.* 8 (2007) 3646–3650. <https://doi.org/10.1021/bm070391a>.
- [133] I. Ushiki, N. Takahashi, T. Shimizu, Y. Sato, M. Ota, R.L. Smith, H. Inomata,

- Adsorption equilibria of rhodium acetylacetonate with MCM-41 , MSU-H , and HMS silica substrates in supercritical carbon dioxide for preparing catalytic mesoporous materials, *J. Supercrit. Fluids.* 120 (2017) 240–248.
<https://doi.org/10.1016/j.supflu.2016.05.032>.
- [134] I. Ushiki, M. Ota, Y. Sato, H. Inomata, VOCs (acetone, toluene, and n -hexane) adsorption equilibria on mesoporous silica (MCM-41) over a wide range of supercritical carbon dioxide conditions: Experimental and theoretical approach by the Dubinin – Astakhov equation, *Fluid Phase Equilib.* 403 (2015) 78–84.
<https://doi.org/10.1016/j.fluid.2015.06.019>.
- [135] I. Ushiki, M. Ota, Y. Sato, H. Inomata, Measurements and Dubinin – Astakhov correlation of adsorption equilibria of toluene, acetone, n-hexane, n-decane and methanol solutes in supercritical carbon dioxide on activated carbon at temperature from 313 to 353 K and at pressure from 4.2 to 15.0 MPa, *Fluid Phase Equilib.* 344 (2013) 101–107. <https://doi.org/10.1016/j.fluid.2013.01.014>.
- [136] O. Aschenbrenner, N. Dahmen, K. Schaber, E. Dinjus, Adsorption of Dimethyl (1,5-cyclooctadiene) platinum on Porous Supports in Supercritical Carbon Dioxide, *Ind. Eng. Chem. Res.* 47 (2008) 3150–3155.
<https://doi.org/10.1021/ie071221h>.
- [137] H. Xing, B. Su, Q. Ren, Y. Yang, Adsorption equilibria of artemisinin from supercritical carbon dioxide on silica gel, *J. Supercrit. Fluids.* 49 (2009) 189–195. <https://doi.org/10.1016/j.supflu.2009.01.003>.
- [138] A. Tarafder, K. Kaczmarek, D.P. Poe, G. Guiochon, Use of the isopycnic plots in designing operations of supercritical fluid chromatography. V. Pressure and density drops using mixtures of carbon dioxide and methanol as the mobile phase, *J. Chromatogr. A.* 1258 (2012) 136–151.
<https://doi.org/10.1016/j.chroma.2012.08.023>.

12 Appendix

12.1 Introduction to REFPROP

REFPROP is said to be based on the most accurate pure fluid and mixture models currently available [138]. It implements three models for the thermodynamic properties of pure fluids: equations of state explicit in Helmholtz energy, the modified Benedict-Webb-Rubin equation of state, and an extended corresponding states (ECS) model. Mixture calculations employ a model that applies mixing rules to the Helmholtz energy of the mixture components, using a departure function to account for the departure from ideal mixing.

12.2 A statistical test for outliers

To compare the Mahalanobis' distances of a set of data to a chi-square distribution with the same degree of freedom is a method to determine whether a data point may be an outlier and whether the data may have a multivariate normal distribution. When the probability is smaller than 0.01, the solute shall be considered as an outlier. This method has been applied for the 17 solutes and the probability of them are all higher than 0.01, therefore none point shall be treated as outlier based on this test.

Table 12.1: Mahalanobis' Distance.

Solute	E	S	A	B	V	L	Mahalanobis' Distance	Probability chi-square cumulative
Toluene	0.58	0.63	0.00	0.12	0.8573	3.430	2.426	0.877
Benzene	0.56	0.69	0.00	0.12	0.7164	2.958	2.883	0.823
Caffeine	1.48	1.90	0.00	1.27	1.3632	7.793	13.045	0.042
Benzoic Acid	0.75	1.08	0.57	0.44	0.9317	4.533	4.168	0.654
Phenol	0.78	0.90	0.50	0.39	0.7751	3.777	3.516	0.742
Vanillin	1.02	1.46	0.44	0.76	1.1313	5.860	3.135	0.792
Naphthalene	1.27	1.02	0.00	0.17	1.0854	5.332	2.584	0.859
Anthracene	1.99	1.34	0.00	0.23	1.4544	7.706	11.860	0.06
p-Nitrotoluene	0.85	1.20	0.00	0.21	1.0315	4.911	3.929	0.686
Nitrobenzene	0.83	1.26	0.00	0.21	0.8906	4.439	6.398	0.380
Anisole	0.62	0.79	0.00	0.33	0.9160	3.803	2.278	0.893
p-Cresol	0.81	0.85	0.50	0.39	0.9160	4.248	4.173	0.653
o-Nitrophenol	0.96	1.24	0.11	0.35	0.9493	4.769	1.736	0.942
Butyl benzoate	0.64	1.05	0.00	0.46	1.4953	6.022	9.545	0.145
Ethyl benzoate	0.64	1.04	0.00	0.45	1.2135	1.214	8.306	0.217
Pyridine	0.60	0.82	0.00	0.40	0.6753	0.675	5.972	0.426
Nicotinamide	1.04	1.68	0.49	0.94	0.9317	0.932	10.046	0.123

12.3 Experimental data for LSER

Table 12.2: Experimental $\ln k$ at 4 pressures of SIL-60.

SOLUTES	150 bar	200 bar	250 bar	300 bar
Toluene	-2.70	-2.51	-2.34	-1.61
Benzene	-2.70	-2.51	-2.34	-1.65
Caffeine	1.75	1.94	1.99	2.81
Benzoic Acid	0.14	0.20	0.29	1.33
Phenol	0.24	0.34	0.39	1.40
Vanillin	0.65	0.62	0.58	1.83
Naphthalene	-1.61	-1.46	-1.44	-0.91
Anthracene	-0.67	-0.80	-0.84	-0.32
p-Nitrotoluene	-1.14	-1.20	-1.01	-0.01
Nitrobenzene	-1.05	-1.15	-0.97	-0.09
Anisole	-1.81	-2.14	-1.74	-0.32
p-Cresol	0.20	0.23	0.38	1.58
o-Nitrophenol	-1.27	-1.36	-1.17	0.08
Butylbenzoate	-1.68	-1.51	-1.51	-1.61
Ethyl Benzoate	-1.63	-1.36	-1.42	-1.35
Pyridine	0.33	0.47	0.55	1.88
Nicotinamide	2.77	3.03	3.40	3.82

Table 12.3: Experimental $\ln k$ at 4 pressures of SIL-100.

SOLUTES	150 bar	200 bar	250 bar	300 bar
Toluene	-2.48	-2.42	-2.55	-2.59
Benzene	-2.44	-2.37	-2.51	-2.51
Caffeine	0.77	0.60	0.49	0.39
Benzoic Acid	-0.63	-0.78	-0.86	-0.93
Phenol	-0.49	-0.60	-0.69	-0.75
Vanillin	-0.14	-0.31	-0.42	-0.50
Naphthalene	-1.57	-1.89	-1.99	-2.04
Anthracene	-1.22	-1.42	-1.50	-1.53
p-Nitrotoluene	-1.62	-1.70	-1.84	-1.89
Nitrobenzene	-1.54	-1.63	-1.77	-1.80
Anisole	-2.11	-2.12	-2.26	-2.29
p-Cresol	-0.51	-0.63	-0.73	-0.77
o-Nitrophenol	-1.46	-1.77	-1.89	-1.95
Butylbenzoate	-1.93	-2.12	-2.29	-2.32
Ethyl Benzoate	-1.93	-2.01	-2.15	-2.15
Pyridine	-0.35	-0.44	-0.49	-0.54
Nicotinamide	1.67	1.60	0.77	1.45

Table 12.4: Experimental $\ln k$ at 4 pressures of SIL-300.

SOLUTES	150 bar	200 bar	250 bar	300 bar
Toluene	-2.32	-2.71	-3.06	-3.21
Benzene	-2.32	-2.71	-3.03	-3.08
Caffeine	0.10	-0.17	-0.36	-0.51
Benzoic Acid	-1.46	-1.92	-1.93	-2.03
Phenol	-1.36	-1.68	-1.87	-1.98
Vanillin	-1.05	-1.37	-1.60	-1.75
Naphthalene	-1.92	-2.38	-2.69	-2.85
Anthracene	-1.81	-2.21	-2.51	-2.66
p-Nitrotoluene	-1.84	-2.27	-2.58	-2.73
Nitrobenzene	-1.80	-2.18	-2.51	-2.66
Anisole	-2.11	-2.56	-2.88	-2.98
p-Cresol	-1.36	-1.70	-1.89	-1.99
o-Nitrophenol	-1.83	-2.28	-2.58	-2.75
Butylbenzoate	-2.00	-2.48	-2.83	-2.95
Ethyl Benzoate	-1.95	-2.48	-2.73	-2.90
Pyridine	-1.24	-1.46	-1.64	-1.72
Nicotinamide	1.06	0.88	0.78	0.69

Table 12.5: Experimental $\ln k$ at 4 pressures of SIL-300

SOLUTES	150 bar	200 bar	250 bar	300 bar
Toluene	-1.44	-1.44	-1.50	-1.47
Benzene	-1.43	-1.38	-1.47	-1.46
Caffeine	0.84	0.64	0.42	0.13
Benzoic Acid	1.96	1.83	1.67	1.50
Phenol	-0.36	-0.46	-0.61	-0.78
Vanillin	0.32	0.18	0.00	-0.22
Naphthalene	-1.14	-1.19	-1.30	-1.42
Anthracene	-1.11	-1.25	-1.30	-1.35
p-Nitrotoluene	-1.00	-1.06	-1.21	-1.39
Nitrobenzene	-0.99	-1.04	-1.15	-1.28
Anisole	-1.28	-1.43	-1.39	-1.43
p-Cresol	-0.38	-0.49	-0.64	-0.82
o-Nitrophenol	-1.03	-1.09	-1.21	-1.35
Butylbenzoate	-1.19	-1.27	-1.38	-1.51
Ethyl Benzoate	-1.17	-1.21	-1.32	-1.45

Table 12.6: Experimental $\ln k$ at 8 temperatures of SIL-60.

SOLUTES	25 °C	30 °C	35 °C	40 °C	45 °C	50 °C	55 °C	60 °C
Toluene	-2.32	-2.24	-2.19	-2.07	-2.09	-2.00	-1.85	-1.66
Benzene	-2.24	-2.22	-2.14	-2.04	-2.09	-2.02	-1.98	-1.76
Caffeine	1.77	1.87	2.10	2.39	2.54	2.78	2.84	2.87
Benzoic Acid	-0.03	0.11	0.29	0.63	0.74	1.01	1.18	1.22
Phenol	0.19	0.25	0.32	0.51	0.53	0.65	0.69	0.73
Vanillin	0.48	0.56	0.69	0.87	0.93	1.09	1.22	1.26
Naphthalene	-1.68	-1.47	-1.24	-1.14	-1.07	-0.95	-0.80	-0.71
Anthracene	-1.04	-0.93	-0.68	-0.59	-0.50	-0.29	-0.01	0.04
p-Nitrotoluene	-1.43	-1.25	-0.84	-0.92	-0.83	-0.67	-0.43	-0.36
Nitrobenzene	-1.37	-1.20	-0.82	-0.92	-0.80	-0.61	-0.43	-0.36
Anisole	-1.91	-1.75	-1.47	-1.43	-1.37	-1.24	-1.08	-0.97
p-Cresol	0.15	0.25	0.58	0.51	0.54	0.66	0.78	0.82
o-Nitrophenol	-1.50	-1.08	-0.91	-0.97	-0.96	-0.83	-0.59	-0.51
Butylbenzoate	-1.74	-1.55	-1.20	-1.09	-0.98	-0.87	-0.63	-0.55
Ethyl Benzoate	-1.70	-1.43	-1.15	-1.07	-0.97	-0.86	-0.65	-0.57
Pyridine	0.56	0.53	0.57	0.73	0.64	0.71	0.69	0.73
Nicotinamide	3.12	3.27	3.50	3.68	3.71	3.81	4.11	4.14

Table 12.7: Experimental $\ln k$ at 8 temperatures of SIL-100.

SOLUTES	25 °C	30 °C	35 °C	40 °C	45 °C	50 °C	55 °C	60 °C
Toluene	-1.94	-2.87	-2.98	-2.97	-3.08	-2.90	-2.92	-2.60
Benzene	-1.96	-2.84	-2.98	-2.97	-3.12	-3.03	-3.06	-2.70
Caffeine	1.56	1.72	1.91	2.13	2.35	2.58	2.74	2.79
Benzoic Acid	-0.07	-0.19	-0.05	0.14	0.35	0.62	0.89	0.94
Phenol	0.04	-0.06	-0.01	0.08	0.16	0.26	0.35	0.42
Vanillin	0.26	0.19	0.27	0.39	0.51	0.67	0.81	0.86
Naphthalene	-1.38	-2.03	-1.99	-1.87	-1.78	-1.53	-1.40	-1.21
Anthracene	-1.07	-1.48	-1.37	-1.22	-1.06	-0.83	-0.60	-0.50
p-Nitrotoluene	-1.19	-1.68	-1.59	-1.48	-1.44	-1.32	-1.15	-1.00
Nitrobenzene	-0.96	-1.65	-1.57	-1.47	-1.43	-1.28	-1.11	-0.95
Anisole	-1.29	-2.32	-2.28	-2.19	-2.12	-1.93	-1.75	-1.50
p-Cresol	0.01	-0.07	-0.01	0.08	0.17	0.29	0.37	0.44
o-Nitrophenol	-1.27	-1.81	-1.67	-1.52	-1.46	-1.37	-1.30	-1.13
Butylbenzoate	-1.37	-2.12	-2.01	-1.84	-1.58	-1.41	-1.35	-1.17
Ethyl Benzoate	-1.31	-2.03	-1.92	-1.76	-1.55	-1.41	-1.36	-1.17
Pyridine	0.26	0.15	0.16	0.20	0.23	0.29	0.31	0.38
Nicotinamide	2.95	3.16	3.30	3.46	3.60	3.71	3.78	3.82

Table 12.8: Experimental $\ln k$ at 8 temperatures of SIL-300.

SOLUTES	25 °C	30 °C	35 °C	40 °C	45 °C	50 °C	55 °C	60 °C
Toluene	-3.43	-3.33	-3.31	-3.01	-2.96	-2.64	-2.44	-2.44
Benzene	-2.98	-3.29	-2.95	-3.04	-3.02	-2.49	-2.44	-2.46
Caffeine	-0.53	-0.47	-0.42	-0.34	-0.27	-0.15	-0.06	0.02
Benzoic Acid	-1.94	-1.91	-1.94	-1.84	-1.82	-1.62	-1.54	-1.61
Phenol	-1.85	-1.83	-1.83	-1.77	-1.73	-1.61	-1.52	-1.52
Vanillin	-1.56	-1.55	-1.53	-1.45	-1.41	-1.30	-1.21	-1.20
Naphthalene	-2.72	-2.68	-2.62	-2.53	-2.53	-2.19	-2.03	-2.19
Anthracene	-2.68	-2.62	-2.56	-2.43	-2.32	-2.13	-1.97	-2.00
p-Nitrotoluene	-2.62	-2.56	-2.49	-2.20	-2.34	-2.06	-2.00	-2.03
Nitrobenzene	-2.35	-2.42	-2.46	-2.31	-2.34	-2.04	-1.96	-2.05
Anisole	-2.85	-2.88	-2.95	-2.72	-2.77	-2.38	-2.22	-2.30
p-Cresol	-1.83	-1.84	-1.88	-1.77	-1.75	-1.61	-1.54	-1.55
o-Nitrophenol	-2.46	-2.60	-2.54	-2.31	-2.36	-2.18	-2.02	-2.10
Butylbenzoate	-2.88	-2.88	-2.87	-2.65	-2.72	-2.35	-2.24	-2.30
Ethyl Benzoate	-2.81	-2.74	-2.75	-2.70	-2.61	-2.27	-2.08	-2.23
Pyridine	-1.55	-1.55	-1.60	-1.53	-1.52	-1.43	-1.39	-1.41
Nicotinamide	0.62	0.64	0.67	0.73	0.78	0.86	0.93	0.97

Table 12.9: Experimental $\ln k$ at 8 temperatures of SIL-Aerogel.

SOLUTES	25 °C	30 °C	35 °C	40 °C	45 °C	50 °C	55 °C	60 °C
Toluene	-2.05	-1.94	-1.76	-1.64	-1.61	-1.60	-1.56	-1.55
Benzene	-2.01	-1.85	-1.69	-1.62	-1.62	-1.54	-1.52	-1.33
Caffeine	0.21	0.29	0.41	0.55	0.66	0.73	0.80	0.89
Benzoic Acid	0.55	0.83	1.17	1.50	1.72	1.94	2.11	2.28
Phenol	-0.93	-0.83	-0.72	-0.63	-0.56	-0.52	-0.47	-0.43
Vanillin	-0.53	-0.39	-0.28	-0.10	0.01	0.14	0.23	0.34
Naphthalene	-1.75	-1.67	-1.49	-1.39	-1.34	-1.31	-1.26	-1.24
Anthracene	-1.64	-1.61	-1.46	-1.38	-1.35	-1.30	-1.22	-1.14
p-Nitrotoluene	-1.68	-1.56	-1.32	-1.27	-1.18	-1.19	-1.13	-1.07
Nitrobenzene	-1.57	-1.48	-1.34	-1.24	-1.18	-1.15	-1.12	-1.06
Anisole	-1.91	-1.79	-1.64	-1.52	-1.61	-1.45	-1.40	-1.44
p-Cresol	-0.98	-0.88	-0.76	-0.65	-0.59	-0.54	-0.50	-0.46
o-Nitrophenol	-1.69	-1.57	-1.41	-1.30	-1.21	-1.18	-1.12	-1.09
Butylbenzoate	-1.95	-1.82	-1.60	-1.49	-1.42	-1.38	-1.30	-1.27
Ethyl Benzoate	-1.84	-1.75	-1.54	-1.44	-1.38	-1.33	-1.28	-1.26

Table 12.10: Experimental $\ln k$ at 7 modifier concentrations of SIL-60.

SOLUTES	5 vol.%	7.5 vol.%	10 vol.%	12.5 vol.%	15 vol.%	17.5 vol.%	20 vol.%
Toluene	-3.31	-2.35	-2.21	-2.36	-1.89	-1.57	-1.49
Benzene	-3.11	-2.29	-2.19	-2.22	-1.87	-1.62	-1.37
Caffeine	2.78	2.06	1.58	1.44	1.17	1.00	0.86
Benzoic Acid	0.59	0.25	-0.07	-0.18	-0.42	-0.54	-0.62
Phenol	0.66	0.30	-0.02	-0.09	-0.33	-0.47	-0.57
Vanillin	0.88	0.60	0.32	0.27	0.04	-0.11	-0.23
Naphthalene	-1.73	-1.57	-1.71	-1.68	-1.40	-1.28	-1.13
Anthracene	-1.00	-0.95	-1.01	-1.00	-1.11	-1.08	-1.04
p-Nitrotoluene	-1.19	-1.32	-1.42	-1.44	-1.24	-1.19	-1.07
Nitrobenzene	-1.09	-1.24	-1.27	-1.22	-1.20	-1.13	-1.02
Anisole	-2.12	-1.85	-1.96	-1.58	-1.63	-1.46	-1.35
p-Cresol	0.65	0.25	-0.03	-0.11	-0.35	-0.50	-0.60
o-Nitrophenol	-1.38	-1.41	-1.53	-1.51	-1.25	-1.21	-1.08
Butylbenzoate	-1.73	-1.72	-1.92	-1.85	-1.60	-1.37	-1.30
Ethyl Benzoate	-1.59	-1.57	-1.53	-1.46	-1.50	-1.39	-1.31
Pyridine	0.99	0.63	0.33	0.27	0.09	0.00	-0.06
Nicotinamide	3.45	3.33	2.75	2.55	2.17	1.88	1.65

Table 12.11: Experimental $\ln k$ at 7 modifier concentrations of SIL-100.

SOLUTES	5 vol.%	7.5 vol.%	10 vol.%	12.5 vol.%	15 vol.%	17.5 vol.%	20 vol.%
Toluene	-2.94	-2.68	-3.04	-2.99	-2.78	-2.49	-2.39
Benzene	-2.82	-2.62	-2.94	-2.86	-2.70	-2.51	-1.87
Caffeine	1.71	1.21	0.88	0.62	0.43	0.26	0.14
Benzoic Acid	-0.21	-0.49	-0.81	-1.05	-1.21	-1.35	-1.26
Phenol	-0.10	-0.44	-0.71	-0.97	-1.14	-1.30	-1.30
Vanillin	0.18	-0.11	-0.35	-0.59	-0.78	-0.96	-1.08
Naphthalene	-1.95	-2.16	-1.87	-2.25	-2.24	-2.18	-1.83
Anthracene	-1.45	-1.56	-1.68	-1.74	-1.75	-1.71	-1.65
p-Nitrotoluene	-1.71	-1.88	-1.89	-1.71	-1.66	-1.61	-1.55
Nitrobenzene	-1.67	-1.74	-1.67	-1.62	-1.59	-1.54	-1.53
Anisole	-2.33	-2.47	-2.61	-2.54	-2.51	-1.77	-1.89
p-Cresol	-0.10	-0.46	-0.74	-0.99	-1.16	-1.33	-1.23
o-Nitrophenol	-1.85	-1.97	-1.77	-1.71	-1.67	-1.57	-1.53
Butylbenzoate	-2.04	-2.44	-2.57	-2.59	-2.61	-2.39	-2.05
Ethyl Benzoate	-1.95	-2.32	-2.43	-2.47	-2.44	-2.29	-1.73
Pyridine	0.14	-0.17	-0.38	-0.56	-0.68	-0.75	-0.83
Nicotinamide	3.13	2.42	1.94	1.57	1.28	1.02	0.80

Table 12.12: Experimental $\ln k$ at 7 modifier concentrations of SIL-300.

SOLUTES	5 vol.%	7.5 vol.%	10 vol.%	12.5 vol.%	15 vol.%	17.5 vol.%	20 vol.%
Toluene	-3.12	-2.94	-2.97	-2.72	-2.12	-1.96	-2.61
Benzene	-2.86	-2.86	-2.97	-2.72	-2.12	-2.23	-1.93
Caffeine	0.55	0.05	-0.30	-0.55	-0.74	-0.91	-1.05
Benzoic Acid	-1.53	-1.75	-1.94	-1.78	-1.73	-1.72	-1.77
Phenol	-1.33	-1.62	-1.79	-1.78	-1.70	-1.71	-1.74
Vanillin	-0.94	-1.29	-1.47	-1.54	-1.55	-1.58	-1.69
Naphthalene	-2.55	-2.57	-2.53	-2.08	-1.94	-1.88	-1.92
Anthracene	-2.26	-2.35	-2.46	-2.46	-2.18	-1.95	-2.15
p-Nitrotoluene	-2.36	-2.41	-2.39	-2.04	-1.94	-1.88	-1.86
Nitrobenzene	-2.32	-2.38	-2.29	-2.02	-1.93	-1.84	-1.84
Anisole	-2.81	-2.74	-2.74	-2.59	-2.07	-1.93	-2.04
p-Cresol	-1.34	-1.62	-1.79	-1.78	-1.73	-1.70	-1.74
o-Nitrophenol	-2.38	-2.48	-2.46	-2.07	-1.95	-1.87	-1.85
Butylbenzoate	-2.36	-2.74	-2.72	-2.51	-2.03	-1.94	-1.99
Ethyl Benzoate	-2.63	-2.65	-2.65	-2.13	-1.99	-1.91	-1.90
Pyridine	-1.09	-1.36	-1.50	-1.49	-1.52	-1.49	-1.57
Nicotinamide	1.99	1.29	0.81	0.45	0.15	-0.09	-0.31

Table 12.13: Experimental $\ln k$ at 7 modifier concentrations of SIL-Aerogel.

SOLUTES	5 vol.%	7.5 vol.%	10 vol.%	12.5 vol.%	15 vol.%	17.5 vol.%	20 vol.%
Toluene	-1.94	-1.76	-1.64	-1.61	-1.60	-1.56	-1.55
Benzene	-1.85	-1.69	-1.62	-1.62	-1.54	-1.52	-1.33
Caffeine	0.29	0.41	0.55	0.66	0.73	0.80	0.89
Benzoic Acid	0.83	1.17	1.50	1.72	1.94	2.11	2.28
Phenol	-0.83	-0.72	-0.63	-0.56	-0.52	-0.47	-0.43
Vanillin	-0.39	-0.28	-0.10	0.01	0.14	0.23	0.34
Naphthalene	-1.67	-1.49	-1.39	-1.34	-1.31	-1.26	-1.24
Anthracene	-1.61	-1.46	-1.38	-1.35	-1.30	-1.22	-1.14
p-Nitrotoluene	-1.56	-1.32	-1.27	-1.18	-1.19	-1.13	-1.07
Nitrobenzene	-1.48	-1.34	-1.24	-1.18	-1.15	-1.12	-1.06
Anisole	-1.79	-1.64	-1.52	-1.61	-1.45	-1.40	-1.44
p-Cresol	-0.88	-0.76	-0.65	-0.59	-0.54	-0.50	-0.46
o-Nitrophenol	-1.57	-1.41	-1.30	-1.21	-1.18	-1.12	-1.09
Butylbenzoate	-1.82	-1.60	-1.49	-1.42	-1.38	-1.30	-1.27
Ethyl Benzoate	-1.75	-1.54	-1.44	-1.38	-1.33	-1.28	-1.26

12.4 Adsorption isotherms fitted into BET

Table 12.14: Fitted BET parameters to the adsorption isotherm of methanol on SIL-60.

T [°C]	a [–]	b_s [mL/g]	b_L [mL/g]	Adj.R ²	RSS
30	32.7 ± 4.9	34.1 ± 9.9	1.68 ± 0.62	0.9869	1.4×10^{-2}
35	34.8 ± 5.1	31.6 ± 9.6	1.50 ± 0.69	0.9871	1.7×10^{-2}
40	34.1 ± 5.0	28.8 ± 9.3	1.45 ± 0.76	0.9873	1.8×10^{-2}
45	34.0 ± 5.1	28.7 ± 9.4	1.63 ± 0.75	0.9873	1.9×10^{-2}
50	39.4 ± 5.3	30.1 ± 8.8	1.67 ± 0.69	0.9894	1.9×10^{-2}
55	40.8 ± 5.0	26.8 ± 7.7	1.60 ± 0.69	0.9916	1.9×10^{-2}
60	44.4 ± 5.1	23.8 ± 7.4	1.17 ± 0.82	0.9923	2.5×10^{-2}

Table 12.15: Fitted BET parameters to the adsorption isotherm of methanol on SIL-100.

T [°C]	a [–]	b_s [mL/g]	b_L [mL/g]	Adj.R ²	RSS
30	17.8 ± 2.3	19.8 ± 7.0	1.19 ± 0.80	0.9914	6.9×10^{-3}
35	17.0 ± 2.1	18.2 ± 6.8	1.14 ± 0.86	0.9919	6.6×10^{-3}
40	17.4 ± 2.2	18.5 ± 6.8	1.21 ± 0.86	0.9920	6.6×10^{-3}
45	18.4 ± 2.2	16.9 ± 7.0	0.867 ± 1.018	0.9921	7.2×10^{-3}
50	18.2 ± 1.9	14.9 ± 6.2	0.681 ± 1.044	0.9942	5.9×10^{-3}
55	19.2 ± 1.9	15.8 ± 6.0	0.855 ± 0.945	0.9948	5.6×10^{-3}
60	19.4 ± 1.9	11.3 ± 6.6	0.253 ± 1.435	0.9950	6.8×10^{-3}

Table 12.16: Fitted BET parameters to the adsorption isotherm of methanol on SIL-300.

T [°C]	a [–]	b_s [mL/g]	b_L [mL/g]	Adj.R ²	RSS
30	7.12 ± 0.29	4.61 ± 0.55	$4.10 \times 10^{-18} \pm 0$	0.9973	1.3×10^{-3}
35	8.24 ± 0.40	5.06 ± 0.68	$2.75 \times 10^{-15} \pm 0$	0.9962	2.1×10^{-3}
40	8.61 ± 0.78	5.30 ± 6.75	$1.61 \times 10^{-10} \pm 2.12$	0.9964	2.1×10^{-3}
45	8.45 ± 0.34	4.47 ± 0.56	$3.30 \times 10^{-15} \pm 0$	0.9973	1.7×10^{-3}
50	8.75 ± 0.39	4.46 ± 2.35	$2.22 \times 10^{-12} \pm 0.83$	0.9972	1.9×10^{-3}
55	9.22 ± 0.70	4.58 ± 6.52	$2.83 \times 10^{-11} \pm 2.20$	0.9977	1.6×10^{-3}
60	10.16 ± 0.48	5.51 ± 1.56	$9.88 \times 10^{-13} \pm 0.43$	0.9972	2.0×10^{-3}

Table 12.17: Fitted BET parameters to the adsorption isotherm of methanol on SIL-Aerogel.

T [°C]	a [–]	b_s [mL/g]	b_L [mL/g]	Adj.R ²	RSS
30	17.5 ± 1.7	7.78 ± 6.21	$7.63 \times 10^{-10*} \pm 1.61$	0.9954	8.6×10^{-4}
35	17.5 ± 1.6	7.68 ± 5.81	0.12 ± 1.52	0.9961	6.9×10^{-3}
40	17.6 ± 1.3	7.07 ± 8.55	$2.15 \times 10^{-12*} \pm 2.66$	0.9965	6.5×10^{-3}
45	17.8 ± 1.5	8.23 ± 5.10	0.43 ± 1.27	0.9969	5.8×10^{-3}
50	18.2 ± 1.5	7.01 ± 5.80	$1.59 \times 10^{-11*} \pm 1.63$	0.9971	6.2×10^{-4}
55	18.8 ± 1.4	8.85 ± 4.84	0.49 ± 1.20	0.9974	5.1×10^{-3}
60	19.2 ± 1.4	7.34 ± 5.37	0.13 ± 1.50	0.9976	5.1×10^{-3}

12.5 Adsorption isotherms fitted into bi-Langmuir

Table 12.18: Fitted bi-Langmuir parameters to the adsorption isotherm of methanol on SIL-60.

T [°C]	q_1 [g/mL]	b_1 [mL/g]	q_2 [g/mL]	b_2 [mL/g]	Adj.R ²	RSS
30	1.72 ± 0.07	9.01 ± 0.89	0.13 ± 0.01	$3 \times 10^{44} \pm 0.00$	0.9985	1.4×10^{-3}
35	1.84 ± 0.09	9.70 ± 1.10	0.13 ± 0.02	$1 \times 10^{45} \pm 0.00$	0.9981	2.2×10^{-3}
40	$5 \times 10^{-15} \pm 0.00$	9.10 ± 0.00	1.74 ± 0.13	16.50 ± 2.90	0.9824	2.2×10^{-2}
45	2.00 ± 15.00	2.00 ± 31.00	1.10 ± 3.40	26.00 ± 57.00	0.9857	1.9×10^{-2}
50	2.32 ± 0.11	9.20 ± 1.00	0.14 ± 0.02	$1 \times 10^{19} \pm 6 \times 10^{31}$	0.9987	1.3×10^{-4}
55	2.67 ± 0.10	8.96 ± 0.75	0.13 ± 0.01	$2 \times 10^{16} \pm 0.00$	0.9990	2.1×10^{-3}
60	2.79 ± 0.12	10.50 ± 1.10	0.13 ± 0.03	$7 \times 10^{32} \pm 2 \times 10^{45}$	0.9983	4.2×10^{-3}

Table 12.19: Fitted bi-Langmuir parameters to the adsorption isotherm of methanol on SIL-100.

T [°C]	q_1 [g/mL]	b_1 [mL/g]	q_2 [g/mL]	b_2 [mL/g]	Adj.R ²	RSS
30	1.47 ± 0.08	7.81 ± 0.93	0.06 ± 0.01	$4 \times 10^{37} \pm 0.00$	0.9979	1.5×10
35	$1 \times 10^{-14} \pm 0.02$	$8.00 \pm 2 \times 10^{13}$	1.36 ± 0.13	11.30 ± 2.30	0.990	7.2×10
40	1.59 ± 0.09	7.09 ± 0.01	0.07 ± 0.01	$2 \times 10^{27} \pm 6 \times 10^{39}$	0.9981	1.4×10
45	1.60 ± 0.10	8.00 ± 0.01	0.06 ± 0.01	$4 \times 10^{45} \pm 0.00$	0.9975	2.0×10
50	1.69 ± 0.09	8.09 ± 0.01	0.05 ± 0.01	$5 \times 10^{35} \pm 0.00$	0.9980	1.8×10
55	1.77 ± 0.09	8.04 ± 0.01	0.06 ± 0.01	$1 \times 10^{35} \pm 0.00$	0.9985	1.5×10
60	2.16 ± 0.17	7.00 ± 0.02	0.06 ± 0.02	$6 \times 10^{17} \pm 1 \times 10^{30}$	0.9976	2.9×10

Table 12.20: Fitted bi-Langmuir parameters to the adsorption isotherm of methanol on SIL-300.

T [°C]	q_1 [g/mL]	b_1 [mL/g]	q_2 [g/mL]	b_2 [mL/g]	Adj.R ²	RSS
30	$0.00 \pm 1 \times 10^4$	$4.60 \pm 3 \times 10^8$	$1.50 \pm 1 \times 10^4$	$4.60 \pm 4 \times 10^2$	0.9970	1.3×10^{-3}
35	$2 \times 10^{-2} \pm 1 \times 10^6$	$5.00 \pm 1 \times 10^6$	$1.60 \pm 1 \times 10^6$	$5.10 \pm 9 \times 10^2$	0.9957	2.1×10^{-3}
40	$2 \times 10^{-9} \pm 1 \times 10^3$	$3.60 \pm 5 \times 10^{11}$	$1.60 \pm 1 \times 10^3$	$5.30 \pm 5 \times 10^2$	0.9959	2.1×10^{-3}
45	0.00 ± 0.00	0.00 ± 0.00	1.89 ± 0.17	4.47 ± 0.59	0.9970	1.7×10^{-3}
50	0.10 ± 0.00	4.50 ± 0.00	1.90 ± 0.00	4.50 ± 0.00	0.9969	1.9×10^{-3}
55	$1.00 \pm 1 \times 10^6$	$4.60 \pm 8 \times 10^5$	$1.00 \pm 1 \times 10^6$	$4.60 \pm 8 \times 10^5$	0.9974	1.6×10^{-3}
60	$7 \times 10^{-8} \pm 1 \times 10^5$	$5.50 \pm 6 \times 10^{10}$	$1.80 \pm 1 \times 10^5$	$5.50 \pm 8 \times 10^2$	0.9969	2.0×10^{-3}

Table 12.21: Fitted bi-Langmuir parameters to the adsorption isotherm of methanol on SIL-Aerogel.

T [°C]	q_1 [g/mL]	b_1 [mL/g]	q_2 [g/mL]	b_2 [mL/g]	Adj.R ²	RSS
30	2.20 ± 1.60	7.80 ± 3.30	$1 \times 10^{-12} \pm 1.90$	$7.80 \pm 9 \times 10^{12}$	0.9949	7.8×10^{-3}
35	2.57 ± 0.18	5.88 ± 0.79	0.04 ± 0.02	$3 \times 10^{32} \pm 0.00$	0.9979	3.3×10^{-3}
40	2.49 ± 0.20	7.10 ± 1.20	0.00 ± 0.02	$2 \times 10^7 \pm 0.00$	0.9960	6.5×10^{-3}
45	2.63 ± 0.48	6.60 ± 1.60	$3 \times 10^{-13} \pm 0.49$	$6.60 \pm 6 \times 10^{12}$	0.9965	7.3×10^{-4}
50	2.59 ± 0.20	7.00 ± 1.10	0.00 ± 0.02	$1 \times 10^6 \pm 0.00$	0.9967	5.5×10^{-3}
55	3.03 ± 0.19	5.28 ± 0.56	0.04 ± 0.01	$2 \times 10^{20} \pm 3 \times 10^{22}$	0.9989	2.0×10^{-3}
60	2.78 ± 0.51	6.90 ± 3.40	$6 \times 10^{-13} \pm 0.44$	$6.90 \pm 1 \times 10^{13}$	0.9972	5.1×10^{-3}

12.6 Paired t-test for correction factor

Table 12.22: Calculation of corrected adsorption constant $K_{eq,L}^{corr}$

	(SIL-60)	(SIL-100)	(SIL-300)	(SIL-Aerogel)
Measured $K_{eq,L}$	16.5	11.2	5.3	7.1
$K'_{eq,L}$	61.6	58.3	24.2	62.5
$K_{eq,L}^{corr}$ (correction factor =0.19*)	11.70	11.08	4.60	11.88

Selected from Table 12.23.

Formula applied in calculation:

Difference of paired observation: $d = K_{eq,L}^{corr} - \text{measured } K_{eq,L}$

Sample mean difference: $\bar{d} = \frac{\sum_{i=1}^n d_i}{n}$

Sample variance: $s_d^2 = \frac{\sum_{i=1}^n (d_i - \bar{d})^2}{n-1}$

Standard error of the mean difference: $s_{\bar{d}} = \frac{s_d}{\sqrt{n}}$

T-statistic: $t = \frac{\bar{d} - \mu_{d0}}{s_{\bar{d}}}$

Null hypothesis: $\mu_d = 0$

Alternate hypothesis: $\mu_d \neq 0$

$K_{eq,L}^{corr} = F K'_{eq,L}$

Table 12.23: Data of paired t-test for correction factor selection.

Correction factor F	$K_{eq,L}^{corr}$ (SIL-60)	$K_{eq,L}^{corr}$ (SIL-100)	$K_{eq,L}^{corr}$ (SIL-300)	$K_{eq,L}^{corr}$ (SIL-Aerogel)	d_2 (SIL-60)	d_2 (SIL-100)	d_3 (SIL-300)	d_4 (SIL-Aerogel)	\bar{d}	$s_{\bar{d}}$	t
0.10	6.16	5.83	2.42	6.25	-10.34	-5.37	-2.88	-0.85	-4.86	3.55	-1.37
0.11	6.78	6.41	2.66	6.88	-9.72	-4.79	-2.64	-0.23	-4.34	3.50	-1.24
0.12	7.39	7.00	2.90	7.50	-9.11	-4.20	-2.40	0.40	-3.83	3.46	-1.11
0.13	8.01	7.58	3.15	8.13	-8.49	-3.62	-2.15	1.03	-3.31	3.43	-0.96
0.14	8.62	8.16	3.39	8.75	-7.88	-3.04	-1.91	1.65	-2.79	3.41	-0.82
0.15	9.24	8.75	3.63	9.38	-7.26	-2.46	-1.67	2.28	-2.28	3.39	-0.67
0.16	9.86	9.33	3.87	10.00	-6.64	-1.87	-1.43	2.90	-1.76	3.38	-0.52
0.17	10.47	9.91	4.11	10.63	-6.03	-1.29	-1.19	3.53	-1.24	3.38	-0.37
0.18	11.09	10.49	4.36	11.25	-5.41	-0.71	-0.94	4.15	-0.73	3.38	-0.22
<u>0.19</u>	<u>11.70</u>	<u>11.08</u>	<u>4.60</u>	<u>11.88</u>	<u>-4.80</u>	<u>-0.12</u>	<u>-0.70</u>	<u>4.78</u>	<u>-0.21</u>	<u>3.40</u>	<u>-0.06</u>
0.20	12.32	11.66	4.84	12.50	-4.18	0.46	-0.46	5.40	0.31	3.42	0.09
0.21	12.94	12.24	5.08	13.13	-3.56	1.04	-0.22	6.03	0.82	3.44	0.24
0.22	13.55	12.83	5.32	13.75	-2.95	1.63	0.02	6.65	1.34	3.48	0.38
0.23	14.17	13.41	5.57	14.38	-2.33	2.21	0.27	7.28	1.85	3.52	0.53
0.24	14.78	13.99	5.81	15.00	-1.72	2.79	0.51	7.90	2.37	3.57	0.66
0.25	15.40	14.58	6.05	15.63	-1.10	3.38	0.75	8.53	2.89	3.62	0.80
0.26	16.02	15.16	6.29	16.25	-0.48	3.96	0.99	9.15	3.40	3.68	0.92
0.27	16.63	15.74	6.53	16.88	0.13	4.54	1.23	9.78	3.92	3.75	1.05
0.28	17.25	16.32	6.78	17.50	0.75	5.12	1.48	10.40	4.44	3.82	1.16
0.29	17.86	16.91	7.02	18.13	1.36	5.71	1.72	11.03	4.95	3.90	1.27
0.30	18.48	17.49	7.26	18.75	1.98	6.29	1.96	11.65	5.47	3.98	1.37

12.7 List of Tables

Table 2.1: Chromatography classifications and their available control parameters [15].	5
Table 2.2: Summary of retention models in RP-HPLC.	15
Table 2.3 Most important properties of silica aerogels. Summarized from [70,71,74,75].	19
Table 3.1: Summary of solutes.	23
Table 3.2: List of employed stationary phases and their textural properties.	24
Table 3.3: Experimental settings for frontal analysis.	31
Table 3.4: Column volumes and total porosities (measured at 30 °C).	34
Table 5.1: Fitted Langmuir parameters to the adsorption isotherm data points of methanol on SIL-60.	48
Table 5.2: Fitted Langmuir parameters to the adsorption isotherm data points of methanol on SIL-100.	48
Table 5.3: Fitted Langmuir parameters to the adsorption isotherm data points of methanol on SIL-300.	49
Table 5.4: Fitted Langmuir parameters to the adsorption isotherm data points of methanol on SIL-Aerogel.	49
Table 5.5: Specific surface area (A_s) and surface concentration of hydroxyl groups ($\Gamma - OH$) of four silica matrices: SIL-60, SIL-100, SIL-300 and SIL-Aerogel.	57
Table 6.1: Solute descriptors used for the LSER analysis [110].	61
Table 6.2: Correlation matrix (Pearson) of the solute descriptors from Table 6.1.	63
Table 6.3: Description of employed methods: each method is a combination of a model (DIM or MRM), adsorption isotherm and a set of fitted parameters [127].	74
Table 6.4: Comparison of methods based on DIMs an MRMs [127].	75
Table 6.5: Regression results for DIMs [127].	83
Table 6.6: Regression results for MRMs [127].	84
Table 12.1: Mahalanobis' Distance.	116
Table 12.2: Experimental $\ln k$ at 4 pressures of SIL-60.	117

Table 12.3: Experimental <i>lnk</i> at 4 pressures of SIL-100.	117
Table 12.4: Experimental <i>lnk</i> at 4 pressures of SIL-300.	118
Table 12.5: Experimental <i>lnk</i> at 4 pressures of SIL-300	118
Table 12.6: Experimental <i>lnk</i> at 8 temperatures of SIL-60.	119
Table 12.7: Experimental <i>lnk</i> at 8 temperatures of SIL-100.	119
Table 12.8: Experimental <i>lnk</i> at 8 temperatures of SIL-300.	120
Table 12.9: Experimental <i>lnk</i> at 8 temperatures of SIL-Aerogel.	120
Table 12.10: Experimental <i>lnk</i> at 7 modifier concentrations of SIL-60.	121
Table 12.11: Experimental <i>lnk</i> at 7 modifier concentrations of SIL-100.	121
Table 12.12: Experimental <i>lnk</i> at 7 modifier concentrations of SIL-300.	122
Table 12.13: Experimental <i>lnk</i> at 7 modifier concentrations of SIL-Aerogel.	122
Table 12.14: Fitted BET parameters to the adsorption isotherm of methanol on SIL-60.	123
Table 12.15: Fitted BET parameters to the adsorption isotherm of methanol on SIL-100.	123
Table 12.16: Fitted BET parameters to the adsorption isotherm of methanol on SIL-300.	124
Table 12.17: Fitted BET parameters to the adsorption isotherm of methanol on SIL-Aerogel.	124
Table 12.18: Fitted bi-Langmuir parameters to the adsorption isotherm of methanol on SIL-60.	125
Table 12.19: Fitted bi-Langmuir parameters to the adsorption isotherm of methanol on SIL-100.	125
Table 12.20: Fitted bi-Langmuir parameters to the adsorption isotherm of methanol on SIL-300.	126
Table 12.21: Fitted bi-Langmuir parameters to the adsorption isotherm of methanol on SIL-Aerogel.	126
Table 12.22: Calculation of corrected adsorption constant <i>K_{eq}, L_{corr}</i>	127
Table 12.23: Data of paired t-test for correction factor selection.	128

12.8 List of Figures

Figure 2.1: Effects of modifiers in SFC [29].	6
Figure 2.2: Principle of the solvation parameter model: interactions related to each solute descriptor. Figure from West et al. [68].	17
Figure 2.3: Application fields of silica aerogels. Extracted from [74].	20
Figure 2.4: Different types of silanol groups and siloxane bridges on the surface of amorphous silica gel [76,77].	21
Figure 3.1: Column packing set-ups. Two set-ups were applied: (a) slurry packing method for Kromasil particles and (b) dry packing for silica aerogel.	25
Figure 3.2: Flow diagram of Waters UPC ² . Blue line: principal connections; green line: to waste. Adapted from the graphical navigator view of Waters' webpage, 2017.	28
Figure 3.3: Ideal breakthrough curve for adsorption of a pure component in frontal analysis.	30
Figure 3.4: An example of breakthrough curves of a staircase frontal analysis of methanol on SIL-300 column. (SFC condition: 200 bar, 40 °C, flow rate 2.0 mL/min, UV 200 nm).	32
Figure 3.5: An example of breakthrough curves of a stepwise frontal analysis of methanol on SIL-60 column. (SFC condition: 200 bar, 40 °C, flow rate 2.0 mL/min, UV 200 nm).	32
Figure 3.6: Density profile between column inlet and outlet of the SIL-60 column at 60 °C with 100% CO ₂ as mobile phase. The x-axis presents the local pressure the column. As the back pressure was applied the density profile ended at 200 bar. The total pressure drops along the columns were observed to be no more than 18 bar. ...	36
Figure 4.1: Retention time of commonly used hold-up tracers on SIL-100 [90]. SFC conditions: 200 bar, 40 °C, injection volume 2 µL, flow rate 2 mL/min. The dashed lines were plotted to guide the eye.	38

Figure 4.2: Chromatogram recorded on injection of a 2 μ L sample of N₂O/methanol solution on the SIL-60 column. The first peak corresponds to N₂O, the second one is the elution peak of methanol, which exhibits strong tailing on silica gel stationary phase. (SFC condition: 200 bar, 60 °C, injection volume 2 μ L, flow rate 2.0 mL/min, 100% CO₂, UV 195 nm). 38

Figure 4.3: Retention time of nitrous oxide and hexane for four different modifiers, 5 vol.% in CO₂. Stationary phase: SIL-100; chromatographic conditions: 200 bar, 40 °C, injection volume 2 μ L, flow rate 2 mL/min..... 39

Figure 4.4: Relationship between the calculated critical pressure (P_c), temperature (T_c), and mass fraction of methanol ($w_{methanol}$) of a CO₂/methanol mixture [17]. The critical temperature keeps on increasing from 0 to 100% methanol, while critical pressure first increases then decreases with increase of methanol percentage reaching a maximum at around 35-40% methanol. The box shows a typical experimental range of methanol as modifier (5-30%). Figure obtained from Saito [15]. 40

Figure 4.5: A $p - T$ phase diagram of pure CO₂ (in blue) or CO₂/methanol mixture at different proportions (in green). Isopycnic lines (equal density) at $\rho = 0.75\text{g/mL}$ of CO₂ or mixture of CO₂-methanol at different compositions were shown. Critical temperature (T_c) and critical pressure (p_c) values were denoted under each composition. Figure obtained from Lesellier et al. [17]. 40

Figure 4.6: Three-dimensional plot of methanol/CO₂ vapor-liquid phase behaviors as a function of $p-T-x_{CO_2}$ (CO₂ mole fraction). The region above the surface is the single phase. The working region of experiments (box in the figure) is situated above the surface and thus in the single-phase region. Figure plotted from data obtained by Yeo et al. [94]. 42

Figure 4.7: Retention time of nitrous oxide at various temperatures. The column was stabilized at each temperature for 4 hours and a half. Within this time, 3 measurements were carried out for each temperature in order to see the stability of the column at a certain temperature. Stationary phases: (A)SIL-60, (B)SIL-Aerogel;

chromatographic conditions: 200 bar, 10 vol.% methanol, injection volume 2 μL , flow rate 2 mL/min..... 44

Figure 4.8: FTIR spectra of SIL-60 treated at 60 to 90 $^{\circ}\text{C}$ and 10 and 20 vol.% methanol in sc- CO_2 (200 bar, flow rate 2 mL/min). The column was stabilized for 30 minutes at each condition before taking the sample. The peaks at 810 cm^{-1} , 960 cm^{-1} and 1100 cm^{-1} are ascribed to Si-O-Si bending, Si-OH stretching and Si-O stretching vibration respectively. The affected peaks at 2400 cm^{-1} are most probably influenced by the measurement technique, which is the degree of compression of the solid sample..... 45

Figure 5.1: Experimental data fitted to the Langmuir, BET and bi-Langmuir model. (Chromatographic condition: stationary phase, silica gel K60 column; mobile phase, CO_2 – methanol, methanol: 0-20% (v/v); column temperature: 60 $^{\circ}\text{C}$; nominal flow rate, 2.0 mL/min). 46

Figure 5.2: Comparison of the methanol adsorption on silica gel in (a) this study with (b) Kern et al. [97] (same stationary phase, same T and p , different method and different equipment), (c) Vajda et al. [98] (different T and p , same method and same equipment) and (d) Vajda et al. [99] (different conditions, different method and same equipment). The values of loading marked by dashed lines are at the methanol concentration of 0.032 g/mL in liquid phase. 51

Figure 5.3: Adsorption isotherms of methanol on four silica matrices at temperature from 30 to 60 $^{\circ}\text{C}$, under a column back pressure of 200 bar. 52

Figure 5.4: Effect of temperature and pressure on the Hildebrand solubility parameter (δ) for supercritical CO_2 . The Hildebrand solubility parameter is an indicator of the solvation power of a fluid. A decrease of the parameter indicates a lower solvation power. Figure obtained from Robards et al.[100]..... 54

Figure 5.5: Loading of methanol at different densities of mobile phase. The density is varied by varying system back pressure (SFC conditions: flow rate 2 mL/min, methanol concentration at 1 vol.%, back pressure at 120, 180, 200 and 240 bar). .. 55

Figure 5.6: Adsorption isotherms of methanol at different column back pressure fitted by Langmuir isotherm. (SFC conditions: SIL-60 column, methanol concentration at 0-20 vol.%, column temperature 50 °C, flow rate 2 mL/min).....	56
Figure 5.7: Surface concentration of methanol ($\Gamma_{methanol}$) and hydroxyl groups ($\Gamma - OH$) on the four silica matrices: SIL-60, SIL100, SIL-300 and SIL-Aerogel. Numbers above the columns are the ratios of the surface concentration of methanol molecules ($\Gamma_{methanol}$) at 20 vol.% methanol to that of hydroxyl groups ($\Gamma - OH$) on silica matrices.	57
Figure 5.8: Coverage of a uniform surface by hard spheres. The circles show the foot- print of each adsorbed molecule; the area outside the circles is the excluded part of the surface. Figure obtained from [87].....	59
Figure 6.1: Natural logarithms of retention factors for four different columns calculated with the minimal (AS, Eq. 34) model vs. experimental values [90]. SFC conditions: 200 bar, 35 °C, injection volume 2 μ L, flow rate 2 mL/min, modifier (methanol) concentration at 5 to 20 vol.%. Dotted line is the line of the best fit.	64
Figure 6.2: Natural logarithms of retention factors for four different columns calculated with the specific models Eq. 35 - Eq. 37 vs. experimental values [90]. SFC conditions: 200 bar, 35 °C, injection volume 2 μ L, flow rate 2 mL/min, modifier (methanol) concentration at 5 to 20 vol.%. Dotted line is the line of the best fit.	65
Figure 6.3: Influence of the concentration of modifier on the goodness of fit. SFC conditions: 200 bar, 35 °C, injection volume 2 μ L, flow rate 2 mL/min.....	66
Figure 6.4: Influence of the pressure of modifier on the goodness of fit. SFC conditions: 35°C, 10 vol.% methanol, injection volume 2 μ L, flow rate 2mL/min.	67
Figure 6.5: Influence of temperature on the goodness of fit. SFC conditions: 200 bar, 5 vol.% methanol, injection volume 2 μ L, flow rate 2 mL/min.	67
Figure 6.6: A schematic diagram of the mixed retention mechanism in a silica packed column [127]. The interaction in the green dashed line contributes to k_c in Eq. 47 and the interaction in red dashed line contributes to k_0	72

Figure 6.7: Retention factors of phenol on different silicas and model fittings according to DIM-Lin-kc [127]. SFC conditions: 200 bar, 40 °C, injection volume 2 μ L, flow rate 2 mL/min.	76
Figure 6.8: Retention factors of various solutes on SIL-60 and model fittings according to DIM-Lin-kc [127]. SFC conditions: 200 bar, 40 °C, injection volume 2 μ L, flow rate 2 mL/min.	77
Figure 6.9: Retention factors of phenol and naproxen on SIL-Aerogel and model fittings according to DIM-Lan-kcK' [127]. SFC conditions: 200 bar, 40 °C, injection volume 2 μ L, flow rate 2 mL /min.....	78
Figure 6.10: Retention factors of toluene on SIL-60 and SIL-Aerogel and model fittings according to method DIM-Lan-kcK' [127]. SFC conditions: 200 bar, 40 °C, injection volume 2 μ L, flow rate 2 mL/min.....	78
Figure 6.11: Retention factors of various solutes on SIL-60 and SIL-Aerogel [127]. SFC conditions: 200 bar, 40 °C, injection volume 2 μ L, flow rate 2 mL/min, modifier (methanol) fraction at 0.1–30 vol.%. The dashed straight lines were plotted to guide the eyes at low coverages.	81
Figure 7.1: Comparison of a and s system constants from the AS model in SIL-60, SIL-100, SIL-300 and SIL-Aerogel stationary phase across different concentrations of modifier in mobile phase. SFC conditions: 200 bar, 35 °C, injection volume 2 μ L, flow rate 2mL/min, modifier concentration at 5 to 20 vol.%.	86
Figure 7.2: System constants from the specific models, Eq. 35, Eq. 36 and Eq. 37 for all silica materials at different modifier concentrations [90]. Error bars represent the standard error of the system constants. SFC conditions: 200 bar, 35 °C, injection volume 2 μ L, flow rate 2 mL/min, modifier (methanol) concentration at 5 to 20 vol.%.	88
Figure 8.1: System constants a and s from the minimal AS model for SIL-60 and SIL-Aerogel stationary phases across different temperature and pressure [90]. Error bars represent the standard error of the system constants. SFC conditions for the top panel: 200 bar, 25 to 60 °C; for the bottom panel: 150 to 200 bar, 45 °C. Other	

conditions: flow rate 2 mL/min, modifier concentration at 10 vol.%, injection volume 2 μ L.	89
Figure 8.2: Influence of the pressure on the retention time and in the peak shape of the representative solutes. Stationary phase: SIL-100. SFC conditions: 35 °C, 10 vol.% methanol, injection volume 2 μ L, flow rate 2 mL/min.	90
Figure 8.3: Influence of the temperature on the retention time and in the peak shape of the representative solutes. Stationary phase: SIL-100. SFC conditions: 200 bar, 5 vol.% methanol, injection volume 2 μ L, flow rate 2 mL/min.	92
Figure 8.4: Retention factors of ketoprofen on SIL-Aerogel at different temperatures and model fitting according to MRM-Lan-kcKM [127]. SFC conditions: 191 bar for 318.15 K, 217 bar for 323.15 K, 242 bar for 328.15 K and 268 bar for 333.15 K, flow rate 2 mL/min, modifier (methanol) fraction at 0.8 to 7.5 vol.%.	94
Figure 8.5: Estimated k_0 values of ketoprofen on SIL-Aerogel at different temperatures. Method DIM-Lan-kcK, DIM-Lan-kcK' and MRM-Lan-kcKM were applied following the procedure explained in section 0.	94
Figure 9.1: Transferability of the retention factors according to Eq. 52 [90]. Reference material: SIL-60, SFC conditions: 200 bar, 40 °C, 10 vol.% methanol, injection volume 2 μ L, flow rate 2 mL/min. Dashed lines indicate 95 % confidence bands.	96

Lebenslauf

Name	Sun
Vorname	Miaotian
Staatsangehörigkeit	Chinese
Geburtsdatum	02.02.1988
Geburtsort, -land	Qingdao, China
09.1995 - 08.2001	Qingdao Sifang Experimental Primary School, China
09.2001 - 08.2004	Qingdao No.53 Middle School, China
09.2004 - 08.2007	Qingdao No. 2 High School, China
09.2007 - 09.2011	East China University of Science and Technology, China Bachelor of Science in Chemical Engineering University of Applied Science Lübeck, Germany Bachelor of Science in Environmental Engineering
10.2011 - 10.2014	Hamburg University of Technology, Germany Master of Science in Chemical and Bioprocess Engineering
11.2014 - 11.2018	Hamburg University of Technology, Germany Research Associate in Institute of Thermal Separation Processes
12.2018 - 05.2021	Freelancer, Germany and United States R & D Consultant
06.2021 - heute	California Department of Cannabis Control, United States Research Scientist